OREGON HEALTH & SCIENCE UNIVERSITY
SCHOOL OF MEDICINE

Exploring the Effects of Novel Design of Contact Lead Sheet Collimation and Filtration of High Energy Electron Fields on Electron Depth Dose Distributions with Application to Uniform Treatment of Small Skin Lesions.

By

Abdulaziz S. Alhussan

A THESIS

Presented to the Department of Radiation Medicine
and the Oregon Health & Science University
School of Medicine
in partial fulfillment of
the requirements for the degree of

Master of Science

August 2020

School of Medicine

Oregon Health & Science University

CERTIFICATE OF APPROVAL

This is to certify that the Master's thesis of

Abdulaziz S. Alhussan

has been approved

Richard J. Crilly, Ph.D.

Malcolm Heard, Ph.D.

Kyle Gallagher, Ph.D.

Andrei Pugachev, Ph.D.

TABLE OF CONTENTS

Page

Page

LIST OF FIGURES

LIST OF TABLES

ACKNOWLEDGEMENTS

I dedicate this thesis to my family and friends. Special thanks to Dr. Richard Crilly for all his support throughout my time of graduate school, especially during the tough time of COVID-19. Many thanks to all my colleagues, everyone in the Radiation Medicine and the Diagnostic Radiology departments, and everybody associated with the Medical Physics Program. I would also like to thank the Kuwait Foundation for the Advancement of Sciences (KFAS) for supporting me financially during my first year of this degree.

ABSTRACT

Purpose: This experiment investigates the effects of using electron beam Cerrobend contact skin collimators in combination with thin metallic scatter foils on electron beam depth dose distribution and isodose curves for small electron fields. The premise is to provide a clinically more uniform treatment for small superficial lesions. This is a test of concept that could potentially open the door for the development of novel electron beam therapy technique applicable for clinical use. The ultimate goal is to produce a quickly accessed, easy to fabricate, reusable device for clinical use with current linear accelerators without the need to modify the design of current linear accelerators' built-in scatter foils or make any other changes to the machine.

Materials & methods: An Elekta Versa HD linear accelerator was used to investigate the dose distributions of *8, 12, and 15 MeV* electron beams for *6 x 6 cm*^{2} applicator, a *2 cm* diameter circular electron fields at a source-to-surface distance (*SSD*) of *100 cm*. Thin flat metallic Pb and Al scatter foils of several thicknesses of less than *2.5 mm* were used. The dose distributions were recorded on Gafchromic™ EBT3 film in a Nomos™ solid water phantom. Calibration films were irradiated with electron beams to confirm the conversion of film intensity to absorbed dose in tissue was correct. All scanned film images were imported and analyzed in *DoseLab*.

Results: The results consist of figures of film profile for every energy and foil thickness combination used, the *PDD* at central axis, and the *10%, 25%, 50%, 80%, 90%* isodose curves. Also, for every energy and foil thickness combination used, tables that include the diameter of the clinically relevant portion of the field, i.e., the *90*% region at depth of maximum dose (D_{max}), the value of the maximum dose, the penumbra sizes *at* D_{max}, D_{90}, D_{50}, *&* D_{25}, as well as the most probable energy (E_{P0}), D_{max} and practical range (R_p). The use of scatter foils on the skin collimator

has been demonstrated to reduce the practical range, the effective energy of electron beams, the *90%* isodose region diameter, the maximum dose and its depth, and to increase the penumbra width at several depths. These effects are especially evident for thicker scatter foils of high Z materials.

Conclusions: The addition of scatter foils did not yield the hypothesized uniform, clinically-desirable, dose distributions. This preliminary work demonstrates that future studies would better focus on different foil material, different foil design and different foil positioning with respect to the skin collimator.

1. INTRODUCTION

In 2018, the number of cancer cases worldwide (excluding non-melanoma skin cancer) exceeded 18 million. [58] With cancer mortality numbers reaching 9.6 million deaths. [58] Of all cancer types, skin cancers are one of the most common cancer types in the world and the most common type of cancer in the United States. [60] Non-melanoma skin cancer alone is responsible for nearly 3 million cases worldwide. [60] Melanoma skin cancer is responsible for 1.59% and 0.64% of cancer incidence and mortality rates, respectively and its mortality numbers are on the rise.[58]

There are several treating options for skin cancer patients, one of which utilizes ionizing radiation in medicine; i.e., radiation therapy. Radiotherapy is a cancer treating procedure that uses ionizing radiation to destroy cancer cells while sparing normal cells. This is done by focusing a beam of high energy photons or particulate radiation (e.g. electrons or protons) on tumors to maximize damage to cancerous cells whilst minimizing damage to critical structures.[18] For skin cancer and near surface cancers, electron beam techniques are dominant due to their unique dosimetric properties. Electron beams display a prominent surface dose, a roughly even dose plateau at depths of maximum dose, and a sharp dose fall-off.[18] This uniqueness helps maximizing dose to tumor and minimizing dose to healthy tissues. This is especially true for large electron fields.[3] However, for irregularly shaped small tumors, the dose profile delivered by small size electron beams becomes less uniform and unpredictable.[54]

The purpose of this study is to investigate a new method to even isodose curves for small electron fields for a more uniform treatment. The proposed method is to use a thin metallic scatter foil on top of a Cerrobend skin collimator that is placed on top of the treatment region. The idea is that the scatter foil will spread out the electron beam mimicking the spread-out of the beam in the linear accelerator's head. This phenomenon along with the focusing of the electron beam by the

skin collimator's aperture is hypothesized to uniformly scatter dose into treatment area. This work functions as a practicability study and presents data from an introductory test into the use of a "skin scatter foil device" for the purpose of improving small electron fields' treatment.

The rest of this work will be divided into six chapters. The next chapter covers the theory behind the use of electron therapy and electron's behavior. Followed by a literature review which discusses published studies regarding current methods to manipulate and improve isodose curves and closing with what research need to be explored. Chapter *4* reviews the materials that has been used to conduct this experiment and the methods that has been followed to construct the experimentation. Chapters *5* presents the data for *8, 12,* and *15 MeV* electron beams in combination with several thicknesses of Al and Pb scatter foils for small electron fields at a fixed SSD. Chapter *6* analyzes and discusses the behavior of the collected data from the preceding chapter and the study limitations. The final chapter draws conclusions and considers directions for future work.

2. BACKGROUND & THEORY

Ionizing radiation, radiation that has enough energy to free electrons from molecules, is proven to be damaging to living cells at high energies.[20] Ionizing radiation can be subdivided based on the rate of energy transfer, better known as linear energy transfer (LET).[20] Neutron's products such as protons, α-particles and heavy charged particles, are high LET particles meaning that they are densely ionizing since they transfer more energy per unit length along their path. In contrast, X-ray and γ-ray radiation produce low LET electrons that are sparsely ionizing because they deposit less energy per unit length along their tracks.[20] DNA damage can be formed by single tracks of highly energetic ionizing radiation, in a single nucleus, in a single cell.[37] Unrepaired or misrepaired damages to genes that control growth and proliferation will primarily result in cell death.[20] This destructive and distinctive characteristic of ionizing radiation is utilized in radiation therapy to damage cancer cells.[51] Electron treatment is one implementation of ionizing radiation for the treatment of certain cancers.

This chapter will discuss, the theory and background behind electron beam treatment. It will mainly follow the journey of electrons in cancer treatment starting from their production in a linear accelerator, to how they interact on a subatomic level, to how they deposit their energy in the medium, and ending with the tissues they are going to encounter as they attack cancer.

2.1 Electron Beam Production

The two types of external beam ionizing radiation used in cancer treatment are: 1) photon beams (x-rays and gamma rays), 2) particle beams (electrons, neutrons, protons, and other heavy charged particles). [18,25] Because these beam types behave differently in terms of penetration depth and energy deposition (*figure 1*), they are used to treat different cancer types based on the tumor location.[4,25] Electrons have very interesting dosimetric properties in which they deposit most of

their energy early in their tracks compared to other charged particles, and have a sharp dose fall-off compared to photons, thus they do not penetrate deep into the body.[27] Therefore, electron beam is mainly used to treat skin cancers and cancers that are close to the surface of the body while sparring deep critical structures.[18]

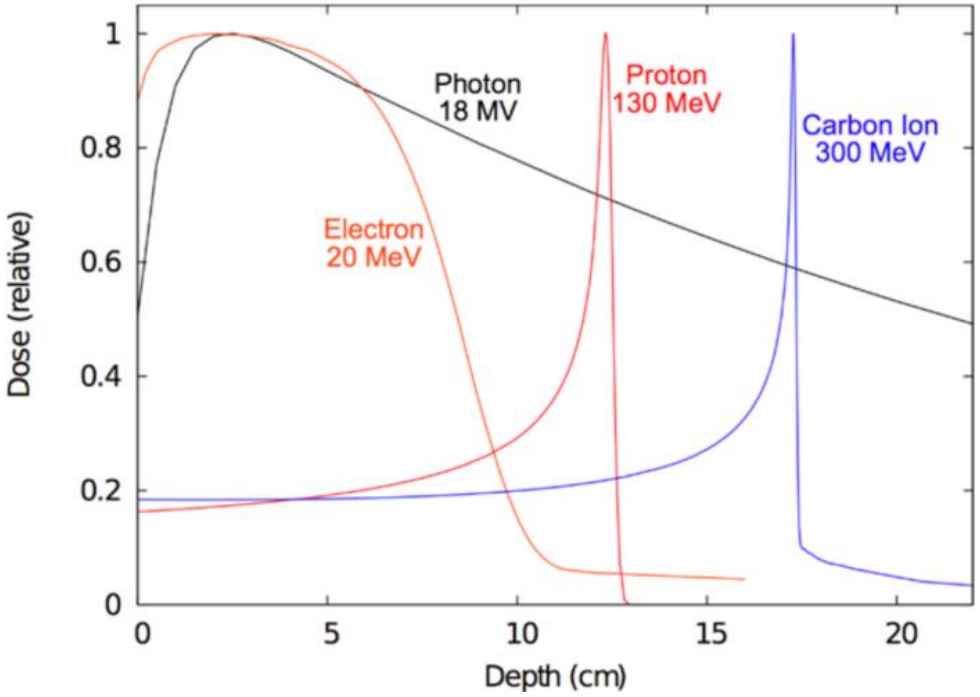

Figure 2.1. Depth dose distribution of different ionization radiation.[27]

Both clinical electron beams and clinical photon beams are generated by linear accelerators.[5,18,39] The birthplace of electrons occurs in the cathode of an electron gun.[5,18] The cathode is made of a filament and a focusing cup.[5,25] When a high filament current is applied, electrons are provided with enough energy to overcome their binding energy (thermionic emission), the focusing cup then focuses the electrons into a beam-shape aimed at the anode.[5,39] The accelerated electrons are then injected into the accelerating waveguide.[18] The temperature of the filament controls the number of electrons injected into the waveguide.[18,25] Radiofrequency microwaves are pulsed into the waveguide by either a klystron or a magnetron, this is synchronized

with the injection of electrons into the waveguide by the electron gun.[25,39] The electrons are then accelerated along the vacuum waveguide by the microwaves passing through a series of small copper holes to focus the beam.[39] A klystron or a magnetron controls the power and the frequency of the microwaves which, along with length of waveguide, determines the energy of the electrons.[18]

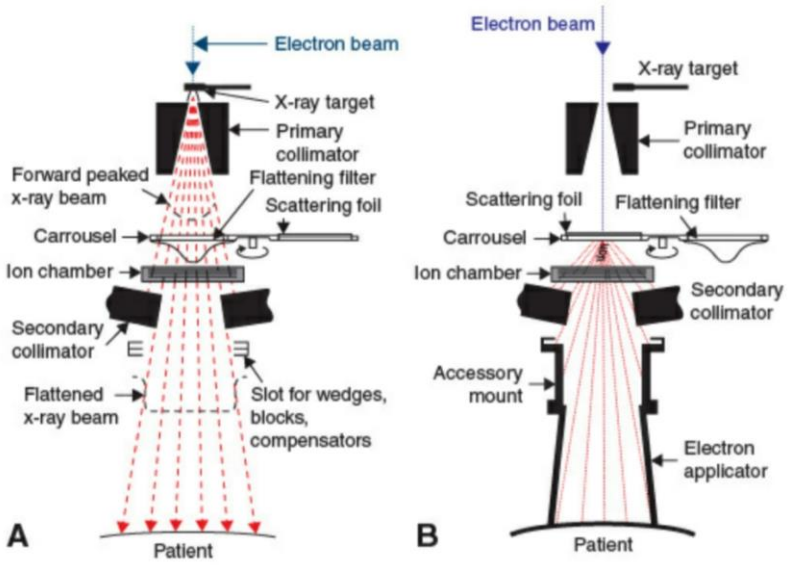

Figure 2.2. A. Photon Beam vs B. Electron beam production.[18]

Two sets of magnets called the steering coils and the focusing coils are used to tighten the energy of the beam and define the electron beam to have a very fine pinhead diameter.[18,39] The beam exits the waveguide and enters the flight tube where it is bent, steered, converged and further focused.[18,39] Unlike photon beams, electron beam does not need a tungsten target or a flattening filter, it does instead require scattering foils and an applicator as shown in figure 2.[18] Scattering foils are thin layers of a high atomic number material that scatter and spread the pencil beam to a wide uniform beam.[5,18] Ideally the scattering foil system consists of two foils; the primary is uniform in thickness while the secondary is thicker in the middle to help flattening the primary foil's electron spread.[18,25,39] Every energy should be matched to its scattering foil to create a useful

beam. This is essential to get the desired scattering of electrons.[25,39] The beam then passes through transmission ionization chambers which are two separate ionization chambers with independent power supplies.[18,39] They are used to monitor the dose of the beam in that their output is cross calibrated with the dose delivered in a standardized setup such that one monitor unit (MU) corresponds to a dose to a point in the standardized setup. All other situations are normalized to the standard setup to allow the amount of MU's needed to deliver a set dose in that particular situation.[39]

Electrons are easily scattered by the ionization chambers, scattering foils and air. The secondary collimator is used to collimate the beam not to cause an additional lateral scattering which would increase the geometric penumbra at the target surface.[39] An electron applicator, which has several open collimators, is used to additionally collimate the beam down to the target and attenuate lateral scatter which would reduce the penumbra.[18] It is attached to the linear accelerator's head, and comes in several sizes. The size of the applicator opening should be smaller than the collimator jaws field size.[18,39] An electron patient specific collimator known as a cutout (made of lead or Cerrobend) could be attached to the applicator's most distal aperture to shape the field. Having the cutout positioned at the end of the applicator helps prevent lateral scatter that would cause smearing of the beam edge.[18,39]

2.2 Electron Interactions

Electrons could pass through an atom without any interactions. However, when they do interact, they interact with either the nucleus of an atom or its orbital electrons.[25,39] Since electrons have a negative charge, they interact by Coulomb interactions.[25] As electrons travel through a medium, there are four possible ways of interaction: a) elastic collision with the nucleus, b) elastic collision with an orbital electron, c) inelastic collision with atomic electrons, d) inelastic collisions

with the nucleus.[25] Elastic collisions cause scattering (e.g. backscattering) of the incident electron without lose or transfer of kinetic energy, hence, no energy or dose is deposited in a tissue.[25] Nevertheless, these two interactions are important in attenuating the beam which results in altering the dose distribution specially between tissues with different atomic numbers.[25,39] Inelastic collisions result in loss of kinetic energy of the incident electron, resulting in energy deposition in a tissue.[25] Inelastic collision between electrons causes either an excitation (movement of an electron to a higher energy level) or an ionization (removal of an electron from an atom).[25] In excitation, as the excited atom deexcites visible light could be produced. While in ionization, the removed electron (secondary electron) results in additional ionizations as it loses its energy in the medium.[5,39] On the other hand, inelastic collisions with the nucleus results in a photons spectrum of energy known as bremsstrahlung due to the braking and the change of direction of electrons as they interact with the nucleus.[5,39] This causes electron beams to have a photon bremsstrahlung tail that deposit negligible energy into the medium (*figure 2.1*).[18] All of these interactions typically occur at different depth in the medium which can be seen in *figure 2.3* that shows electron pear-shaped interaction volume at depths of ~ *2-5μm*.[59] Heat is also generated but causes no harm to the surrounding tissues.[4,6]

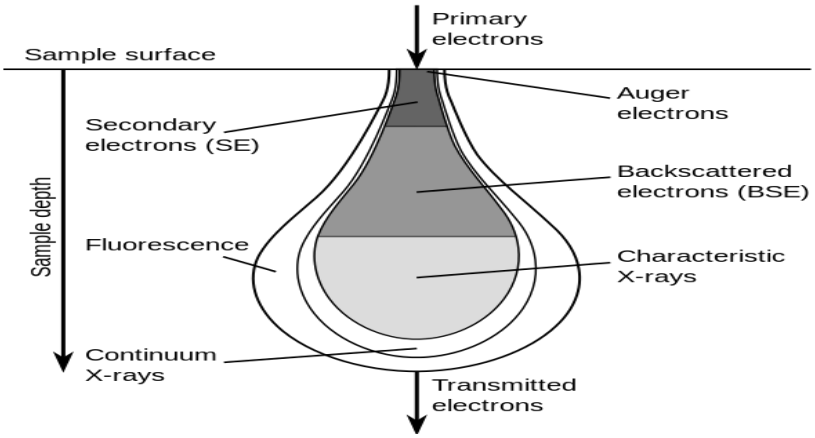

Figure 2.3. Electron interaction volume vs sample depth.[59]

Before electrons exit a linear accelerator, they are practically monoenergetic.[18,25] Once they exit the linear accelerator and interact with its window and the scattering foils, they start depositing energy.[18,39] As they hit the medium, electrons continue losing several eV of energy in numerous number of interactions as they move in a tortuous track until they deposit all of their energy before coming to a stop at the practical range.[18] It refers to the maximum depth that some of these electrons achieve before being absorbed.[18,39] The practical range in cm is roughly estimated as $0.5E_0(MeV)$.[18] Beyond that point, the only dose being deposited in the tissue is from bremsstrahlung tail.[18] Bremsstrahlung radiation increases as the energy of the electron beam and the atomic number of the material increase.[18,25] In water, which represents the majority of the human body, electrons with energies of *1 MeV* and higher have an energy loss rate of ~ *2 MeV/cm*.[18] Thus, as tissue depth increases the average energy of the electron beam decreases linearly.[18] And as the energy of the electron beam decreases scattering becomes more evident particularly with mediums of higher atomic numbers.[18,25]

2.3 Electron Beam Isodose Curves

The dose distribution profile and dose rate of electron beam in a water is primarily dependent on energy of the incident beam, the applicator size, the cutout size, and the source-to-surface distance or SSD.[18,25] For an unchanged field size and SSD, as energy increases, high-value isodose curves get closer to the surface and cover larger areas but are constricted laterally as they move deeper into the medium, while low-value isodose curves expand outwardly with depths due to range straggling (range variations between different electrons due to requiring different number of collisions to completely stop them) (*figure 2.4.*).[59] Also, as the energy increases, there is a rapid dose fall-off laterally with decreasing depths, making the isodose curves close to each other at

shallow depths (< *1 cm*) for higher energy beams and slightly more spread for lower energy beams at the same depth. [18,25,59]

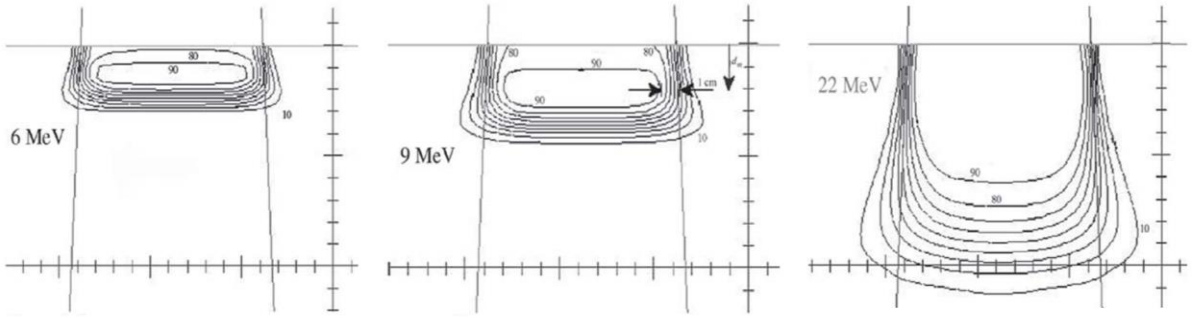

Figure 2.4. Electron beam isodoses in water for 3 different energies while all other variables the same.[59]

Although not advised due to resulting in a significantly lower output, at an extended SSD (*figure 2.5: C & D*), high-value isodose curves get closer to the surface for lower energies but deeper into the medium for higher energies.[29] Isodose curves also get farther away from each other indicating a slower dose fall off and a more dose spread.[29] On the other hand, the effects of having a large field size on isodose curves is clear. As field size increases, the treatment area gets larger, thus the larger the isodose curves get laterally and with depth.[18]

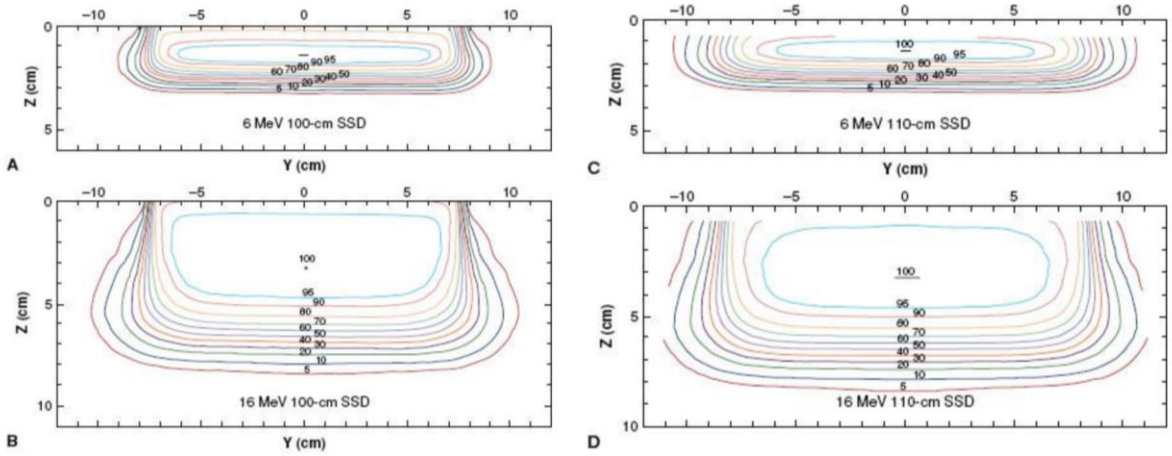

Figure 2.5. Variation of dose distribution with energy and SSD in water.[29]

2.4 Electron Beam Percentage Depth Dose (*PDD*)

Figure 2.6 shows electron percent depth dose (*PDD*) distribution in water for *6, 8,9,12,15* and *18 MeV* electrons vs a *4 MV* photon. The first thing to notice is that electrons have much less skin sparing and much shorter range compared to photons. Skin sparing decreases as the energy of electrons increases making the shape of *PDD* broader plateau at depth of maximum dose with a higher relative surface dose.[18] This is because electrons with higher energy have a slow and a long dose build-up region since they are more forward-scattered with less lateral scatter and do not recoil at relatively larger angles like lower energy electrons. [5,18,25,39] The wide scatter of lower energy electrons results in a sheer dose buildup near the entrance.[18] Roughly speaking, the percent depth dose at the surface for electrons is *75%* at *6 MeV*, *80%* at *9 MeV*, *85%* at *12 MeV*, *90%* at *16 MeV*, and *95%* at *20 MeV*. While the depths in *cm* of the *90%* and *80%* isodose curves are estimated as $E_0(MeV)/3.3$ and $E_0(MeV)/3.0$ respectively.[18,25] These values are of clinical significance since physicians typically want the tumor to be engulfed by the *80%* or *90%* isodose curves because the dose decreases severely beyond the *90%* isodose curve.[18]

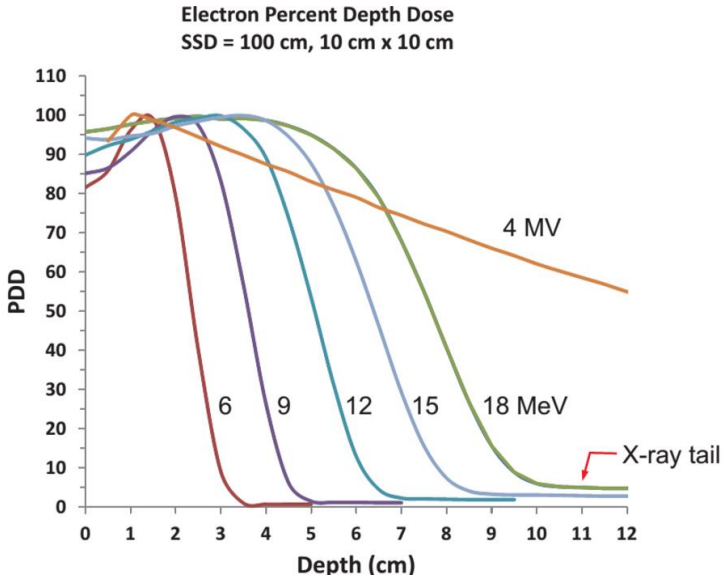

Figure 2.6. Electron beam percent depth dose (PDD) distribution in water for multiple energies vs a 4 MV photon.[18]

Electrons with higher energies penetrate deeper into the medium because they have higher energies to spend (*Figure 2.6).*[18] The depth of the maximum dose also increases with increasing energies until reaching energies above ~ *15 MeV,* as follows: *1.3 cm* for *6 MeV, 2.2 cm* for *8 MeV, 2.8 cm* for *12 MeV, 3.4 cm* for *15 MeV, 1.8 cm* for *18 MeV.*[25] Typical electron beam depth dose parameters for different energies in given in *figure 2.7.*[25] It is also worth mentioning that the bremsstrahlung tail increases in amplitude as the energy of the electron beam increases (*Figure 2.6).*[18] Though, even for electrons with energies of *20 MeV,* the bremsstrahlung tail is less than *5%,* which is of no clinical implications in the majority of cases.[18] These features make electron beam superior to photons in treating superficial tumors typically at depths of around *5 cm.*[42]

Energy (MeV)	R_{90} (cm)	R_{80} (cm)	R_{50} (cm)	R_p (cm)	$\bar{E}(0)$ (MeV)	Surface dose %
6	1.7	1.8	2.2	2.9	5.6	81
8	2.4	2.6	3.0	4.0	7.2	83
10	3.1	3.3	3.9	4.8	9.2	86
12	3.7	4.1	4.8	6.0	11.3	90
15	4.7	5.2	6.1	7.5	14.0	92
18	5.5	5.9	7.3	9.1	17.4	96

Figure 2.7. Electron beam depth dose parameters.[25]

Figure 2.8. shows electron beam PDD in water for different field sizes of the same beam energy. For a decreasing field size, PDD depends on the size of the cutout until it becomes larger than $1.77\bar{E}_{P,0}\,(MeV)^{0.5}$, in other words, until when the distance from the point of interest (central axis) to the field edge is larger in *cm* than $R_{eq} = 0.88\bar{E}_{P,0}\,(MeV)^{0.5}$ (where $E_{P,0}$ is the most probable energy on the surface and differs slightly from the average energy).[18,25] Fields sizes smaller than R_{eq} are called small field sizes, while field sizes equal to or larger than R_{eq} are considered large.[18,25]

Fields smaller than the practical range (of that electron beam energy) have quick dose build-up and a slow dose fall-off, causing less skin sparing, a decrease in the maximum dose and its depth, eventually leading to a lower dose rate.[18] This is because of the decrease of number of electrons scattering into the volume of interest while the scattering out electrons remains the same causing a loss of lateral scatter equilibrium. [18,25]Thus, small fields require individual calibrations to better evaluate their PDDs in tissues. Note that his also happens at the edges of large fields.[18]

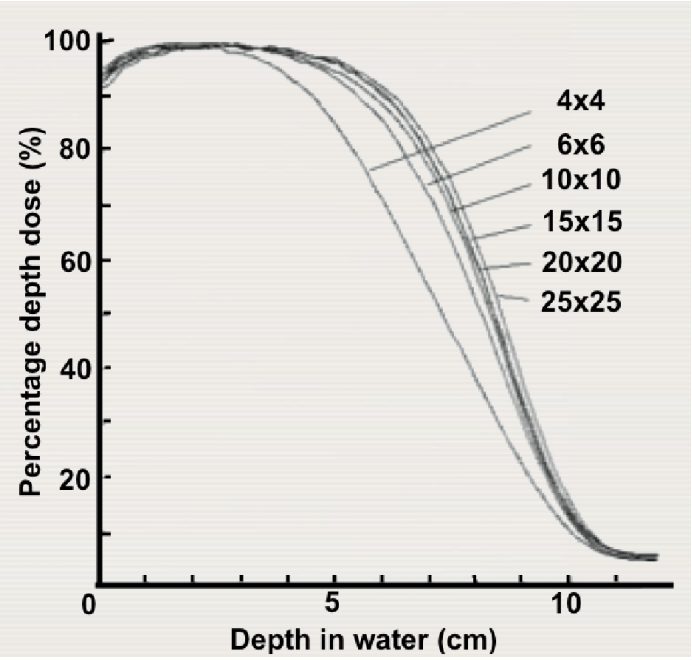

Figure 2.8. Electron beam (PDD) in water for multiple field sizes.[25]

In cases where the applicator or the field size is larger than $10 \times 10\ cm^2$ and electron beam energy of *20 MeV* and lower, or for cutouts larger than $E_P(MeV)^{0.5}$, *PDD* on the central axis remains unchanged and the size and shape of the cutout has very minimal effects on the dose rate.[18,25] This is because of the short range of these electrons which will prevent them from reaching the central axis keeping the number of electrons entering and leaving that region of interest the same, this is called lateral scatter equilibrium (LSE). [5,6]

Typical normalization conditions for electron beam are *SSD = 100 cm, 10 x 10 cm*^{2} applicator and cutout, where the dose rate is set to deliver *1.0 cGy/MU* at depth of maximum dose.[5,18,25,39] Thus, if the applicator was not a *10 x 10 cm*^{2} the relative dose rate has to be calculated by taking into account electron output factor.[18,39] Small cutouts will result in a noteworthy change to the dose rate and dose profile.[18,39] For irregular shaped cutouts the output factor could be measured by estimating an equivalent rectangular *L x W*, then using the geometric mean of the square root of the products of the output factors for *L x L and W x W*.[39] This method could also be used to calculate the depth dose of an irregularly shaped field.[39]

2.5 Skin Cancer and Electron Treatment

Cancer is a disease that involves an abnormal cell division without control and has the potential to invade or spread to other parts of the body.[44] An accumulation of gene mutations, particularly in genes that control proliferation, apoptosis, immortalization, and genetic stability, is thought to cause tumor initiation.[20,21] Most cancers are grouped into one of three groups: carcinomas (malignancies of epithelial cells; most common ~ 90%), sarcomas (rare; solid tumors of connective tissues, such as muscle, bone, fat and cartilage), and leukemias (blood-forming cells) or lymphomas (immune system cells).[13]

It is proposed by Dr. Robert A. Weinberg of the MIT that if humans live long enough everyone will eventually develop cancer.[26] The current human lifetime, from birth to death, risk in the United States of developing cancer is about *40%* or *2* in *5*, and the risk of dying from it is about *21%* or *1* in *5*.[47] Of all cancer types, skin cancer is the most common type of cancer in the United States and its incidence numbers are on the rise. It is estimated that 1 in 5 Americans will develop a skin cancer in their lifetime.[49] Ultraviolet light exposure is the leading cause of skin cancer.[60] Nonmelanomas (basal cell carcinoma and squamous cell carcinoma) and melanoma (noninvasive

and invasive) represent the vast majority of all skin cancer incidences. Surviving rates for nonmelanomas are very high if properly treated, while most skin cancer mortalities are from melanomas.[50]

Surgery, radiation therapy, chemotherapy, photodynamic therapy and biological therapy are used to treat skin cancer. [8,52] Many factors play a role in which treatment to select, such as: cosmetic reasons, tumor location and type, cost, patient's age, medical condition, and availability of treatment.[8,52] As described in previous sections, electron beam dosimetric properties make it an ideal candidate for treatment of superficial cancers. Typically utilized for regional skin cancers in the body or head and neck, total skin Mycosis Fungoides treatment (a rare cutaneous T-cell lymphoma), and in intraoperative therapy for multiple solid tumor locations.[1,6,50,52]

Treatment generally employs a single electron field at an SSD of 100 cm.[25] Beam energy is selected based on the target volume depth, the dose required to be delivered to the target and the acceptable dose to be delivered to critical organs in proximity of the tumor. [8,52] In most treatments, it is desired to have the target volume completely within the 80-95% isodose curves.[25] Field sizes are chosen accordingly. By taking advantage of the rapid dose fall-off beyond the 80% isodose curve, dose to healthy tissue is minimized and dose to the target volume is optimized.[18] Though, in these cases, cautious should be taken not to exceed the prescribed dose to healthy skin tissues which is not spared in electron beam treatments.[18,25]

3. LITERATURE REVIEW

In spite of all the precautions and rigorous planning to spare healthy tissues, electron beam *PDD* and isodose curves are not uniform across the treatment region. Albeit unrealistic, it is sought to have the tumor completely engulfed by at least the 90% isodose curves while healthy tissues are fully spared (*figure 3.1.*). Patients would absolutely benefit from having a uniform treatment of large and small skin lesions since more healthy tissues could be spared. Though, this is difficult to accomplish especially for small size electron fields because of their unpredictable behavior.[3,17,18]

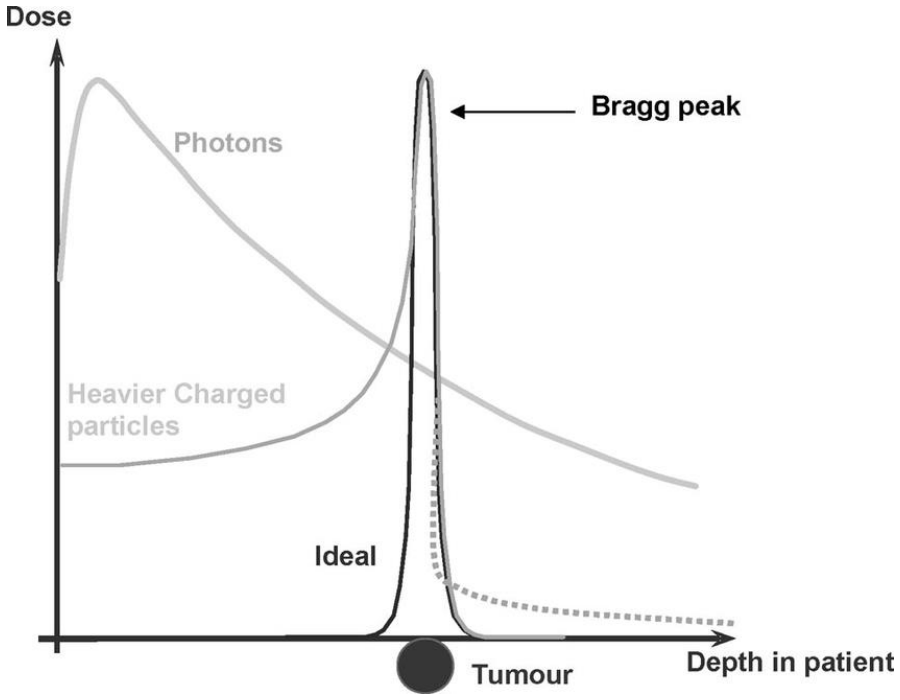

Figure 3.1. Ideal Bragg Peak completely spares healthy tissues while depositing all the dose in the target volume.[62]

The first section of this chapter will discuss current methods used to shape electron beam isodose curves and *PDDs*. The chapter is ending with a section about what research needs to be conducted. The main sources of material were the American Association of Physicists in Medicine (*AAPM*) Wiley online library of medical physics and *PubMed* service of the US National Library of Medicine which comprises more than 27 million citations for biomedical literature.

3.1 Current Techniques to Manipulate Electron Beams

As mentioned in *Chapter 2*, the *PDD* on the central axis in water changes with the beam energy, the field size and *SSD*. These factors are easy to adjust based on the desired dose rate to be delivered. However, due to scatter and the way electrons behave in matter, entirely sparing healthy tissue becomes a real challenge with many factors to consider.

3.1.1. Body Inhomogeneity

The human body is made of tissues of different densities and attenuation properties (bone, lung, water…etc.), making it inhomogeneous. Tissue inhomogeneity does affect the *PDD* and the prescribed dose when using electron beam therapy.[18] For example, in materials with low density such as lungs, electrons have longer range causing isodose curves to spread out tremendously both laterally and with depth, making *PDD* on the central axis more penetrable (*figures 3.2.*).[25] This means that not all of the electron's energy is absorbed in the vicinity of the target, thus delivering less dose than prescribed unless corrected for.[25] Differences in homogeneity is corrected for by knowing the density, electron density and thickness of the materials involved.[18,25]

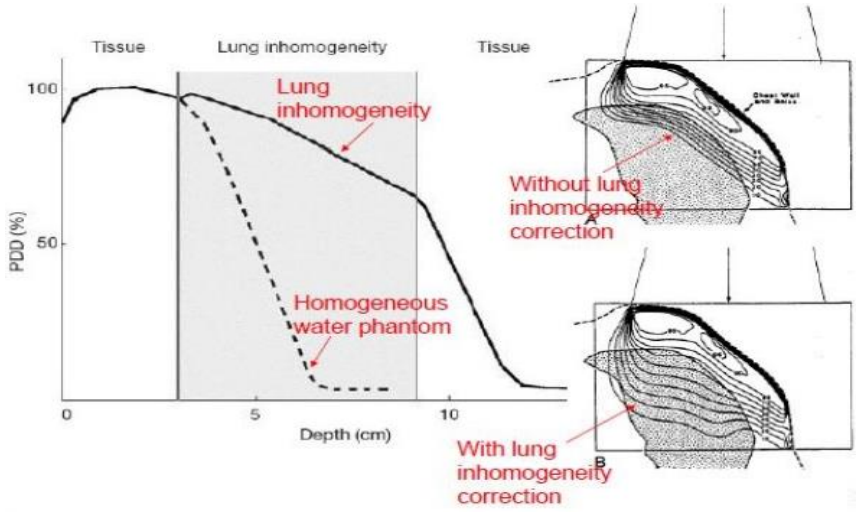

Figure 3.2. Effect of lung inhomogeneity on the PDD distribution and isodose curves of an electron beam (energy: 15 MeV, field: 10×10 cm^2).[25]

On the other hand, a high-density material such as bone or lead (used as a shield superficially on the patient or internally) increases backscatter and attenuation, which could cause hot/cold spots and shifting the isodose curves (*figures 3.3.*).[25,57] Materials with lower density receive a higher dose at the interface with materials of higher density because of the increased scattering of electrons.[25] This concept is important to comprehend for cases of internal shielding and at the interfaces of different density tissues. In these cases, where vital organs are very close to the target volume, an internal shield of a high atomic number material (e.g. Cerrobend) in combination with a material of low atomic number (e.g. Aluminum) is used to reduce dose to healthy tissues.[18,25]

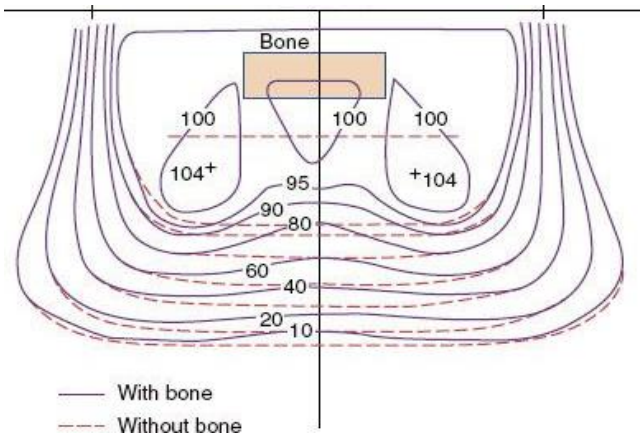

Figure 3.3. Effect of body inhomogeneity on the isodose curves of an electron beam.[29]

3.1.2. Bolus

Surface irregularities should be considered for electron therapy treatments as it could result in a considerable change in isodose curves and the delivered dose (*figure 3.4.*).[25] Therefore, for an irregular surface, a custom-made bolus made of a tissue equivalent material (e.g. wax) of variable or a uniform thickness could be used to level out the surface irregularities for a more uniform treatment.[18] Bolus is also used to increase entrance dose (surface dose) and decreases the range of electron beam, thus sparing distal tissues.[25,48] In *figure 3.5.*, a bolus is used to conform

the isodose curves to the tumor shape. Air gaps between the bolus and the surface of the patient, displacement of bolus, improper pick of bolus thickness, could all lead to errors in the delivered dose.[18,25]

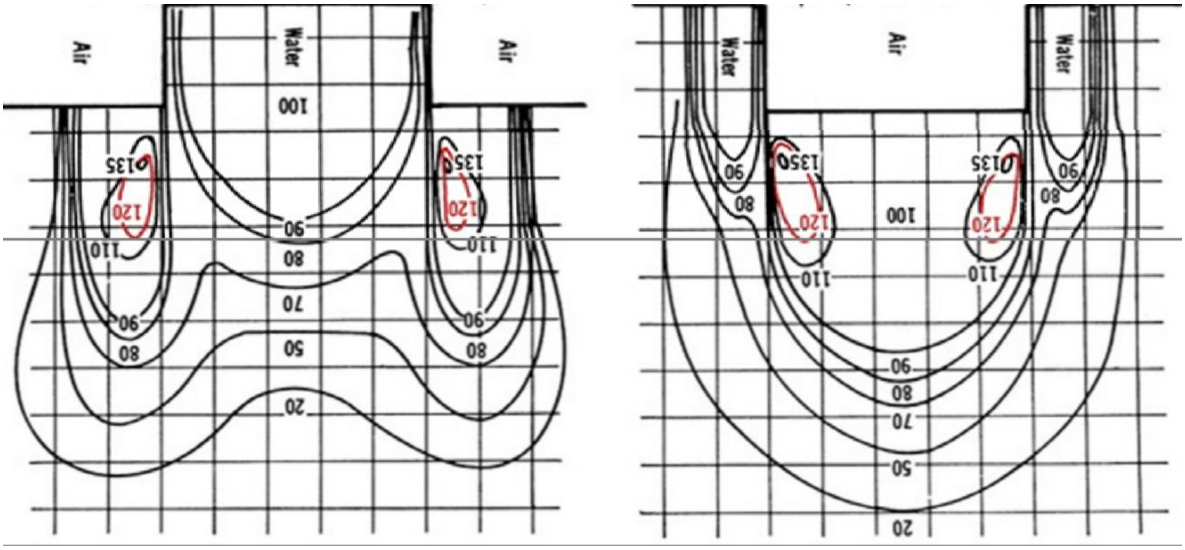

Figure 3.4. Effect of surface contour on the isodose curves of an electron beam (energy: 17 MeV, field: 10×10 cm^2).[25]

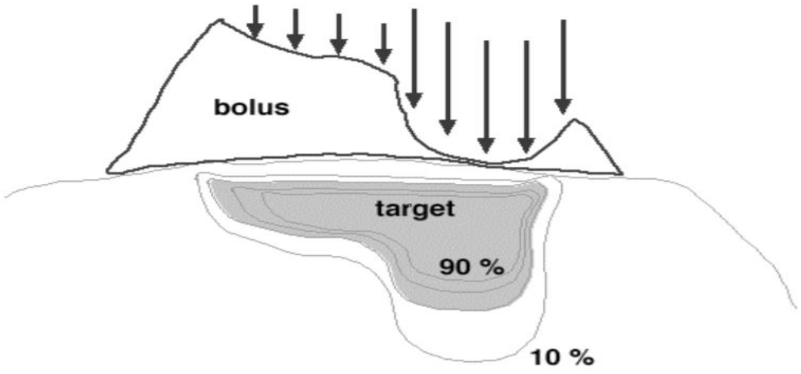

Figure 3.5. The effect of using a bolus on the isodose curves of an electron beam.[25]

3.1.3. Conformal Electron Therapy

Other techniques that could be utilized to improve electron beam treatment are energy and/or intensity modulated electron beam therapy.[22] These are electron conformal therapy that use

a single or multiple electron beam with the goal of delivering a homogeneous dose distribution to the PTV by having the *90%* isodose line encompassing the PTV while minimizing dose to critical tissues.[22,23,24,36] Intensity modulation optimizes electron fields beamlets energy, weight and intensity patterns using multi-leaf collimator or multiple field cutouts.[22] This technique typically has lower skin dose but larger MU, longer treatment times, and increased deep tissue doses.[23]

On the other hand, energy modulation could be continuous using bolus filtration or discrete using multiple energy beams.[22,23] In Bolus Electron Conformal Therapy (Bolus ECT), a customized bolus of different thickness is utilized with one electron beam to conform the *90%* isodose curve to contain the PTV which increases skin dose, minimizes dose to normal tissues and improves PTV dose homogeneity.[24] The Bolus ECT is designed by a bolus generating software based on the treatment planning system plan. It is then sent electronically to the manufacturer to be manufactured, and finally, is sent to the facility for usage.[24] In Segmented-Field Electron Conformal Therapy multiple electron fields of energy and weight are used to have the distal surface of the PTV within the *90%* isodose line.[23] Although this technique has lower skin dose, it does have larger MU, longer treatment times, and dose inhomogeneity from abutting fields. [23,24,36]

3.1.4. Beam Obliquity

Beam obliquity has a huge effect on electron beam isodose curves. *Figure 3.6.* shows an example of a *20 MeV* beam incident normally and obliquely on a surface. Notice that the maximum dose increases to *115%* for the oblique incidence with a more laterally spread out isodose lines compared to the bulging out of isodose lines with depth in the normal incidence beam.[14] Obliquity also changes *PDD* due to the increased electron fluence which adds dose of some high scatter angle electrons to the central axis (*figure 3.7.*).[18,25] Increasing the angle of obliquity increases the dose at the surface, increases the maximum dose and shifts its depth closer to the surface, decreases

the depth penetration, increases the practical range, and increases the bremsstrahlung tail.[14,18,25] It is also important to point out that oblique beams have nonuniform isodose curves across the target volume.[14,53]

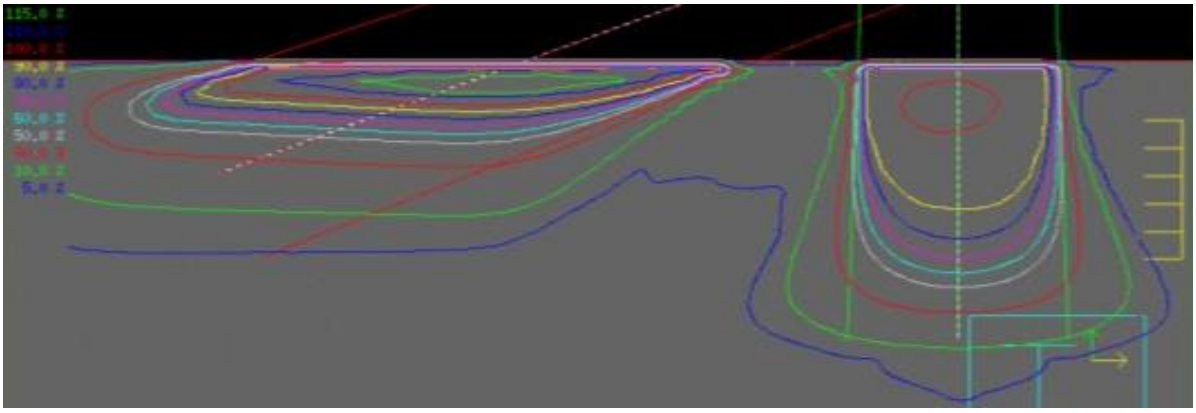

Figure 3.6. Electron beam isodoses for a 20 MeV beam oblique beam vs a normal beam.[14]

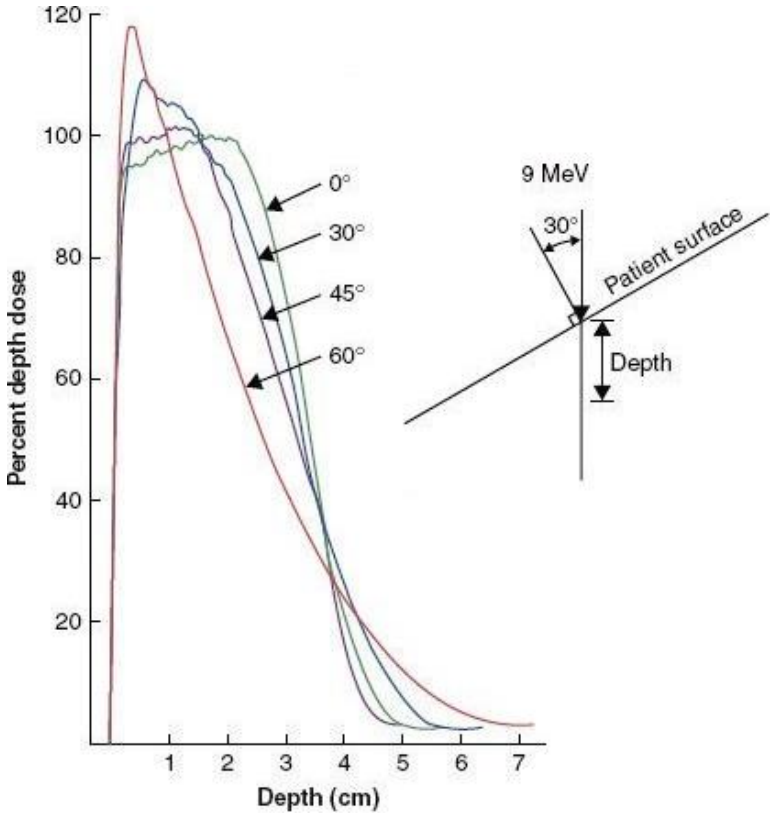

Figure 3.7. Electron beam percent depth dose (*PDD*) distribution in water for a 9 MeV beam for multiple angles.[29]

3.1.5. Air Gap

Another factor to consider that changes a *PDD* profile is the air gap between the patient and the cutout. This air gap is usually set at *5 cm*.[18] An air gap value of more than *5 cm*, would diverge low-value isodose lines and converge high-value isodose curves; hence it would increase the penumbra (*figure 3.8.*).[28]

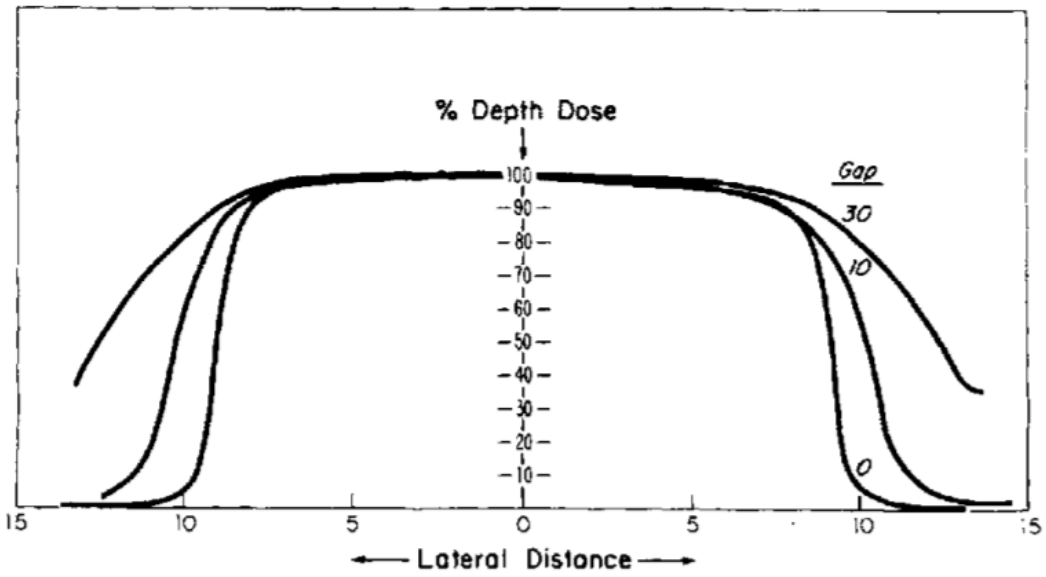

Figure 3.8. An example of electron beam lateral dose distribution profile at the depth of maximum dose vs air gaps in *cm*.[28]

3.1.6. Abutting Fields

Under some certain circumstances (e.g. very large tumors) and for certain tumor types electron/electron or electron/photon field matching could be used.[39] Typically, using abutting electron fields (fields that are not irradiating a common volume) causes hot and cold spots due to big penumbra and the inflamed isodose curves.[39] *Figure 3.9.* shows isodose lines of an abutment between two *19 MeV* electron fields of different sizes with three different gap sizes between the two fields. An overlap/underlap is inevitable which causes hot and cold spots.[25] Therefore, to avoid

cold spots, electron fields are abutted at the surface. The overlap at depth results in an increase in hot-spot doses and a decrease in cold-spot doses as the gap between the adjacent fields decreases.[25]

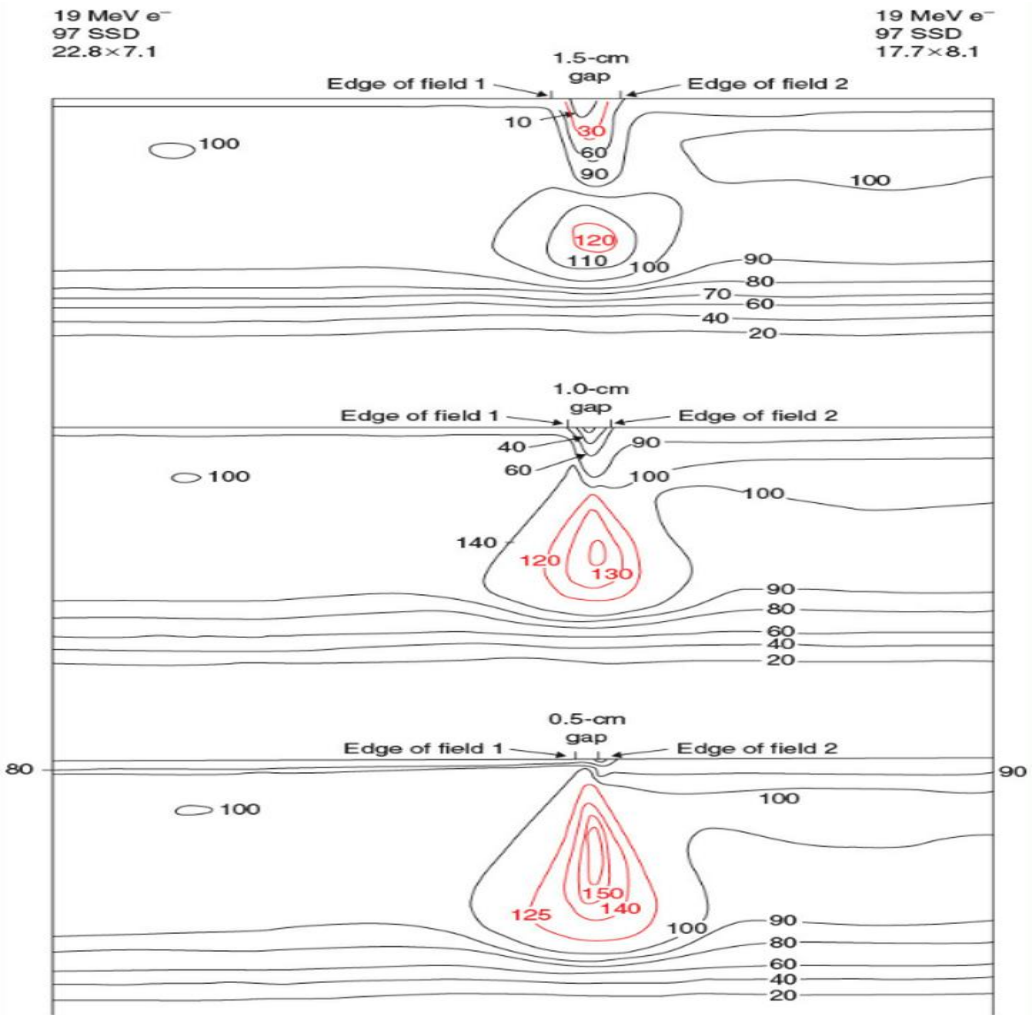

Figure 3.9. Electron/electron beam abutting: **A:** Electron beam at standard SSD of 100 cm. **B:** Electron beam at extended SSD of 120 cm.[25]

Figure 3.10. on the other hand, is an example of abutting a photon field with an electron field, **A** with a an SSD of a *100 cm* and **B** with an SSD of a *120 cm*. The extended SSD causes a larger hotspot on the photon side of the field.[25] Another use of a combination of electron/photon fields is the mixing of intensity modulated electron and photon beams (*figure 3.11.*) This technique results in a sharp dose fall-off and sharp penumbras with depth, and an increase in skin dose.[31]

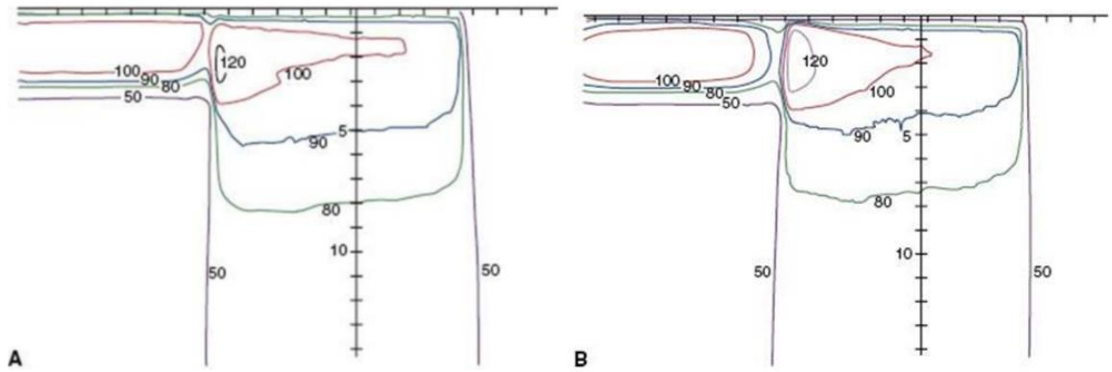

Figure 3.10. Electron/photon beam abutting: **A:** Electron beam at standard SSD of 100 cm. **B:** Electron beam at extended SSD of 120 cm.[25]

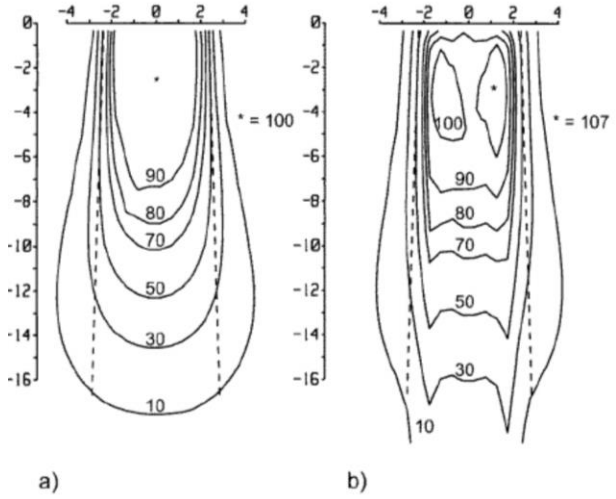

Figure 3.11. Isodose plots of a flat, *40 MeV* electron beam (a), and a *40 MeV/25 MV* mixed beam with an on-axis mix ratio of *0.8/0.2*. Dose values are percentages of the corresponding central axis maximum doses. The field size is approximately $5 \times 5\ cm^2$ at a source to surface distance of *87.5 cm*. The broken lines correspond to the field widths.[31]

3.1.7. Electron Arc Therapy

Electron arc therapy is a technique used to treat curved superficial (usually large) tumors by using an arc of electron beams.[25] *PDD* shape in this complicated technique depends on: beam energy, *w*: the width of the field, d_i: isocenter depth, *f*: the distance from source to axis, surface curvatures, the third level collimation, and the secondary collimator defined field shape (*figure 3.12.*).[25] Where β is the characteristic angle (represents a continuous rotation in which a point at

the surface receives a portion of dose from the beam at every angle) and is a function of *w*, d_i, and *f* (*figure 3.13*).[25] β is determined based on the sought *PDD* profile. In this treatment, photon dose from bremsstrahlung is of concern at the isocenter because of the collective contribution from all beams, and it is inversely proportional to β.[25]

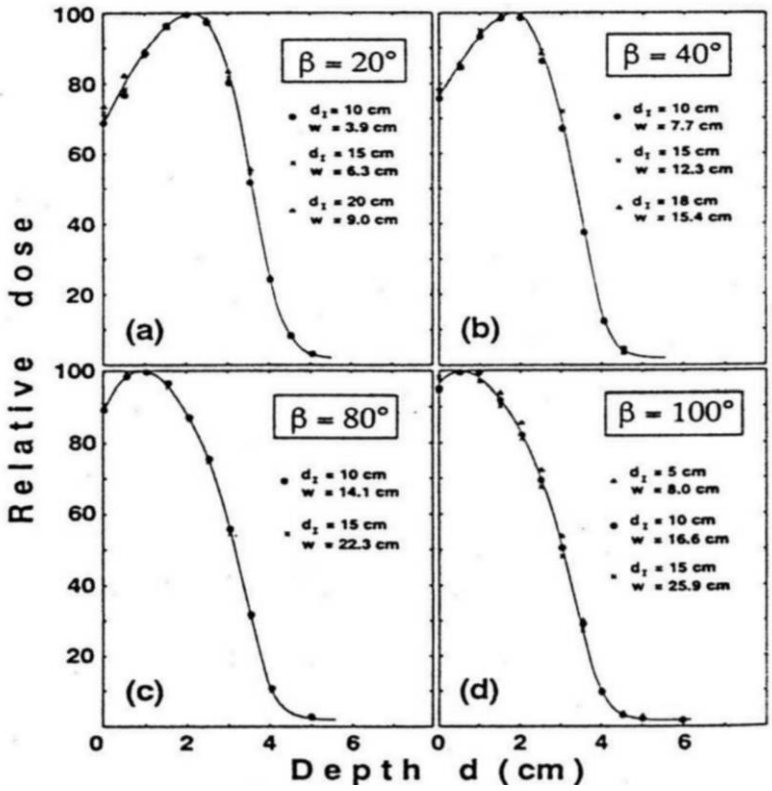

Figure 3.12. PDD for electron arc therapy as a function of β for several combinations of *w* and *di*.[25]

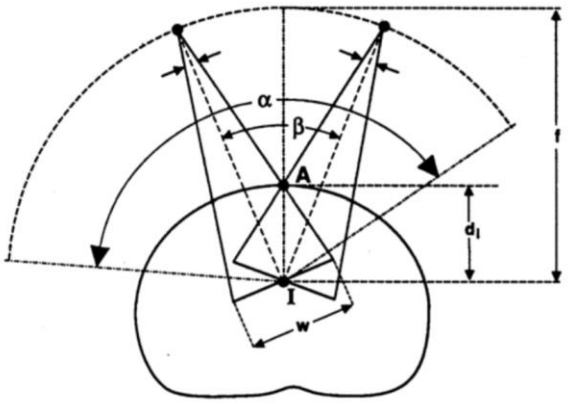

Figure 3.13. Electron arc therapy geometry, α is the angle of the arc treatment.[25]

3.1.8. Very High Energy Electrons Beam

New innovative techniques that uses electron beams to treat cancer has also been emerging. One unique example is the use of very high energy electron beam to treat deep tumors (*figure 3.14.*). This method uses magnetic lens to focus electron beams of *50-2000 MeV,* that can be shaped to the tumor volume or scanned to several volumetric elements of the tumor (*figure 3.15.*).[30] Monte Carlo simulations in water phantom have shown that these focused beams have the advantage of delivering very small entrance and exit doses, and less dose to normal tissues compared to using collimated electron beams with the same energies (*figure 3.14.*).[30] This happens because the strength of the magnetic fields in the phantom enables the concentration of dose into the target volume by decreasing lateral scatter.[30]

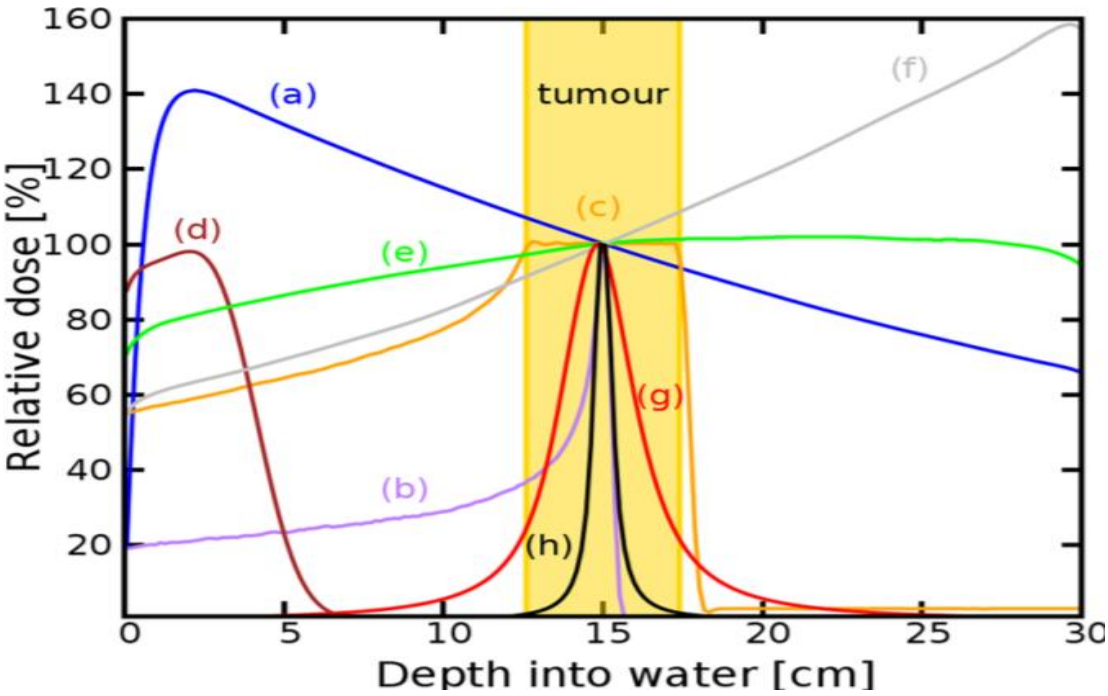

Figure 3.14. PDD curves in a water phantom for: (a) 6 MV Photons, (b) Bragg peak 147MeV protons, (c) spread-out Bragg peak, (d) 10 MeV electrons, (e) collimated 200 MeV electrons, (f) collimated 2GeV electrons, (g) 200MeV electrons focused at 15 cm, (h) 2GeV electrons focused at 15 cm. Curves are normalized to the dose at 15 cm except for the 10 MeV electron beam, which is normalized to its peak dose.[30]

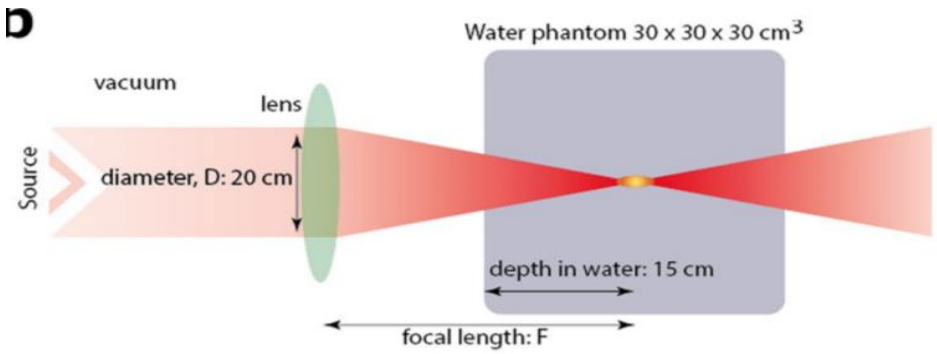

Figure 3.15. Electron beam focused into a water phantom by an ideal magnetic lens.[30]

3.1.9. Skin Collimator

In a more simplistic manner, a field-defining skin collimator (made of lead or Cerrobend) can be used in small field electron treatments to have a more clinically useful dose distribution by reducing penumbra and protecting critical structures (*figure 3.16.*).[18,25] The skin collimator inner edge conforms the border of the radiation field used for treatment, while the outer edge must be wide enough to stop the penumbra and scattered electrons formed by the larger field size of the applicator.[29] Skin collimators should be in direct contact with the skin for the sharpest penumbra (*figure 3.16.*).[11,35] However, as air gap between the skin collimator and the surface decreases, skin surface dose increases and the transmitted dose from bremsstrahlung photons increases and it is higher than that without the use of skin collimator.[29] Even though, the depth dose is defined by the skin collimator size, the dose output is approximated by the size of the cutout.[18]

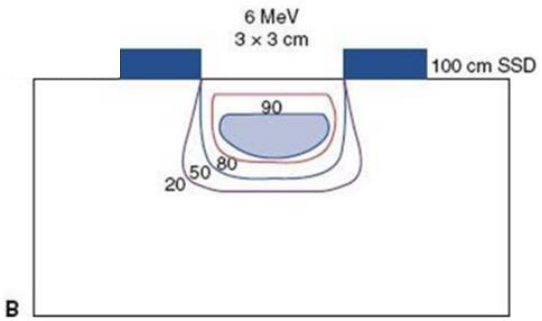

Figure 3.16. Isodose curves of skin collimation in water for small electron fields formed by a collimation at the surface with a *6x6 cm*^{2} applicator insert *10 cm* above the patient.[29]

3.1.9.1 Beveled Skin Collimator Edges

An experiment conducted last year at OHSU by Harrison Ludewig as part of his Master's thesis studied the feasibility of Cerrobend skin collimators with beveled top edges of several different angles for small fields of a *2 cm* circular diameter.[33] The dose distributions for the different Cerrobend angles showed an increase in the maximum dose in the field when compared to the standard *0*^{o} skin collimator currently in use for small electron fields.[33] It is concluded that larger angled beveled edges resulted in decreasing the clinically useful 90% isodose line.[33]

3.1.9.2 Skin Collimator Interactions

Cutouts and skin collimators used to shape the field and protect normal tissues are usually made of lead or Cerrobend, a.k.a. Lipowitz metal (an alloy made, by weight, of 50% bismuth, 27% lead, 13% cadmium, and 10% tin).[33,43] These materials are widely used due to their high Z number, inexpensive value, availability and practicality. Electron's collisional and radiative losses differ in water vs in high Z materials (e.g. lead or Cerrobend) (*figure 3.17.*).[18] For collisional, the energy loss rate in the medium is dependent on its electron density and is greater for low Z materials than for high Z materials.[18] This is because high atomic number materials have tightly bound electrons and lower number of electrons per gram compared to low atomic number materials.[18] On the other hand, radiation losses are proportional to the energy of the electron and to Z^2. Radiation loss becomes significant relative to the collisional loss at *~8 MeV* for lead and *~50 MeV* for water.[18]

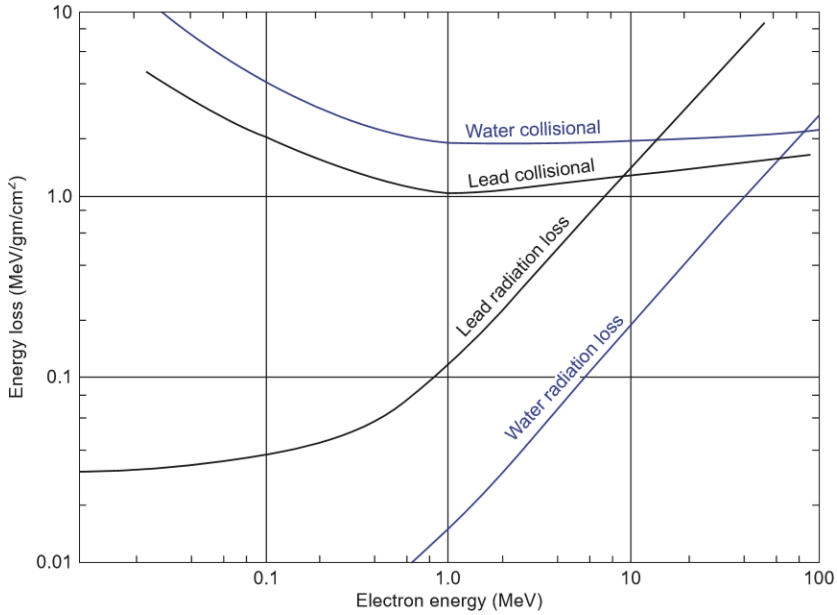

Figure 3. 17. The rate of energy loss vs electron energy for water and lead.[18]

3.1.9.3 External Shielding

In cases of external shielding, it is crucial to consider the required shield thickness for *5%* permitted transmission taking into account the practicality of the shield weight on the patient's surface (*figure 3.18.*).[18] For lead, the required thickness could be given by: $t_{Pb}(mm) = 0.5E_0(MeV) + 1$, and for Cerrobend, the thickness is given by: $t_c(mm) = 1.2t_{Pb}(mm)$.[18,25] Note that smaller field sizes require less shield thickness due to the less scattering occurring. External shielding (e.g. shield thickness) is of importance to us for small fields (smaller than what is required for a maximum lateral dose build-up) and for high energy electron beams because it results in a change in the dose rate, as well as, the dose distribution (*section 2.3*).

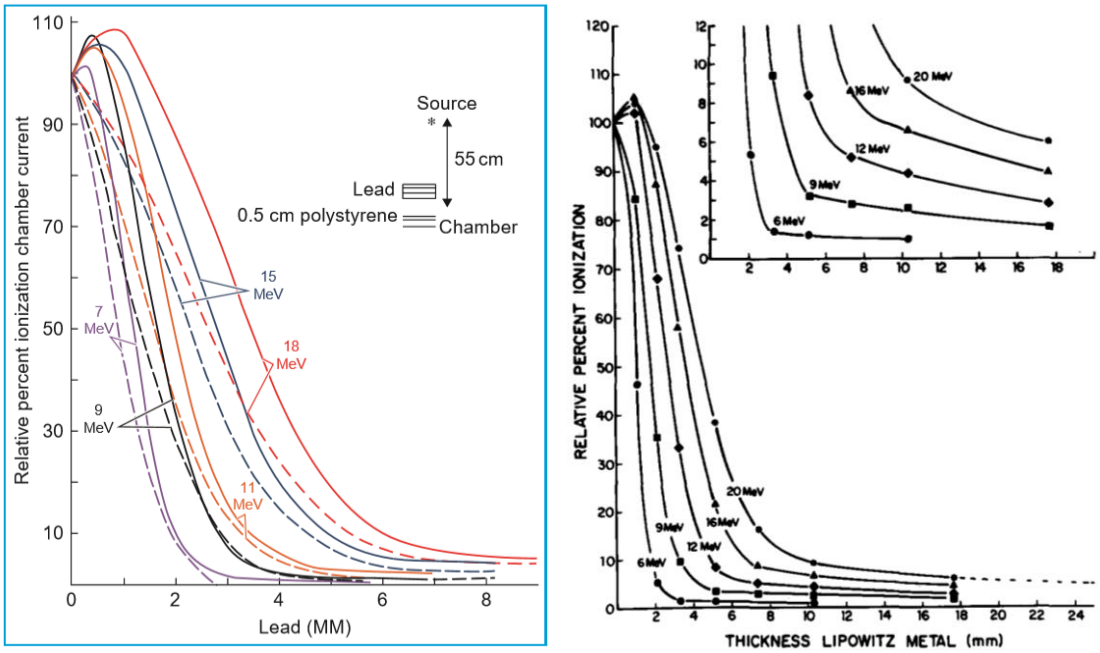

Figure 3. 18. Transmission curves for lead (left) and Cerrobend (right) for a range of electron beam energies. For lead: solid lines are for *10.5 × 10.5 cm* field size and dashed lines are for *6.3 × 6.3 cm* field size. For Cerrobend: *at 4 × 4 cm* field size and *100 cm SSD*.[18 & 43]

3.1.9.4 Internal Shielding

In internal shielding (such as for buccal mucosa and eyelid lesions) lead shielding is used to protect the critical structures beyond the tumor region.[18] In these cases, electron backscatter to the target volume could increase the dose rate significantly (*figure 3.19*). Therefore, it is recommended to use a low Z material (e.g. wax or aluminum) between the internal shield and the critical structure.[18] An important aspect in internal shielding is the placement depth of the lead shield in the patient. This has a significant effect on the dose distribution as illustrated in *figure 3.20*.[18] As distance between the patient surface and the lead placement depth increases the dose enhancement decreases exponentially.[18]

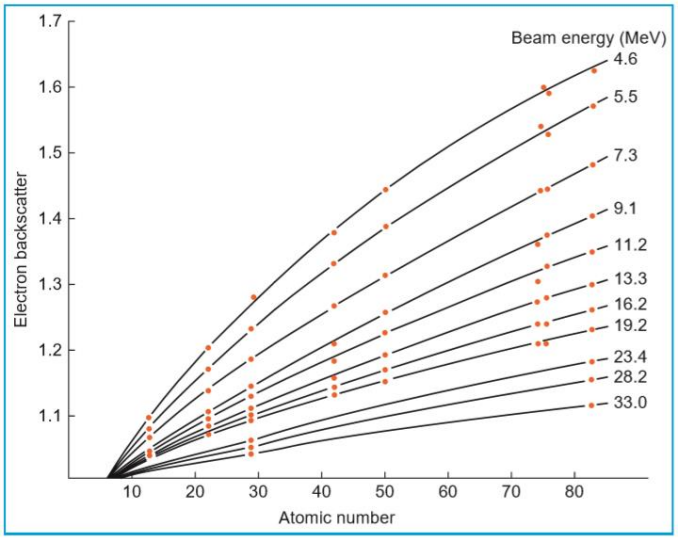

Figure 3. 19. Electron Backscatter factor as a function of Atomic number for various electron energies.[18]

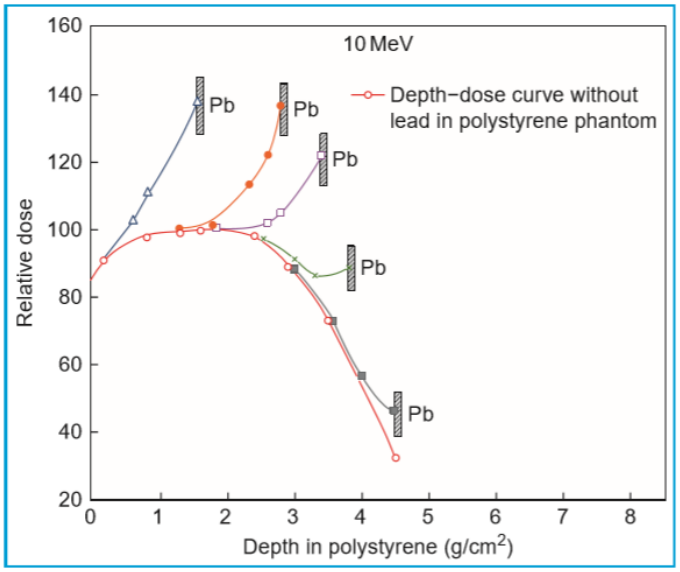

Figure 3. 20. Effect of lead placement depth on dose distribution for *10 MeV* electron beam.[18]

3.1.10. Scatter Foils

Electron beams are broadened and flattened as they hit the dual foil scattering system to produce a clinically useful beam.[32] Foils are made of thin high Z material targets in Elekta machines and are located near the exit window.[32] The primary flat shaped foil is used to broaden the pencil beam while the secondary gaussian shaped foil is used flatten the beam by scattering the

more penetrating central portion of the beam outwardly, thus improving beam uniformity.[32,41] *Figure 3.21* shows a more uniform beam distribution when dual scatter foil system is used. Ionizing radiation contributing to electron beam dose is in the form of electrons of the primary beam, scatter foils x-rays, scattered electrons from the jaws and applicator, and applicator x-rays.[32]

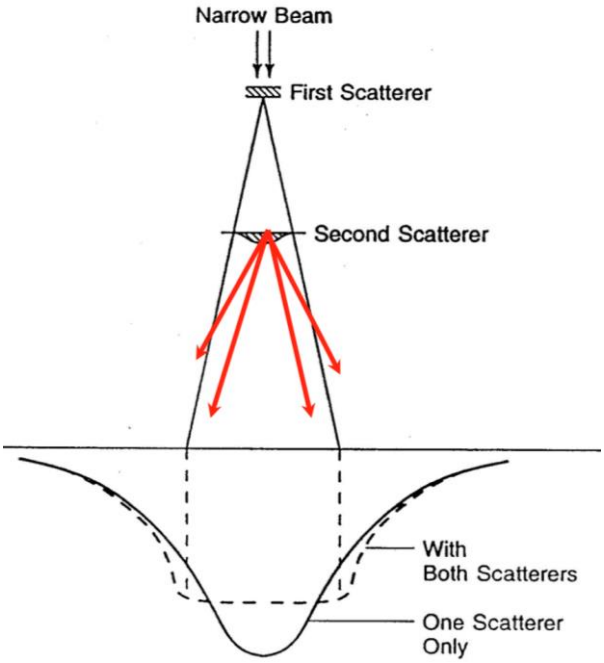

Figure 3. 21. An illustration of a dual scattering fuel system.[32]

3.1.10.1 Optimizing Scatter Foil System

A number of papers discussed optimizing foil systems in linear accelerators for different electron beam energies in terms of their design parameters, number of foils used, foils material, and foils thickness.[1,7,10,12,32,56] For example, Connell & Seuntjens (2014) investigated the possibility of producing custom made scatter foils for MERT to achieve beam broadening for high energy beams.[12] They concluded that the optimal scatter foil for very large field sizes would be made of lower Z material and would be flat in shape, where its thickness would vary based on the energy used.[12]

3.1.10.2 Other Scatter Foil Usages

Other papers experimented with adding scattering foils by the exit window in the direction of the pencil electron beam line for improvement of electron beam treatments Ye et al. (2005), or to model electron scatter through different materials Ross et al. (2008).[46,61] The former showed a better dose uniformity and a rapid dose fall-off of electron total skin irradiation patients treated with a single large electron field for monoenergetic *6.72 MeV* electrons at a treatment distance of *382 cm* with the addition of a *0.6 cm* thick PMMA energy degrader inserted into the wedge slot, and aluminum scatter foils (*12 x 12 x 0.6 cm*^{3}) positioned at a *100 cm* from the source.[61] While Ross et al. (2008) made use of metallic scatter foils of several materials with multiple thickness to model electron transport through materials.[46]

3.1.10.3 Scatter Foils and Magnet Collimators

Phaisangittisakul et al. (2003) applied an interesting approach for controlling electron range and fluence for a more desired dose distribution using magnet collimators and thin metallic foils filters.[40] In their experiment, they used a range of electron energies, and several types of foils materials of different thicknesses placed at the top surface of a magnetic collimator. The magnetic collimator (*12 cm* in length, maximum field strength of *2.0 T,* field opening ranges from *3x3* to *10x10 cm*^{2}) placed at the end of the electron cone, *80 cm* from a virtual source and 10 cm away from the water phantom.[40]

They also demonstrated a spread-out peak enhancement using the magnetic collimators for higher energy electrons.[40] Of the metals they used, higher Z materials such as lead showed large attenuated and more photon contamination while lower Z materials such as aluminum showed lower bremsstrahlung contamination and better depth dose

enhancement.[40] It was also found that the metal foils not only worsen skin sparring due to scatter but also eliminate the horns of high isodose curves at the low depth as a result of the more attenuation (they diverge and transverse through extra thickness of foil) peripheral electrons go through compared to central electrons (*figure 3.22*).[40] A great potential of uniform dose distribution and improved dose homogeneity is experimentally established for targets of specific depth and shape (e.g. rectangular targets) when optimizing the beam parameters and foil thickness in conjunction with magnetic collimators ((*figure 3.22).*[9,34,40]

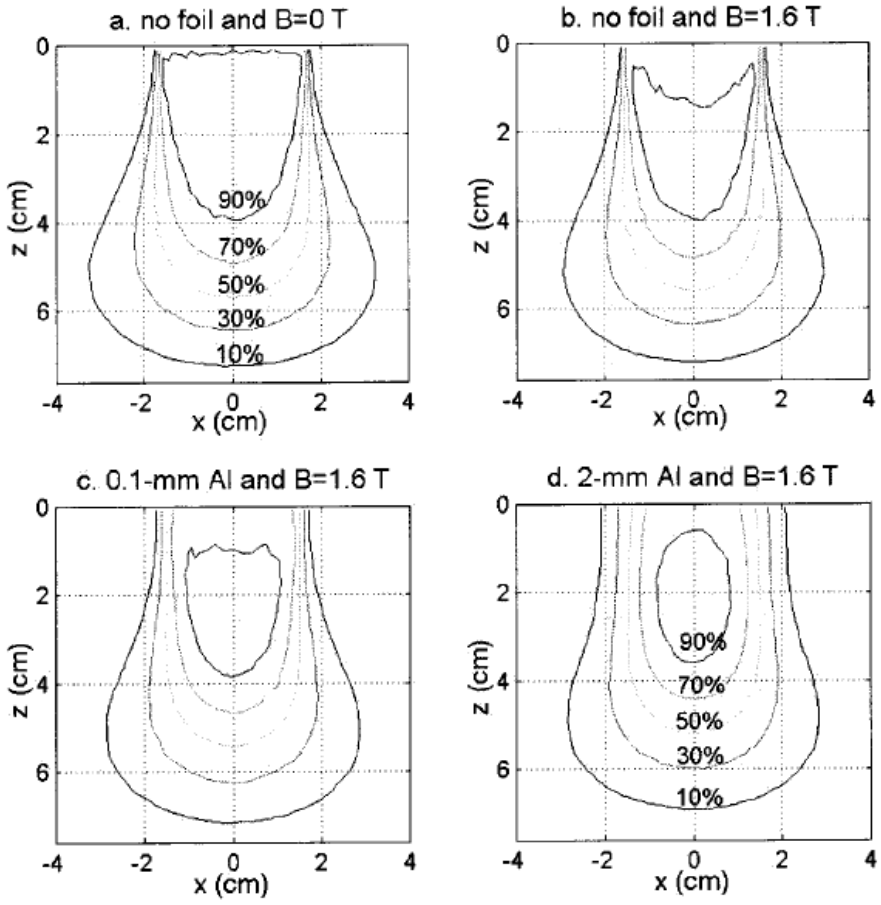

Figure 3. 22. Isodose curves for 15 MeV electrons for several different cases of magnetic fields strength and foil thickness.[40]

3.2 Needed Research & Research Goals

Numerous devices are available nowadays for delivery of very personalized electron therapy such as cutout inserts, skin collimators, eye shields, and bolus. Experiments to optimize current linacs' scatter foil systems have also been conducted. Nevertheless, no actual study to test the use of an additional skin scatter foil over a skin collimator for small field skin lesions has been found in the literature. Thus, the next chapter will be an experiment to test the usage of a thin sheet of metallic scattering foil on top of a skin collimator with the premise of shielding more healthy tissues and better distributes dose into the tumor by filtering high energy electrons, and improving/manipulating the isodose lines for a more uniform treatment free of hot/cold spots. This is a test of concept experiment that could potentially open the door for the development of novel electron beam therapy technique. The goal is to produce a quickly accessed, easy to fabricate, reusable device for clinical use with current linear accelerators without the need to modify the design of linacs' built-in scatter foils or add magnetic collimators.

4. MATERIALS & METHODS

This chapters consists of two sections. The first covers the materials used to run the trials for this project. The second section explains the experiment's design and setup.

4.1. Materials

4.1.1. Linear Accelerator

All experiments for this project were conducted at Oregon Health & Science University Radiation Medicine department using Elekta Versa HD linear accelerator, linac 3, which is commissioned for both electron and photon treatments (*figure 4.1.*). This linear accelerator is able to deliver various energies of photon beams up to *18 MV* with and without flatting filters, in addition to electron beams of *4, 6, 8, 9, 12, 15,* and *18 MeV*.[19] It has *80-pair* of tungsten multi-leaf collimators (MLCs) with a leaf width of *5 mm*, an interleaf gap < 0.1 mm, a leaf speed of *3.5 cm/s*, and a maximum field size of *40 x 40 cm*^{2}.[55]

Figure 4.1. OHSU's Linac3, Elekta HD Versa linear accelerator.

4.1.2. Applicator

Elekta Versa HD comes with several electron applicator sizes (*6 x 6, 10 x 10, 14 x 14 and 20 x 20 cm*^{2}) that could be attached to the linear accelerator treatment's head. *Figure 4.2.* shows an example of a *10 x 10 cm*^{2} Elekta Versa HD's applicator. All applicators used in this experiment are square in shape.

Figure 4.2. Elekta HD Versa's *10 x 10 cm*^{2} electron applicator.

4.1.3. Cutout inserts

Since this experiment is just a prove of concept, for simplicity, no cutout inserts were used at the end of the applicator. Instead, only skin collimators placed at the surface of the phantom were used.

4.1.4. Skin collimators

Skin collimators made of Cerrobend placed directly on top of the phantom were used as the cutouts for this experiment. The skin collimators have circular aperture of a *2 cm* in diameter representing a small electron field (*figure 4.3*). They are square in shape and extend beyond the treatment area collimated by the applicator to protect the phantom from any scattered electron

contamination. The Cerrobend skin collimators were fabricated on site by pouring melted Cerrobend into Cerrobend molds of the desired shape.

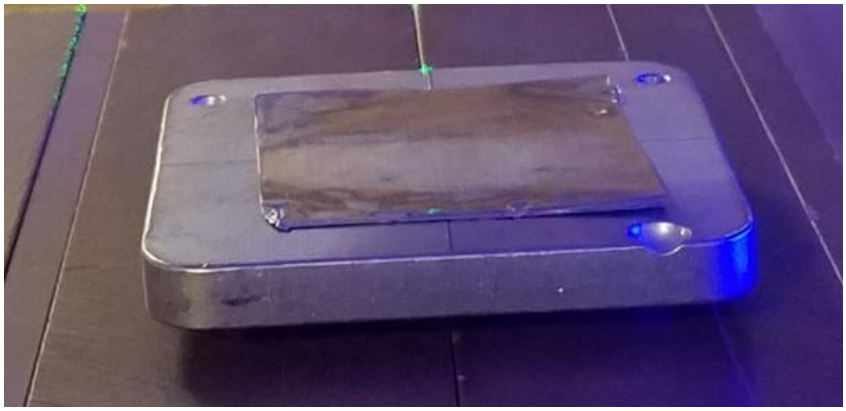

Figure 4.3. Skin collimator used in this experiment with lead foils on top.

4.1.5. Metal sheets

Two metallic flat scatter foil sheet materials were used in this experiment, lead and aluminum. The lead foils, produced by Nuclear Associates, were of *0.1524 mm* thickness each and the 3003 H14 aluminum foils were of *0.635 mm* thickness each. These two materials were chosen to represent the high range and the low range of Z atomic number, respectively, due to their availability, affordability, practicality and their robust results when used in similar experiments. The metallic sheet was placed on top of the skin collimator covering the circular open field as shown in *figure 4.3*. Various sheet thicknesses were used for this experiment.

Figure 4.4. 0.635 mm Aluminum scatter foil.

4.1.6. Solid Water Phantom

Nomos solid water phantom was utilized in this experiment as a direct representation of water, thus tissue, due to their similar electron densities. The solid water blocks are *30 x 30 cm*^{2} in surface area by several different thicknesses of *0.2 cm, 0.3 cm, 1 cm, 2 cm, 3 cm, 4 cm, 5 cm,* and *6 cm*. Once phantom was created, each half of the phantom has dimensions of *30 x 30 x 9 cm*^{3} (*figure 4.5*). The phantom thickness was chosen to represent a real-life situation of enough material for a correct backscatter dose. Tape and clamps were used to hold the solid water blocks together to minimize motion and to eliminate air gaps between the phantom and the film. The thickest blocks were placed on the inside, to ensure a homogenous medium around the film.

Figure 4.5. Half of the solid water phantom used in this experiment.

4.1.7. Film Dosimetry

Gafchromic Film™ EBT3 was used in this experiment due to its superior spatial resolution, its wide dose range, and its practicality for this experiment. [15,48] Film dosimetry is widely used for electron beam dose distribution since it has the advantage of showing a complete set of isodose

lines in the plane of the film.[48] Film is mainly used for relative dosimetry as opposed to absolute dosimetry.[18] The optical density (OD) of the film is proportional to dose because the collision stopping power ratio in emulsion and in water changes slowly with the energy of the electron beam, thus, making film energy independent and near tissue equivalent.[15,38] All these features of film align perfectly with the goals of this experiment for small electron field dosimetry. Films from the same batch were used in all experiments and films were developed at approximately the same time to improve accuracy of measurements. Precautions should be taken when using film, and many factors could cause error in the results obtained from film, such as: film alignment (*figure 4.6*), temperature, physical damage, presence of ionizing radiation or sunlight, oil from handling (gloves should be worn), scanning orientation, and time before scanning.[18, 38,48] All films front face bottom right corners were marked with a marker to maintain orientation consistency when scanning (*figure 4.7*). Films were cut into smaller pieces for the several scans. After usage, films were placed in envelops for protection and were kept for at least 24 hours to develop before being scanned.

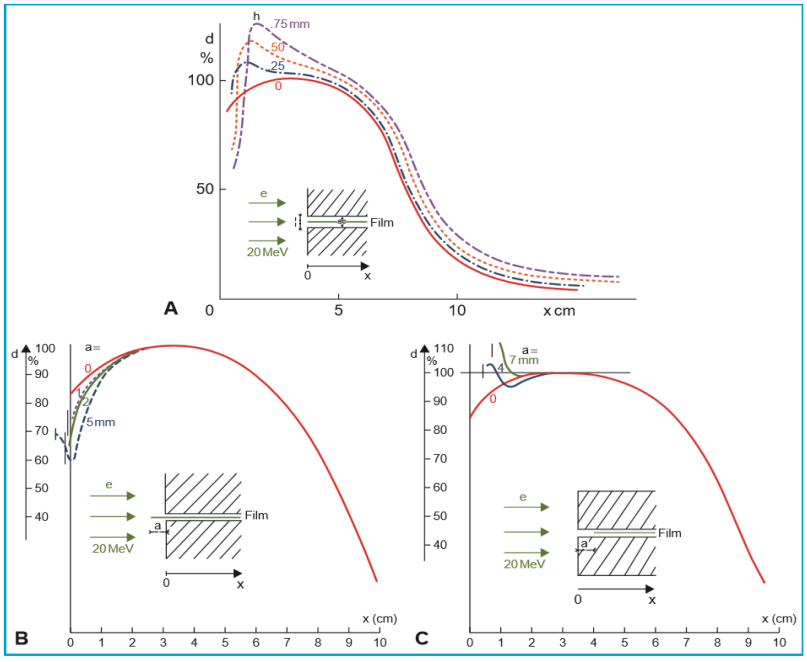

Figure 4.6. Film artifacts caused by A: air gaps between the phantom and the film, B: film extending beyond the phantom, and C: film recessed within the phantom.[18]

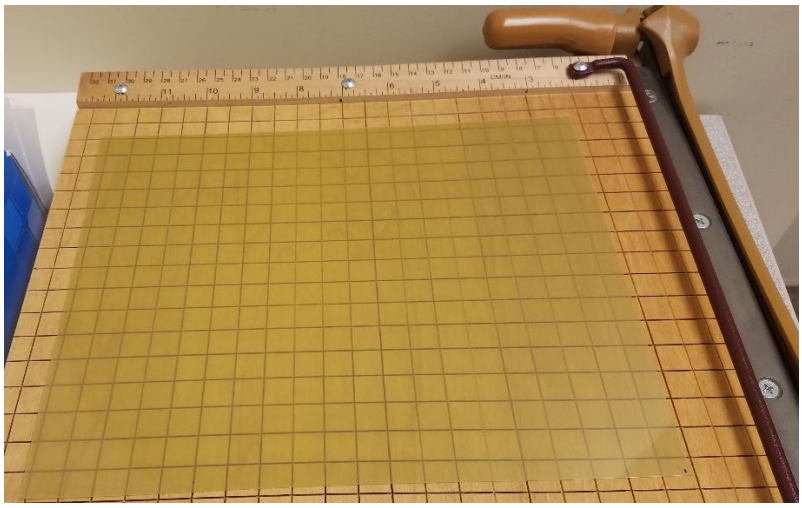

Figure 4.7. Film orientation when first removed from the batch.

4.1.8. Film Scanner

All films were scanned using Epson Expression 10000XL film scanner.[16] Films were positioned face down in the top center part of the scanner. Gloves were worn at all time when handling the film for its protection. Details on the scanner settings used are shown in *figure 4.8*. These images were saved and analyzed in *DoseLab*, *section 4.2.3*.

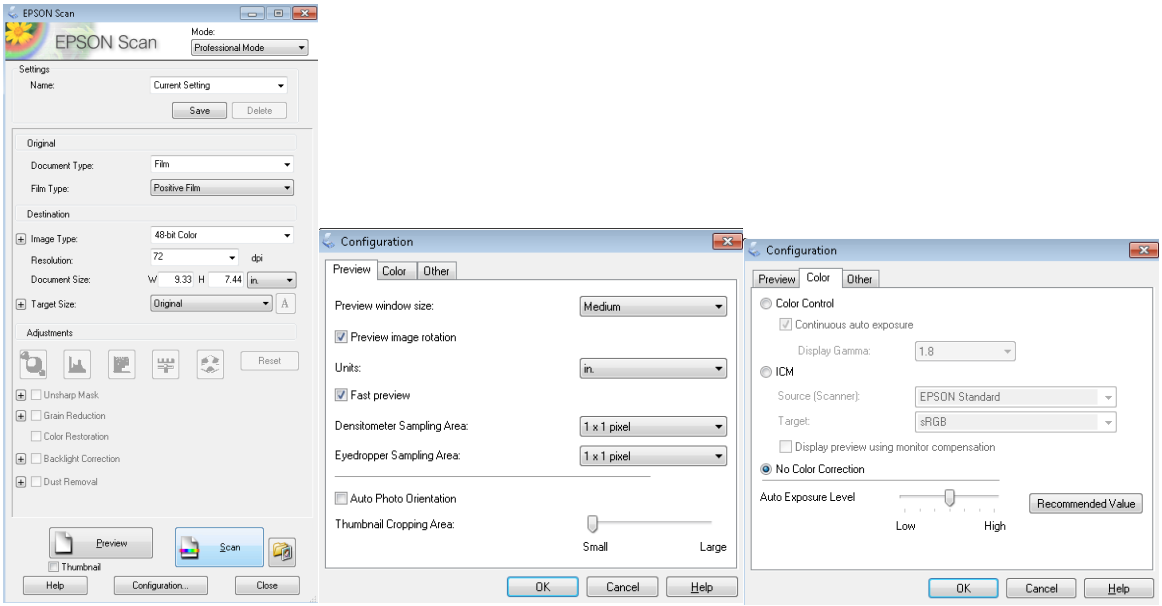

Figure 4.8. Scanner setting used to properly scan Gafchromic Film.[15,16]

4.2. Methods

The goal of this experiment is to understand the behavior of isodose lines when a metallic scatter foil is placed directly over a skin collimator for small electron fields of high energy electrons. That being said, three variables were changed; the scatter foil material, the scatter foil thickness, the energy of the electron beam. The other parameters that were kept constant in this experiment are: SSD, beam obliquity, applicator field size, usage of cutouts, scatter foil shape/design and dimensions, skin collimator thickness, skin collimator field size, and phantom thickness. Oregon Health & Science University Linac 3's electron beams are calibrated to deliver *1 cGy/MU* at depth of maximum dose for SSD of *100 cm* for *10 x 10 cm^2* physics field.

4.2.1. Calibration Scans

For this experiment, three different electron beam energies were used: *8, 12,* and *15 MeV*. Calibration films were placed horizontally, face-up, centrally on top of the *30 x 30 x 9 cm^3* for acceptable backscatter, and underneath phantom blocks of thickness equal to the depth of maximum dose for the energy used sufficient for adequate build-up based on the beam energy according to *figure 2.8.* and *section 2.4*. A *10 x 10 cm^2* was used for all calibration irradiation. The phantom was centered in the electron field. The calibration scans setup is shown in *figure 4.8.*, and full setup parameters are given in *tables 1-3*. Calibration is fundamental to assure the accuracy of the instruments and to control the detectability of the measurement.

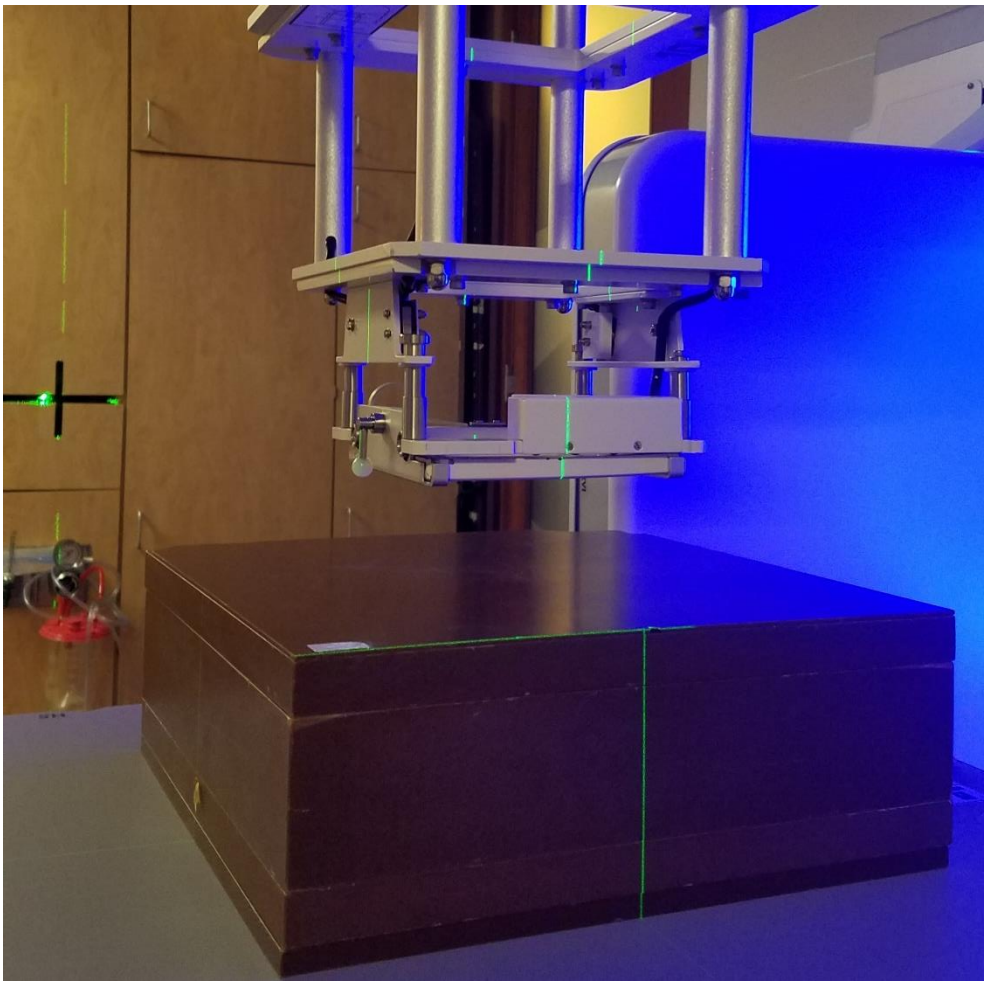

Figure 4.9. The calibration horizontal scan setup.

To assure correct calibration, additional vertical calibration irradiation for each beam energy were taken, settings given in *tables 4-6.* Vertical irradiation were taken through the top uncut edge of the film as opposed to any cut edges. For the vertical scans, film was placed vertically between the two halves of the phantom blocks parallel to the beam, the top edge of the film was aligned with the surface of the phantom to avoid artifacts. *Figure 4.10.* shows the calibration vertical scan setup taken in a head-to-toe orientation, where the head side represent the couch's side closer to the linac's head and the toe side represents the couch's side farther away from the linac's head. The upper and lower ranges of MUs were chosen for proper characterization of low and high isodose lines.

Table 1: Parameters used for calibration horizontal irradiation for *8 MeV* electron beam.

Parameter	Settings
Beam Energy	*8 MeV*
SSD	*100 cm*
Applicator Size	*10 x 10 cm^2*
Bottom Phantom Thickness	*30 x 30 x 9 cm^3*
Top Phantom Thickness	*30 x 30 x 2.2 cm^3*
Film Size	*5 x 20 cm^2*
Monitor Units (MU)	*0, 50, 100, 200, 300, 400, 500, 600, 700, 800*

Table 2: Parameters used for calibration horizontal irradiation for *12 MeV* electron beam.

Parameter	Settings
Beam Energy	*12 MeV*
SSD	*100 cm*
Applicator Size	*10 x 10 cm^2*
Bottom Phantom Thickness	*30 x 30 x 9 cm^3*
Top Phantom Thickness	*30 x 30 x 2.8 cm^3*
Film Size	*5 x 20 cm^2*
Monitor Units (MU)	*0, 50, 100, 200, 300, 400, 500, 600, 700, 800*

Table 3: Parameters used for calibration horizontal irradiation for *15 MeV* electron beam.

Parameter	Settings
Beam Energy	*15 MeV*
SSD	*100 cm*
Applicator Size	*10 x 10 cm^2*
Bottom Phantom Thickness	*30 x 30 x 9 cm^3*
Top Phantom Thickness	*30 x 30 x 3.4 cm^3*
Film Size	*5 x 20 cm^2*
Monitor Units (MU)	*0, 50, 100, 200, 300, 400, 500, 600, 700, 800*

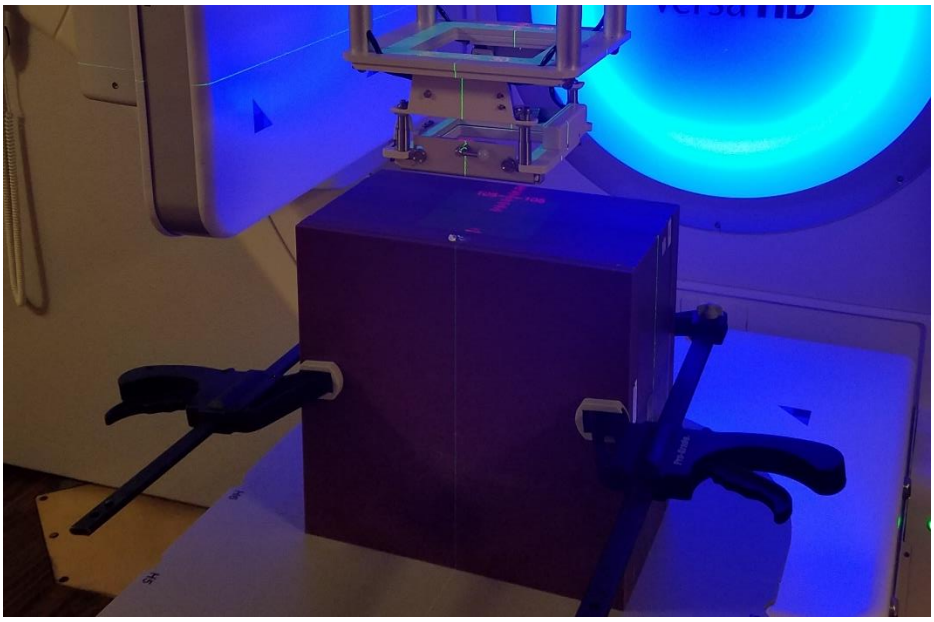

Figure 4.10. The calibration vertical scan setup.

Table 4: Parameters used for calibration vertical irradiation for *8 MeV* electron beam.

Parameter	Settings
Beam Energy	*8 MeV*
SSD	*100 cm*
Applicator Size	*10 x 10 cm^2*
Right half Phantom Thickness	*30 x 30 x 9 cm^3*
Left half Phantom Thickness	*30 x 30 x 9 cm^3*
Film Size	*15 x 10 cm^2*
Monitor Units (MU)	*600*

Table 5: Parameters used for calibration vertical irradiation for *12 MeV* electron beam.

Parameter	Settings
Beam Energy	*12 MeV*
SSD	*100 cm*
Applicator Size	*10 x 10 cm^2*
Right half Phantom Thickness	*30 x 30 x 9 cm^3*
Left half Phantom Thickness	*30 x 30 x 9 cm^3*
Film Size	*15 x 10 cm^2*
Monitor Units (MU)	*600*

Table 6: Parameters used for calibration vertical irradiation for *15 MeV* electron beam.

Parameter	Settings
Beam Energy	*15 MeV*
SSD	*100 cm*
Applicator Size	*10 x 10 cm^2*
Right half Phantom Thickness	*30 x 30 x 9 cm^3*
Left half Phantom Thickness	*30 x 30 x 9 cm^3*
Film Size	*15 x 12 cm^2*
Monitor Units (MU)	*600*

4.2.2. Scatter Foil Vertical Scans

For this experiment, the following variables were used: three different electron beam energies of *8, 12,* and *15 MeV*, two scatter foil materials Pb and Al, totaling in *4* different thicknesses for Al: *0.635, 1.27, 1.905,* and *2.54 mm*, and *4* thicknesses for Pb: *0.1524, 0.4572, 0.762*, and *1.0668 mm.* For all runs, calibration films were placed vertically between the two halves of the *30 x 30 x 9 cm^3* phantom in a head-to-toe orientation, with the uncut edge aligned with the phantom surface. The phantom was centered in the electron field. A *6 x 6 cm^2* applicator was used as this would realistically represent a small field setting. The skin collimator of *2 cm* circular diameter was placed directly on the phantom surface and centered. Skin collimators used have enough thickness for electron shielding with an acceptable *5%* transmission according to the Cerrobend's equation in *section 3.1.9.3* and figure *3.18.* The vertical scatter foil scans full setup is shown in figure *4.10.*, and setup parameters are given in *tables 9-16*.

Figure 4.11. The vertical scans setup for all experiments.

Table 7: Parameters used for Pb scatter foil vertical irradiation for *8 MeV* electron beam.

Parameter	Settings
Beam Energy	*8 MeV*
SSD	*100 cm*
Applicator Size	*6 x 6 cm^2*
Right half Phantom Thickness	*30 x 30 x 9 cm^3*
Left half Phantom Thickness	*30 x 30 x 9 cm^3*
Scatter Foil Material	*Pb*
Scatter Foil Thicknesses	*0.1524, 0.4572, 0.762, and 1.0668 mm*
Skin Collimator Thickness	*10.5 mm*
Film Size	*5 x 10 cm^2*
Monitor Units (MU)	*600*

Table 8: Parameters used for Pb scatter foil vertical irradiation for *12 MeV* electron beam.

Parameter	Settings
Beam Energy	*12 MeV*
SSD	*100 cm*
Applicator Size	*6 x 6 cm^2*
Right half Phantom Thickness	*30 x 30 x 9 cm^3*
Left half Phantom Thickness	*30 x 30 x 9 cm^3*
Scatter Foil Material	*Pb*
Scatter Foil Thicknesses	*0.1524, 0.4572, 0.762, and 1.0668 mm*
Skin Collimator Thickness	*10.5 mm*
Film Size	*5 x 10 cm^2*
Monitor Units (MU)	*600*

Table 9: Parameters used for Pb scatter foil vertical irradiation for *15 MeV* electron beam.

Parameter	Settings
Beam Energy	*15 MeV*
SSD	*100 cm*
Applicator Size	*6 x 6 cm^2*
Right half Phantom Thickness	*30 x 30 x 9 cm^3*
Left half Phantom Thickness	*30 x 30 x 9 cm^3*
Scatter Foil Material	*Pb*
Scatter Foil Thicknesses	*0.1524, 0.4572, 0.762, and 1.0668 mm*
Skin Collimator Thickness	*10.5 mm*
Film Size	*5 x 12 cm^2*
Monitor Units (MU)	*600*

Table 10: Parameters used for Al scatter foil vertical irradiation for *8 MeV* electron beam.

Parameter	Settings
Beam Energy	*8 MeV*
SSD	*100 cm*
Applicator Size	*6 x 6 cm^2*
Right half Phantom Thickness	*30 x 30 x 9 cm^3*
Left half Phantom Thickness	*30 x 30 x 9 cm^3*
Scatter Foil Material	*Al*
Scatter Foil Thicknesses	*0.635, 1.27, 1.905, and 2.54 mm*
Skin Collimator Thickness	*10.5 mm*
Film Size	*5 x 10 cm^2*
Monitor Units (MU)	*600*

Table 11: Parameters used for Al scatter foil vertical irradiation for *12 MeV* electron beam.

Parameter	Settings
Beam Energy	*12 MeV*
SSD	*100 cm*
Applicator Size	*6 x 6 cm^2*
Right half Phantom Thickness	*30 x 30 x 9 cm^3*
Left half Phantom Thickness	*30 x 30 x 9 cm^3*
Scatter Foil Material	*Al*
Scatter Foil Thicknesses	*0.635, 1.27, 1.905, and 2.54 mm*
Skin Collimator Thickness	*10.5 mm*
Film Size	*5 x 10 cm^2*
Monitor Units (MU)	*600*

Table 12: Parameters used for Al scatter foil vertical irradiation for *15 MeV* electron beam.

Parameter	Settings
Beam Energy	*15 MeV*
SSD	*100 cm*
Applicator Size	*6 x 6 cm^2*
Right half Phantom Thickness	*30 x 30 x 9 cm^3*
Left half Phantom Thickness	*30 x 30 x 9 cm^3*
Scatter Foil Material	*Al*
Scatter Foil Thicknesses	*0.635, 1.27, 1.905, and 2.54 mm*
Skin Collimator Thickness	*10.5 mm*
Film Size	*5 x 12 cm^2*
Monitor Units (MU)	*600*

4.2.3. DoseLab Analysis

All scanned film images, calibration + measurement + blank, were imported to *DoseLab. DoseLab* reads an unexposed film image and uses it to convert exposed film images into OD.[15] All film scans should be taken using an identical region of interest on the film scanner, i.e., all film images should have the exact same dimensions; otherwise, the data will be susceptible to error.[15,16] A blank unexposed film was used in order to perform a 2D uniformity correction and calculate a net OD values for each pixel of the selected RGB channel (Red channel for doses up to 1000 cGy) of the exposed films (calibration and measurement), where*: Net OD = log(blank/measured).* Net OD is used so that the exposed films are compared to the baseline of the blank unexposed film.[15] The resulted new OD images are then saved as a 16-bit TIF image. The calibration filmstrips were then analyzed individually and a third order polynomial calibration curve from OD to dose was

created manually for each of the three energies used using the ROI method described in *DoseLab* manual.[15] Calibration was then applied and the measurement film scans were converted from OD into dose images using the appropriate Excel calibration table. The resulted images were then analyzed thoroughly using the many tools built in *DoseLab* and are presented in *chapter 5*.

5. RESULTS

This chapter contains the summarized data from the experiment described in *chapter 4*. The results consist of figures and tables constructed in *DoseLab* and *Microsoft Excel*. A written description is accompanied.

5.1. PDDs & Isodose Curves

This section contains *PDDs* and isodose curves of all measurements taken in this experiment. Note that, for the *8 MeV* energy, doses in the calibration curve were increased *109%* (by using *0.109* dose conversion) in order to get a dose at maximum depth equal to *600 cGy*. For the *15 MeV* energy, doses in the calibration curve were decreased to *84.5%* (by using 0.0845 dose conversion) in order to yield a dose at maximum depth equal to *600 cGy*. These two adjustments were done to be able to compare the results since the depths of the maximum dose for the calibration measurements were incorrect. The results consist of figures of film profile for every energy and foil thickness combination used, the *PDD* at central axis, and the *10%, 25%, 50%, 80%, 90%* isodose curves. Also for every energy and foil thickness combination used, tables that include the diameter of the clinically relevant portion of the field, i.e., the *90*% region at depth of maximum dose (D_{max}), the value of the maximum dose, the penumbra sizes (distance between *20%* and *80%* field edges on all sides *at* D_{max}, D_{90}, D_{50}, D_{25}), as well as the most probable energy (E_{P0}), D_{max} and practical range (R_p) are provided.

The “Single Image Analysis” tool was utilized to analyze all the scans. The film profiles in units of dose (*cGy)* were generated in *Doselab* using the method described in *section 4.2.3.* The isodose curves were generated using “isodose image” option from the “Analysis” tab. The *PDDs* at central axis, D_{max}, E_{P0}, and R_p, were provided using the machine QA tab then “depth dose film”. The “Image profiler” tool under the analysis tab was used to find the diameter of the clinically relevant portion of the field and the penumbra sizes.

The exact method used to find the *90%* isodose field width was choosing a “horizontal profile” from the “profile type” section, then using the horizontal profile at D_{max} (found in the previous step), then moving the curser on the horizontal film profile and recording the X_1 and X_2 values on both sides of the peak that corresponds to a *y* value of *0.9*MaximumDose cGy* which represent the *90%* isodose (*x= X, y = 0.9*MaximumDose*). The difference between X_1 and X_2 values equals the *90%* isodose curve diameter at depth of maximum dose. Similarly, penumbra sizes were found at depth of D_{max}, D_{90}, D_{50}, D_{25} (by having a peak value in the horizontal profile corresponding to a dose of *1*MaximumDose, 0.9*MaximumDose, 0.5*MaximumDose and 0.25*MaximumDose cGy*, respectively). The difference between the *X* values in the two location of (*x= X_1, y= 0.8*dose*) and (*x= X_2, y= 0.2*dose*) yields the size of the penumbra, where *0.8* and *0.2* corresponds to the *80%* and *20%* lines.

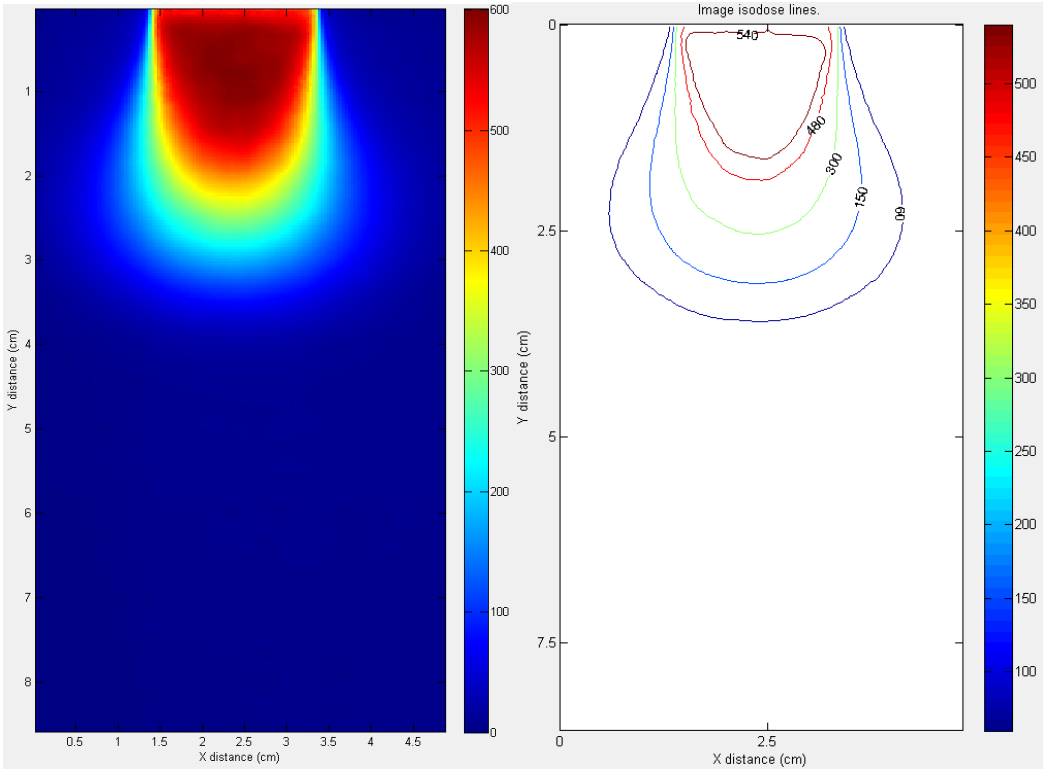

Figure 5.1. Image profile (left) and Isodose lines (right: *10%, 25%, 50%, 80%, 90%* isodose curves) for *no foil, 8 MeV* at *600 MUs*.

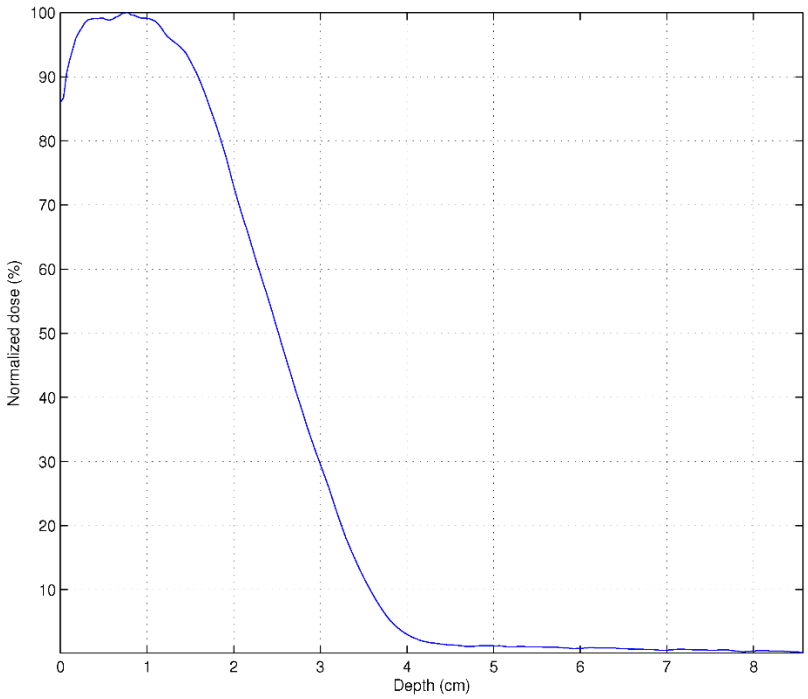

Figure 5.2. Normalized dose *PDD* at central axis for *no foil, 8 MeV* at *600 MUs*.

Table 13: Results for *no* scatter foil for *8 MeV* electron beam.

Parameter	Results
Beam Energy	*8 MeV*
Foil Material	*none*
Foil Thickness	*0 mm*
Most probable Energy E_{P0}	*7.44 MeV*
Maximum dose, and D_{max}	*600 cGy @ 0.78 cm*
Practical Range R_p	*3.63 cm*
Diameter of *90%* @ D_{max}	*1.44 cm*
Penumbra Size D_{max}, D_{90}, D_{50}, D_{25}	*0.26, 0.71, 1.06, and 1.10 cm*

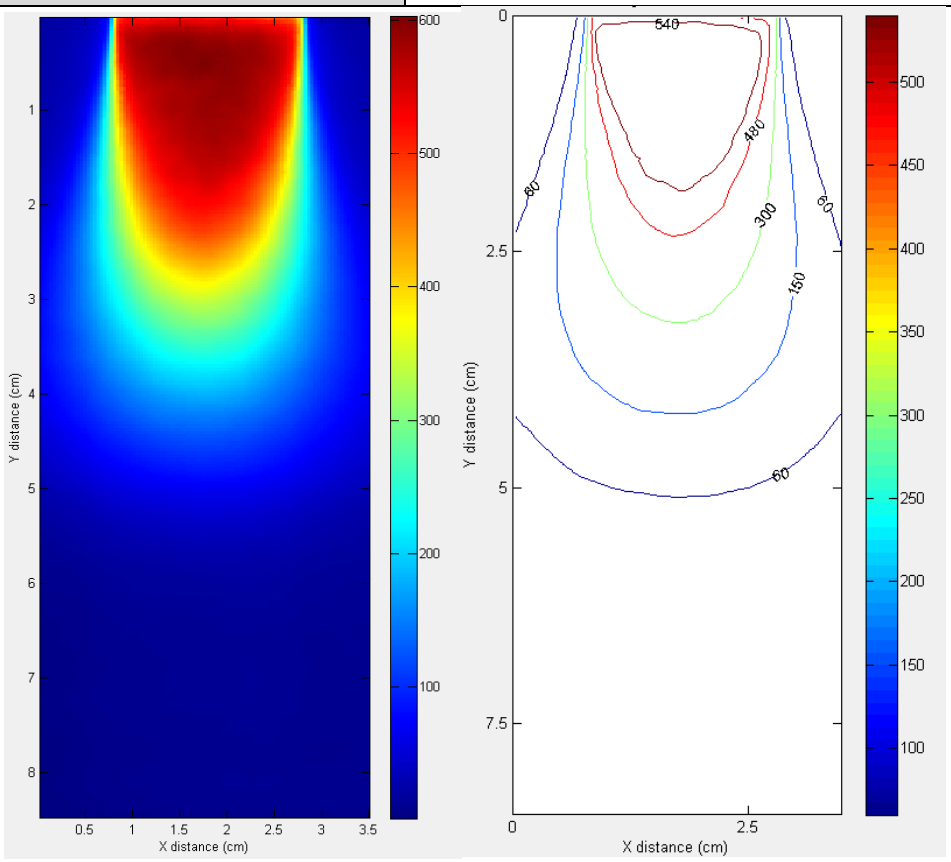

Figure 5.3. Image profile (left) and Isodose lines (right: *10%, 25%, 50%, 80%, 90%* isodose curves) for *no* scatter foil, *12 MeV* at *600 MUs*.

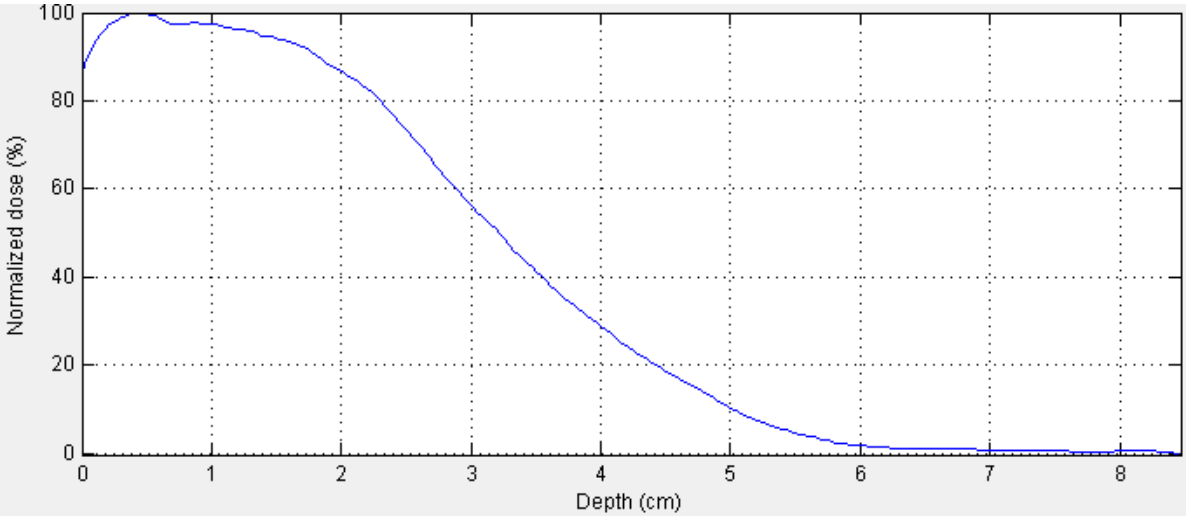

Figure 5.4. Normalized dose *PDD* at central axis for *no* scatter foil, *12 MeV* at *600 MUs*.

Table 14: Results for *no* scatter foil for *12 MeV* electron beam.

Parameter	Results
Beam Energy	*12 MeV*
Foil Material	*none*
Foil Thickness	*0 mm*
Most probable Energy E_{P0}	*9.91 MeV*
Maximum dose, and D_{max}	*600 cGy @ 0.46 cm*
Practical Range R_p	*4.87 cm*
Diameter of *90% @* D_{max}	*1.68 cm*
Penumbra Size D_{max}, D_{90}, D_{50}, D_{25}	*0.14, 0.61, 1.14, and 1.52 cm*

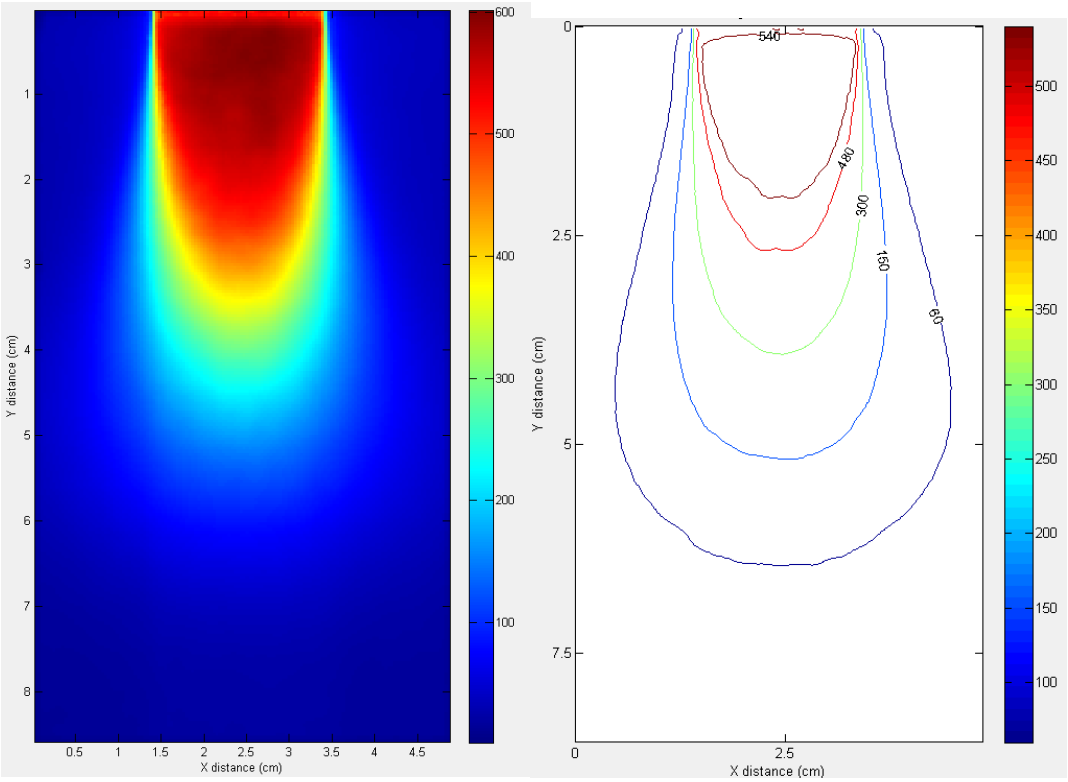

Figure 5.5. Image profile (left) and Isodose lines (right: *10%, 25%, 50%, 80%, 90%* isodose curves) for *no* scatter foil, *15 MeV* at *600 MUs*.

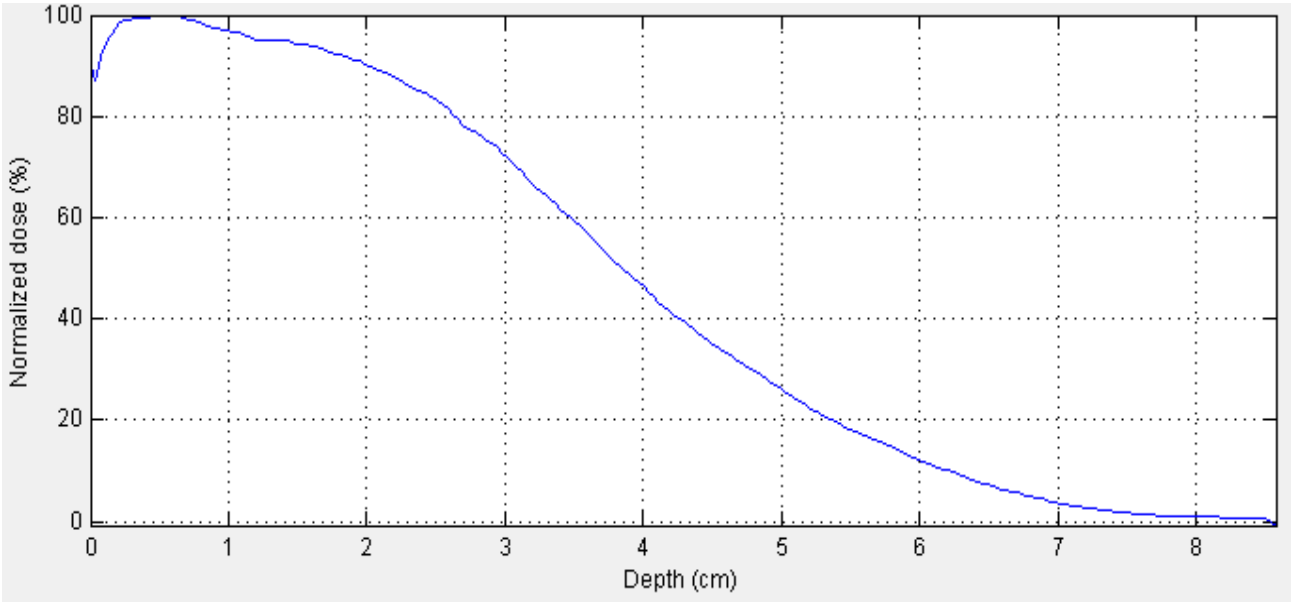

Figure 5.6. Normalized dose *PDD* at central axis for *no* scatter foil, *15 MeV* at *600 MUs*.

Table 15: Results for *no* scatter foil for *15 MeV* electron beam.

Parameter	Results
Beam Energy	*15 MeV*
Foil Material	*none*
Foil Thickness	*0 mm*
Most probable Energy E_{P0}	*11.79 MeV*
Maximum dose, and D_{max}	*600 cGy @ 0.53 cm*
Practical Range R_p	*5.80 cm*
Diameter of *90%* @ D_{max}	*1.87 cm*
Penumbra Size D_{max}, D_{90}, D_{50}, D_{25}	*0.11, 0.50, 1.235, and 1.45 cm*

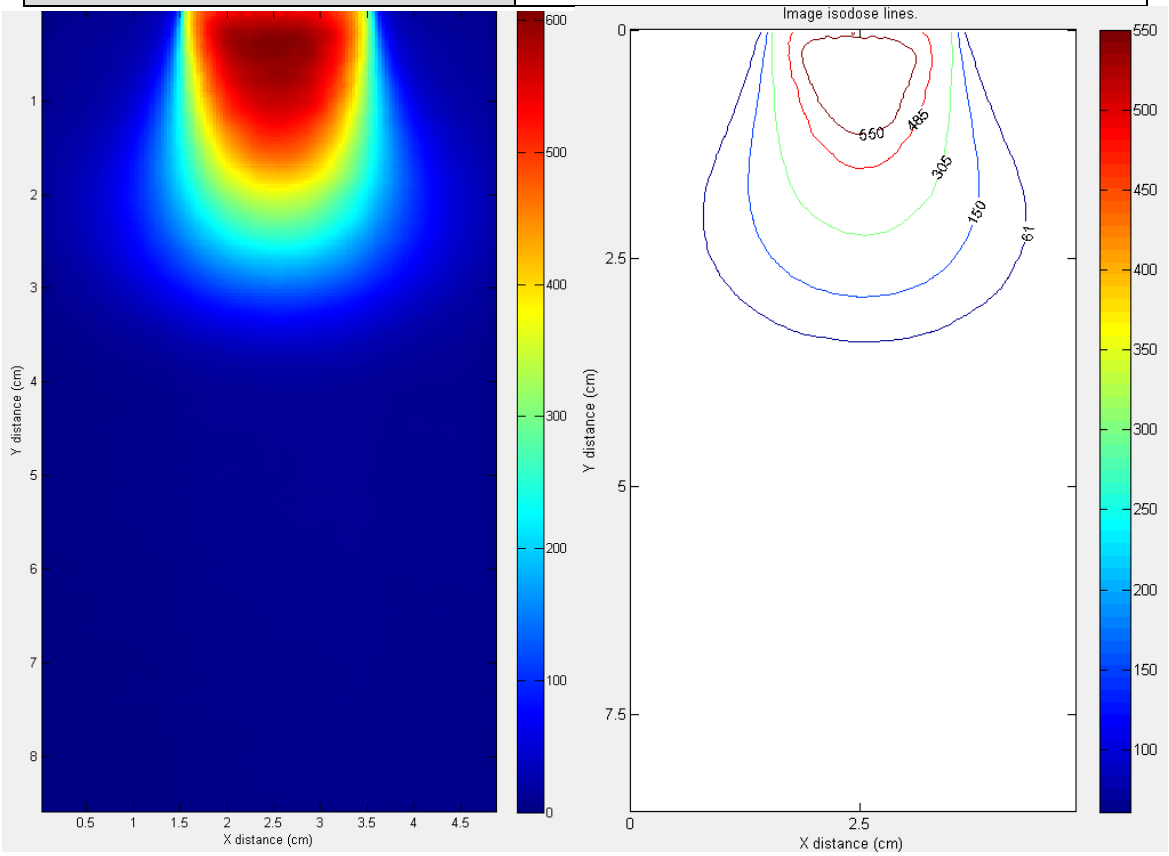

Figure 5.7. Image profile (left) and Isodose lines (right: *10%, 25%, 50%, 80%, and 90%* isodose curves) for *0.635 mm* Al, *8 MeV* at *600 MUs*.

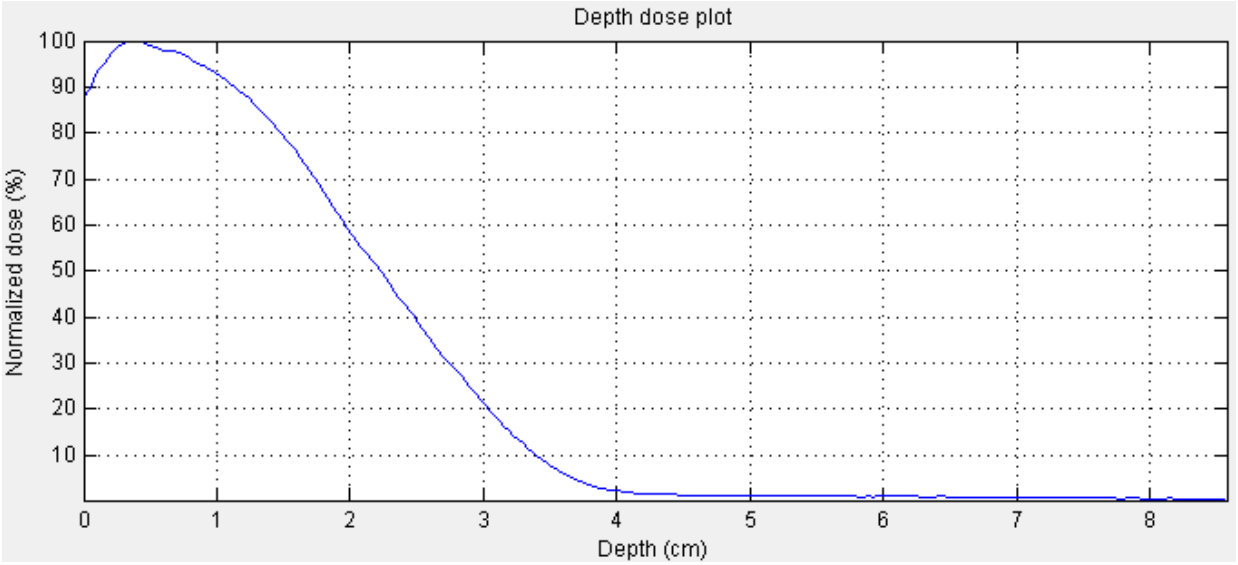

Figure 5.8. Normalized dose *PDD* at central axis for *0.635 mm* Al, *8 MeV* at *600 MUs*.

Table 16: Results for *0.635 mm* Al scatter foil for *8 MeV* electron beam.

Parameter	**Results**
Beam Energy	*8 MeV*
Foil Material	*Al*
Foil Thickness	*0.635 mm*
Most probable Energy E_{P0}	*7.20 MeV*
Maximum dose, and D_{max}	*608 cGy @ 0.35 cm*
Practical Range R_p	*3.51 cm*
Diameter of *90% @* D_{max}	*1.22 cm*
Penumbra Size D_{max}, D_{90}, D_{50}, D_{25}	*0.33, 0.65, 1.05, and 1.14 cm*

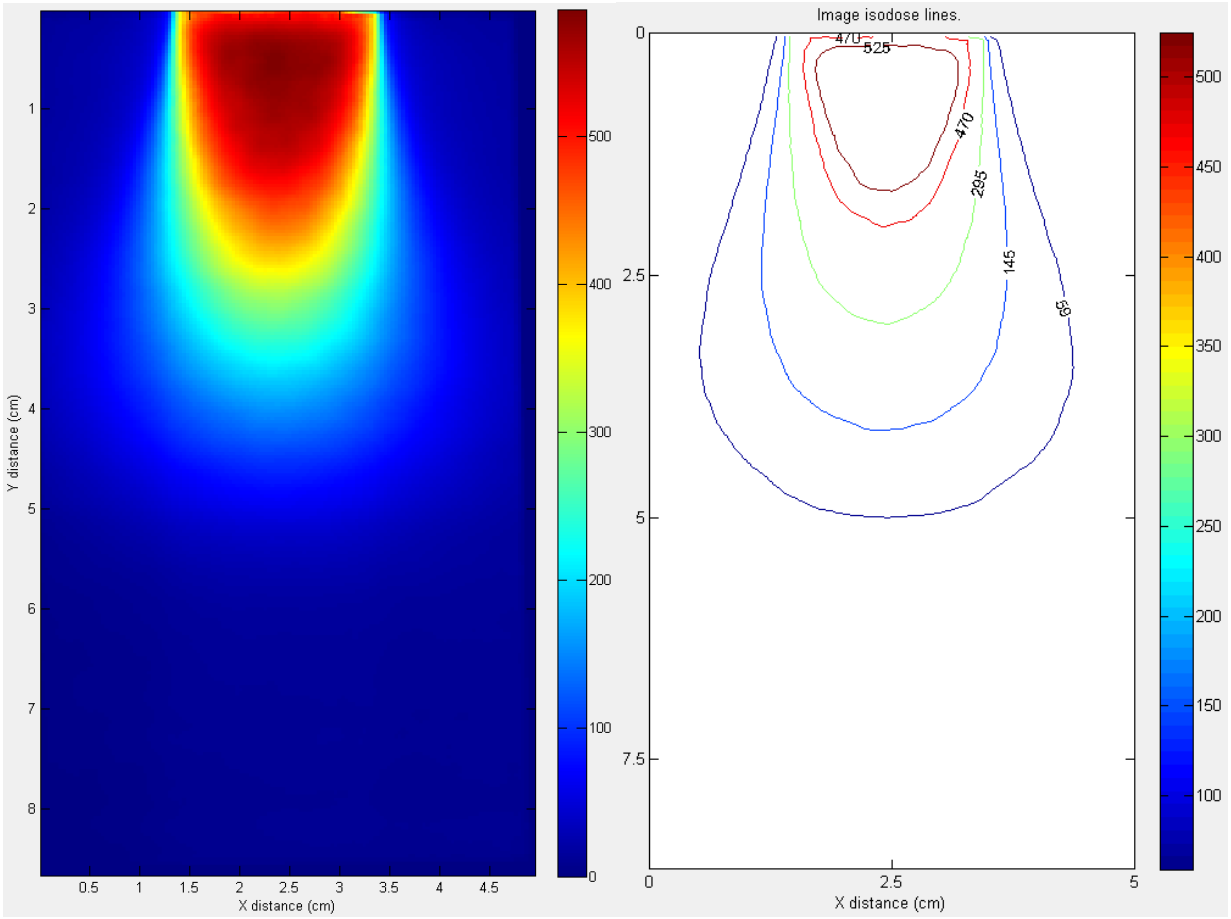

Figure 5.9. Image profile (left) and Isodose lines (right: *10%*, *25%*, *50%*, *80%*, *90%* isodose curves) for *0.635 mm* Al, *12 MeV* at *600 MUs*.

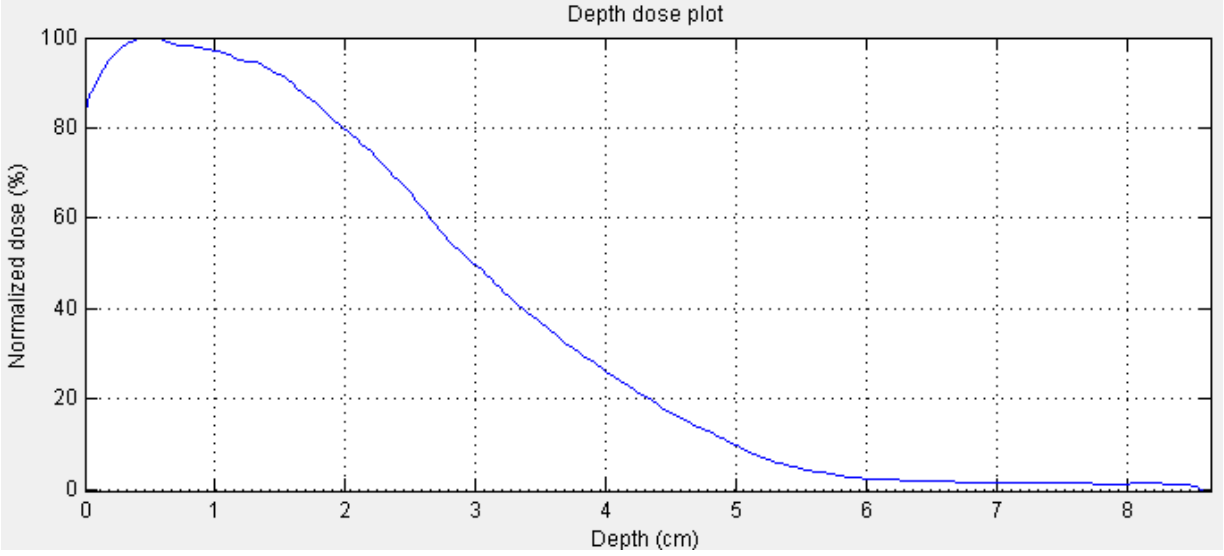

Figure 5.10. Normalized dose *PDD* at central axis for *0.635 mm* Al, *12 MeV* at *600 MUs*.

Table 17: Results for *0.635 mm* Al scatter foil for *12 MeV* electron beam.

Parameter	Results
Beam Energy	*12 MeV*
Foil Material	*Al*
Foil Thickness	*0.635 mm*
Most probable Energy E_{P0}	*9.78 MeV*
Maximum dose, and D_{max}	*585 cGy @ 0.46 cm*
Practical Range R_p	*4.80 cm*
Diameter of *90%* @ D_{max}	*1.46 cm*
Penumbra Size D_{max}, D_{90}, D_{50}, D_{25}	*0.28, 0.66, 1.17, and 1.46 cm*

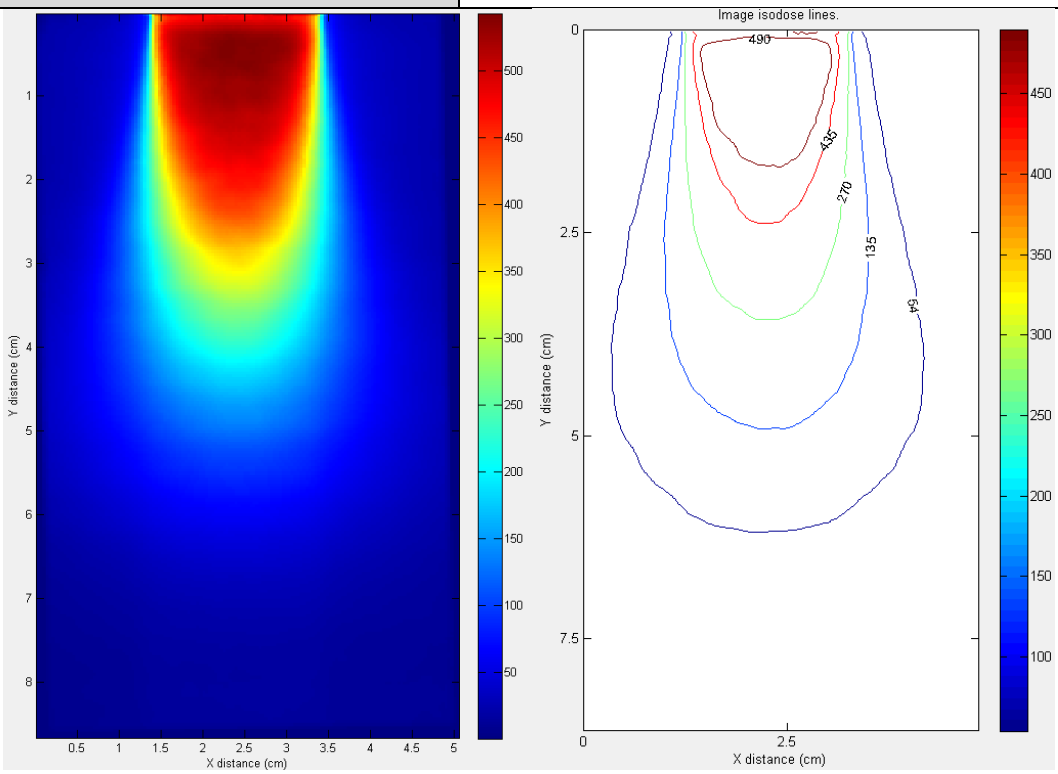

Figure 5.11. Image profile (left) and Isodose lines (right: *10%, 25%, 50%, 80%, 90%* isodose curves) for *0.635 mm* Al, *15 MeV* at *600 MUs*.

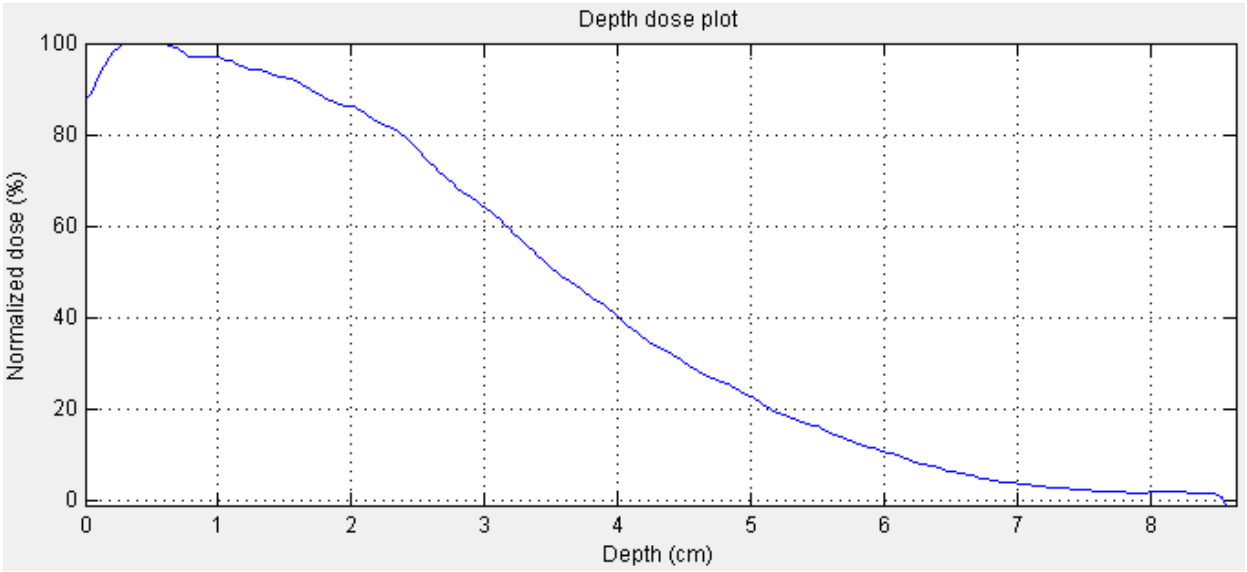

Figure 5.12. Normalized dose *PDD* at central axis for *0.635 mm* Al, *15 MeV* at *600 MUs*.

Table 18: Results for *0.635 mm* Al scatter foil for *15 MeV* electron beam.

Parameter	Results
Beam Energy	*15 MeV*
Foil Material	*Al*
Foil Thickness	*0.635 mm*
Most probable Energy E_{P0}	*11.59 MeV*
Maximum dose, and D_{max}	*543 cGy @ 0.35 cm*
Practical Range R_p	*5.70 cm*
Diameter of *90% @* D_{max}	*1.60 cm*
Penumbra Size D_{max}, D_{90}, D_{50}, D_{25}	*0.19, 0.54, 1.17, and 1.58 cm*

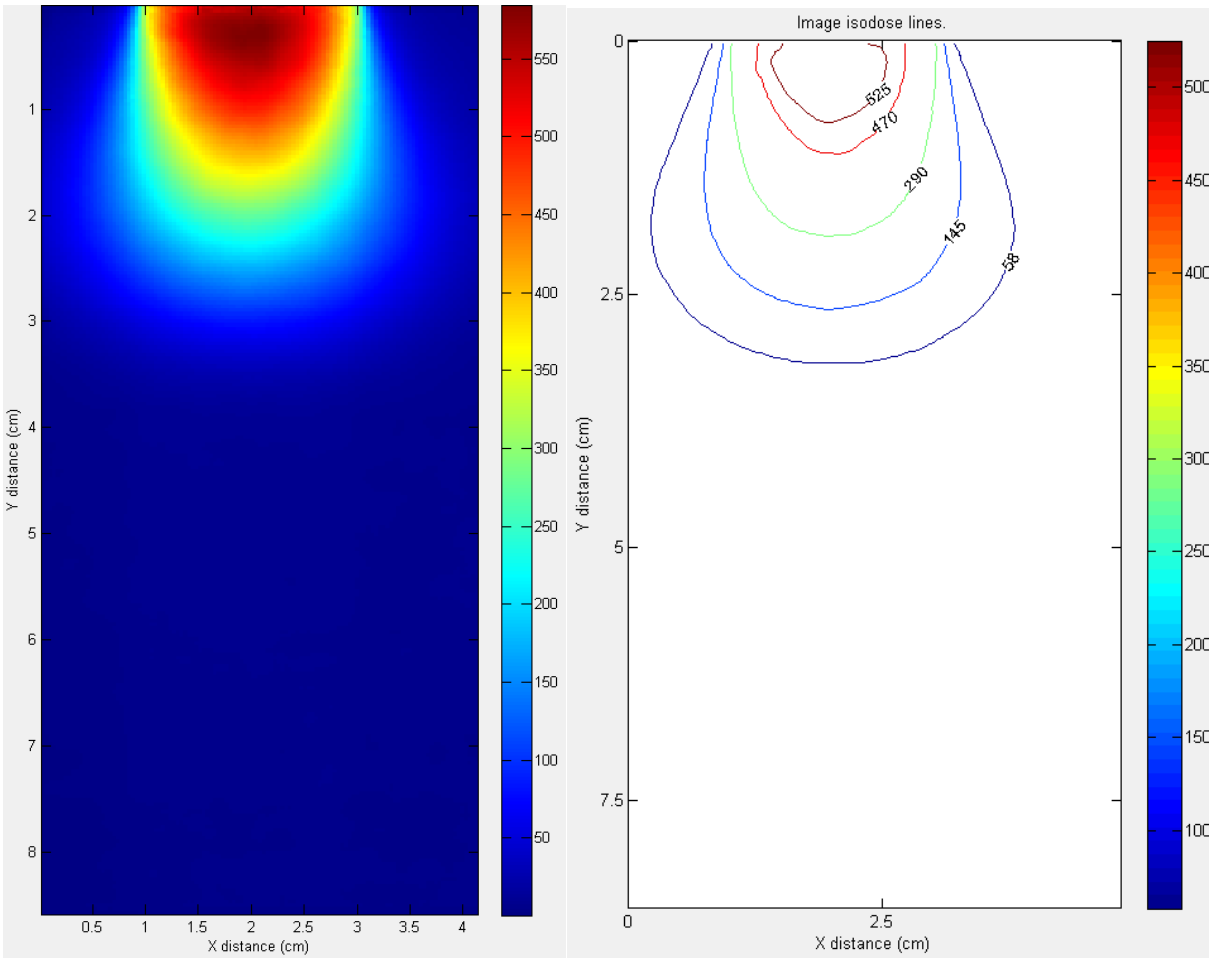

Figure 5.13. Image profile (left) and Isodose lines (right: *10%*, *25%*, *50%*, *80%*, *90%* isodose curves) for *1.27 mm* Al, *8 MeV* at *600 MUs*.

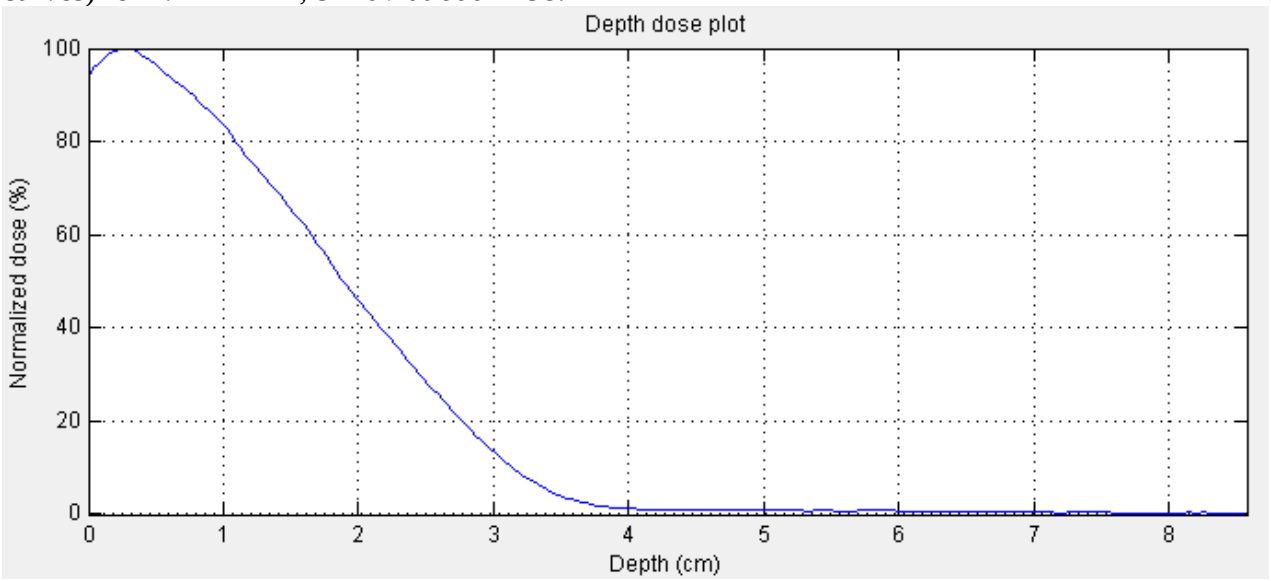

Figure 5.14. Normalized dose *PDD* at central axis for *1.27 mm* Al, *8 MeV* at *600 MUs*.

Table 19: Results for *1.27 mm* Al scatter foil for *8 MeV* electron beam.

Parameter	Results
Beam Energy	*8 MeV*
Foil Material	*Al*
Foil Thickness	*1.27 mm*
Most probable Energy E_{P0}	*6.55 MeV*
Maximum dose, and D_{max}	*584 cGy @ 0.28 cm*
Practical Range R_p	*3.18 cm*
Diameter of *90%* @ D_{max}	*1.11 cm*
Penumbra Size D_{max}, D_{90}, D_{50}, D_{25}	*0.41, 0.65, 1.10, and 1.20 cm*

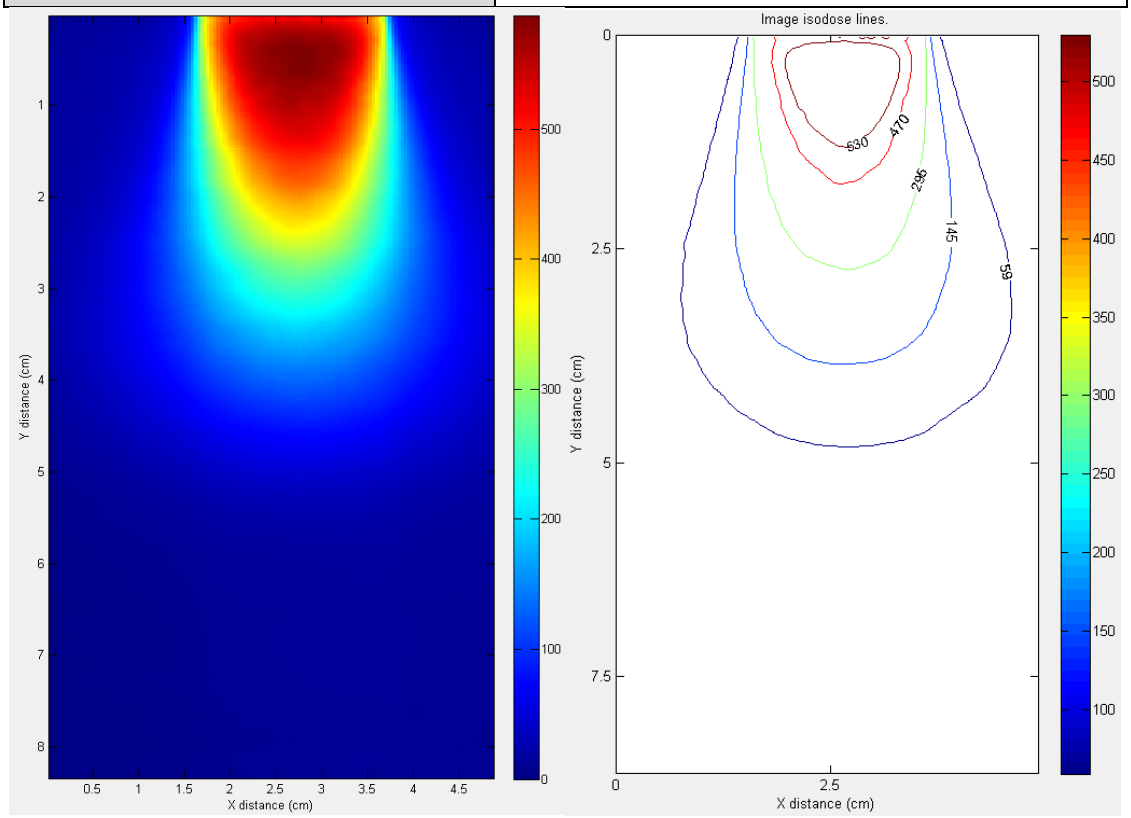

Figure 5.15. Image profile (left) and Isodose lines (right: *10%, 25%, 50%, 80%, 90%* isodose curves) for *1.27 mm* Al, *12 MeV* at *600 MUs*.

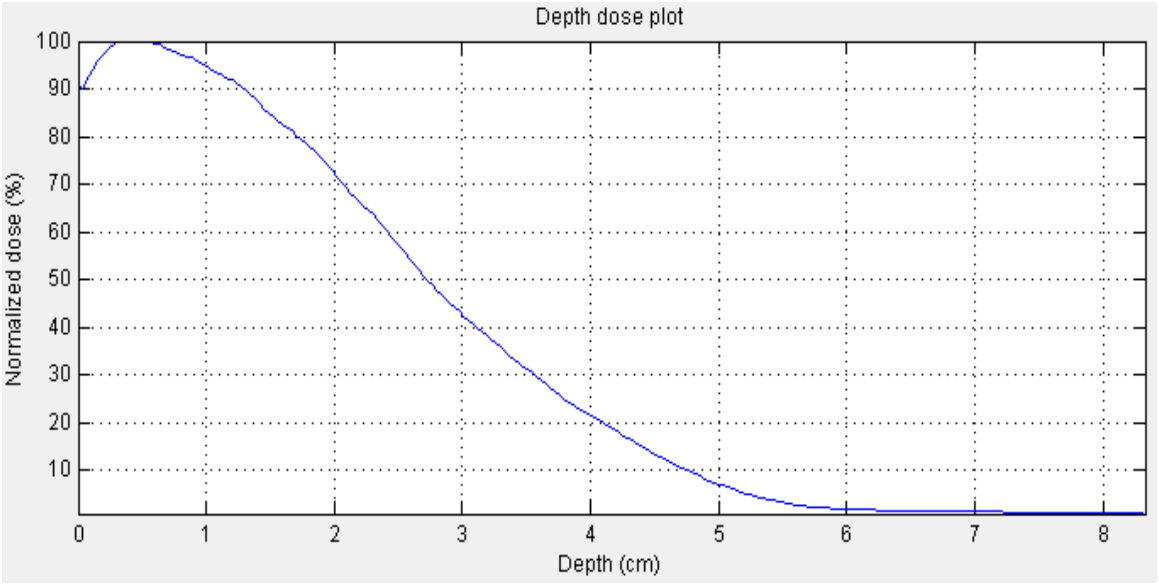

Figure 5.16. Normalized dose *PDD* at central axis for *1.27 mm* Al, *12 MeV* at *600 MUs*.

Table 20: Results for *1.27 mm* Al scatter foil for *12 MeV* electron beam.

Parameter	Results
Beam Energy	*12 MeV*
Foil Material	*Al*
Foil Thickness	*1.27 mm*
Most probable Energy E_{P0}	*9.06 MeV*
Maximum dose, and D_{max}	*588 cGy @ 0.35 cm*
Practical Range R_p	*4.44 cm*
Diameter of *90% @* D_{max}	*1.34 cm*
Penumbra Size D_{max}, D_{90}, D_{50}, D_{25}	*0.35, 0.67, 1.26, and 1.52 cm*

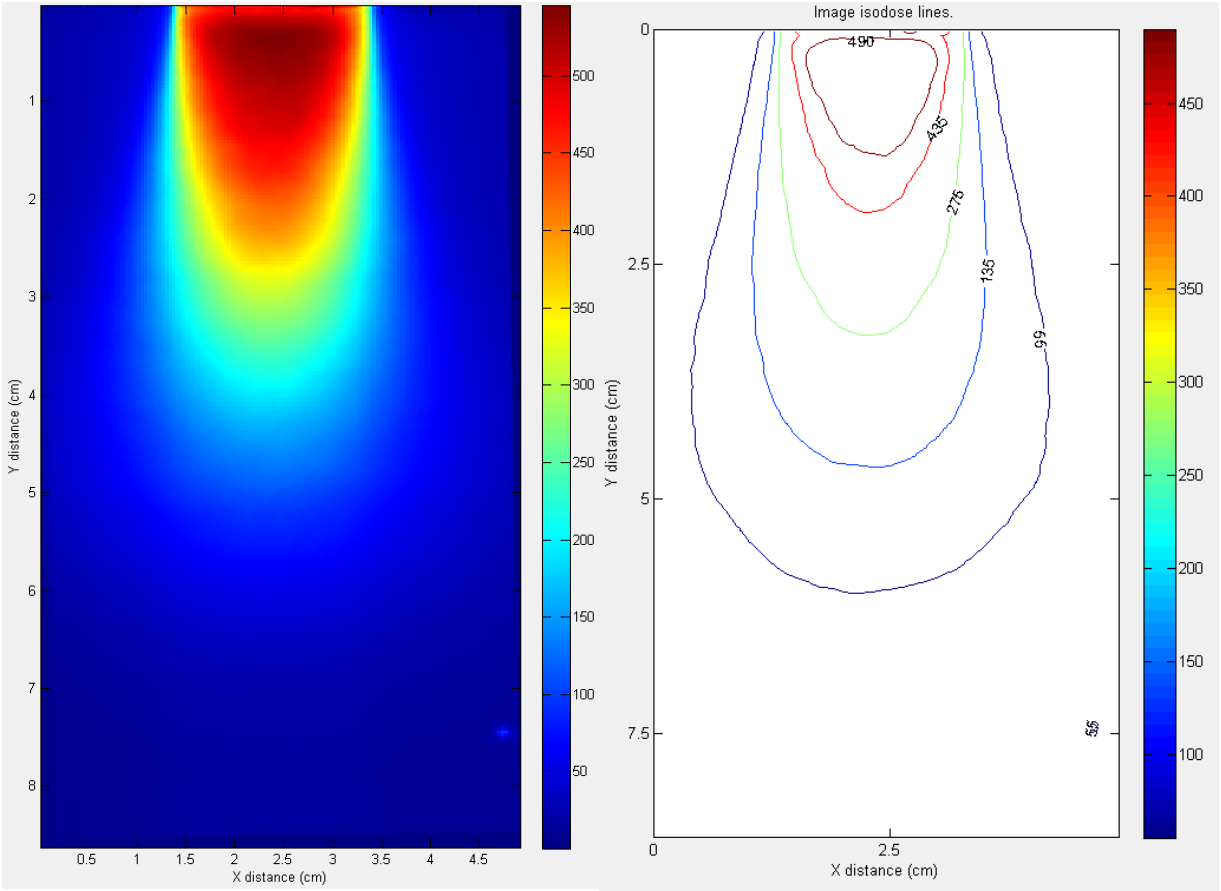

Figure 5.17. Image profile (left) and Isodose lines (right: *10%, 25%, 50%, 80%, 90%* isodose curves) for *1.27 mm* Al, *15 MeV* at *600 MUs*.

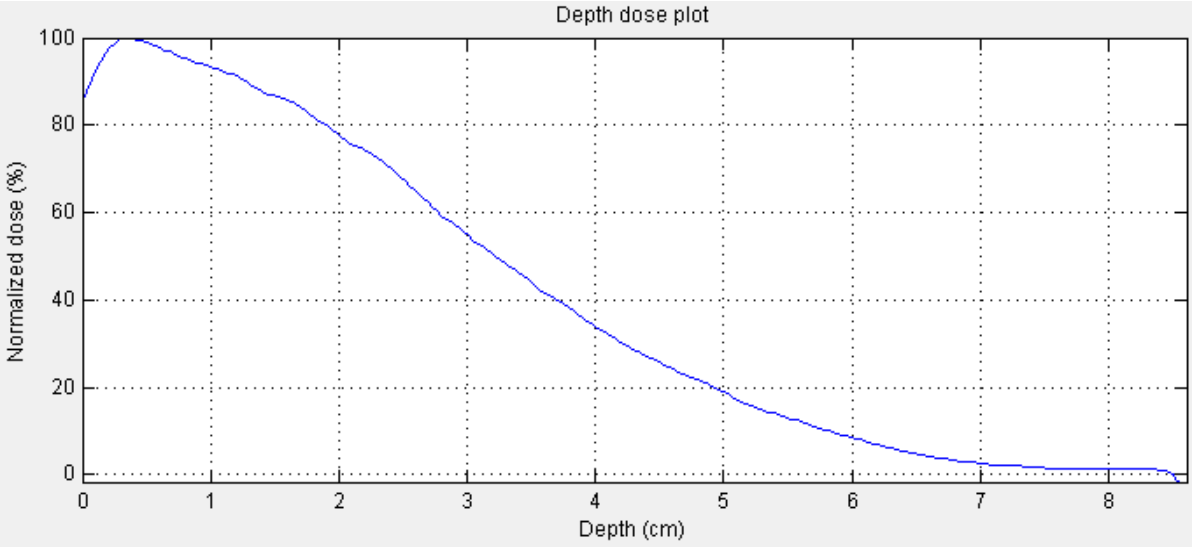

Figure 5.18. Normalized dose *PDD* at central axis for *1.27 mm* Al, *15 MeV* at *600 MUs*.

Table 21: Results for *1.27 mm* Al scatter foil for *15 MeV* electron beam.

Parameter	Results
Beam Energy	*15 MeV*
Foil Material	*Al*
Foil Thickness	*1.27 mm*
Most probable Energy E_{P0}	*11.20 MeV*
Maximum dose, and D_{max}	*546 cGy @ 0.35 cm*
Practical Range R_p	*5.51 cm*
Diameter of *90%* @ D_{max}	*1.38 cm*
Penumbra Size D_{max}, D_{90}, D_{50}, D_{25}	*0.27, 0.547, 1.13, and 1.63 cm*

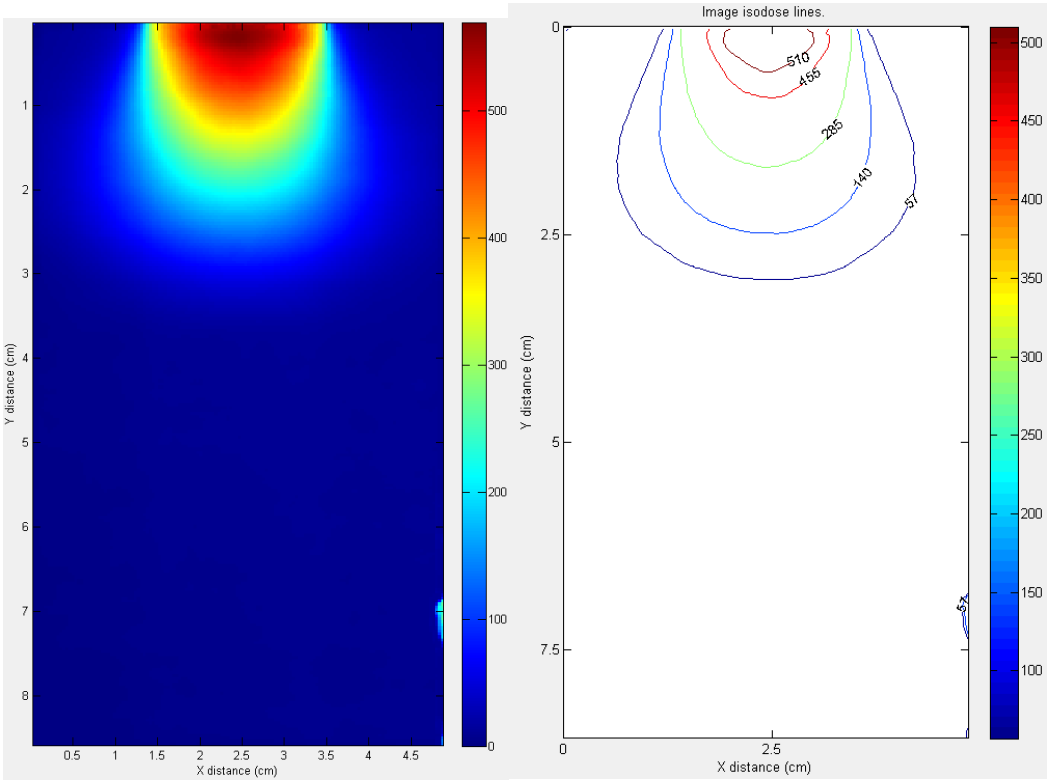

Figure 5.19. Image profile (left) and Isodose lines (right: *10%, 25%, 50%, 80%, 90%* isodose curves) for *1.905 mm* Al, *8 MeV* at *600 MUs*.

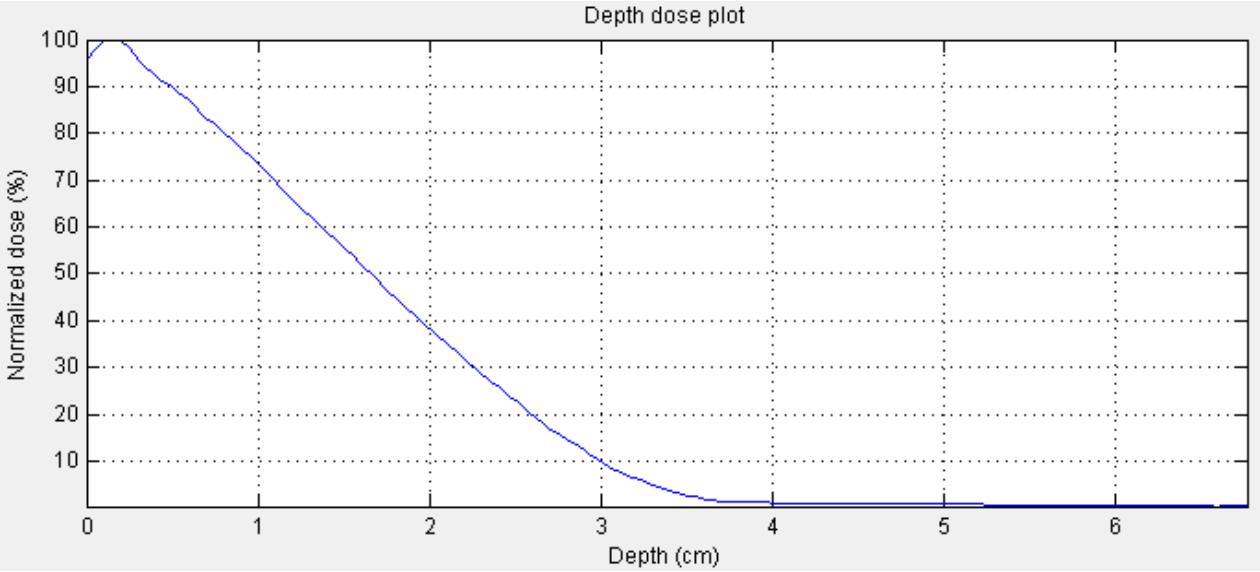

Figure 5.20. Normalized dose *PDD* at central axis for *1.905 mm* Al, *8 MeV* at *600 MUs*.

Table 22: Results for *1.905 mm* Al scatter foil for *8 MeV* electron beam.

Parameter	Results
Beam Energy	*8 MeV*
Foil Material	*Al*
Foil Thickness	*1.905 mm*
Most probable Energy E_{P0}	*6.33 MeV*
Maximum dose, and D_{max}	*570 cGy @ 0.18 cm*
Practical Range R_p	*3.07 cm*
Diameter of *90% @* D_{max}	*1.06 cm*
Penumbra Size D_{max}, D_{90}, D_{50}, D_{25}	*0.48, 0.57, 1.10, and 1.20 cm*

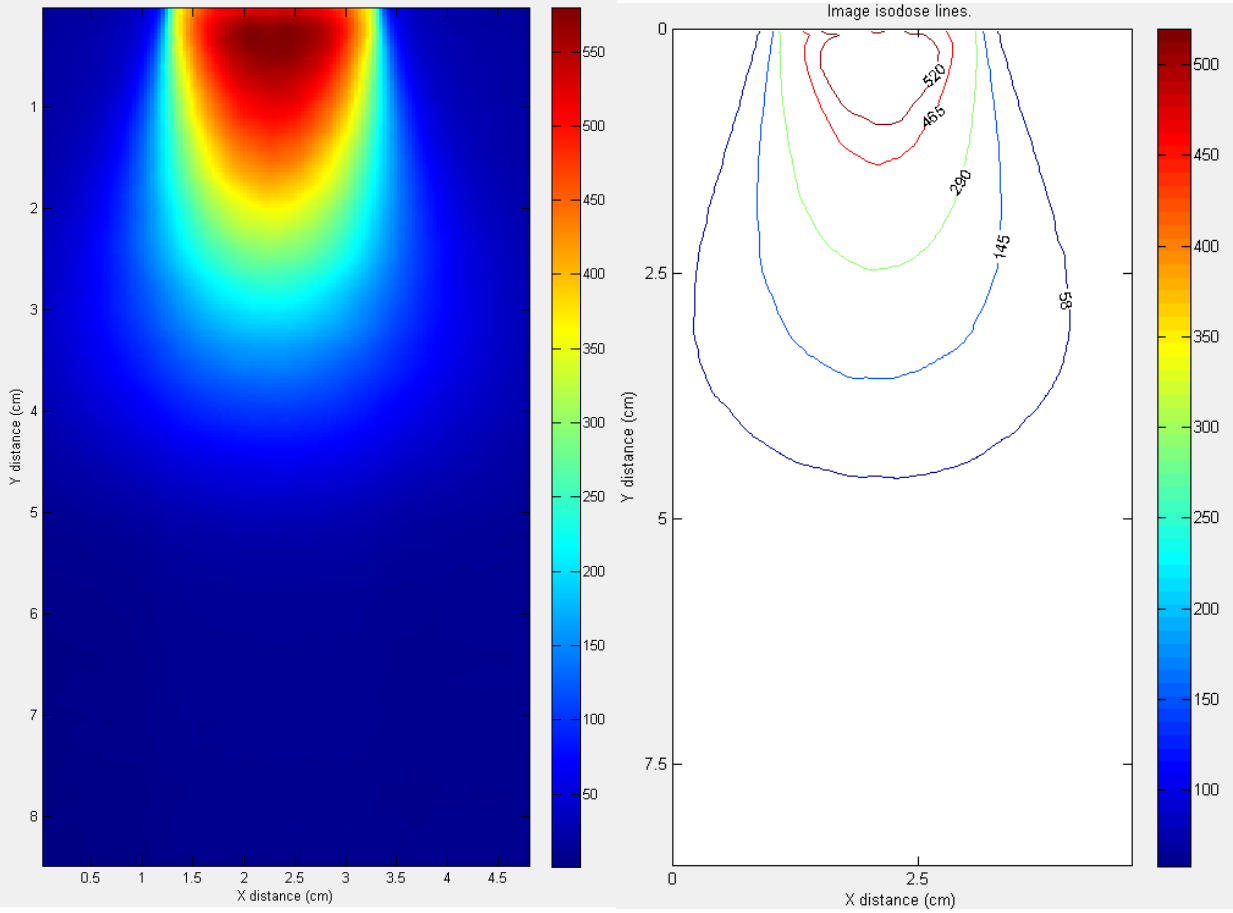

Figure 5.21. Image profile (left) and Isodose lines (right: *10%, 25%, 50%, 80%, 90%* isodose curves) for *1.905 mm* Al, *12 MeV* at *600 MUs*.

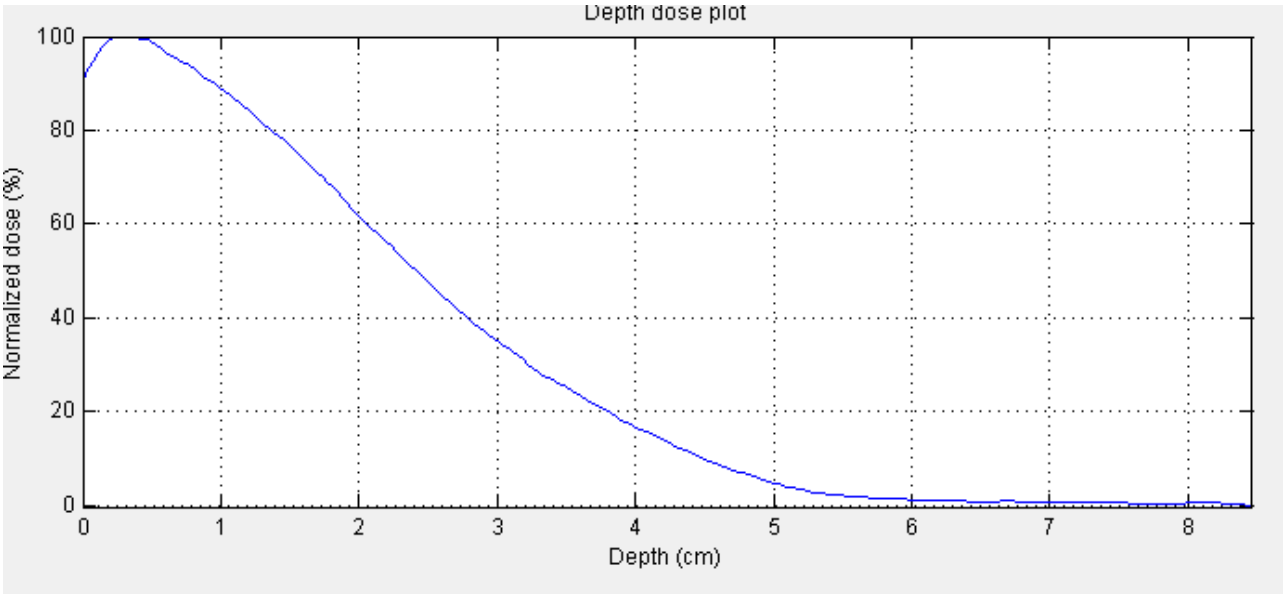

Figure 5.22. Normalized dose *PDD* at central axis for *1.905 mm* Al, *12 MeV* at *600 MUs*.

Table 23: Results for *1.905 mm* Al scatter foil for *12 MeV* electron beam.

Parameter	Results
Beam Energy	*12 MeV*
Foil Material	*Al*
Foil Thickness	*1.905 mm*
Most probable Energy E_{P0}	*8.61 MeV*
Maximum dose, and D_{max}	*579 cGy @ 0.28 cm*
Practical Range R_p	*4.22 cm*
Diameter of *90%* @ D_{max}	*1.20 cm*
Penumbra Size D_{max}, D_{90}, D_{50}, D_{25}	*0.38, 0.62, 1.13, and 1.70 cm*

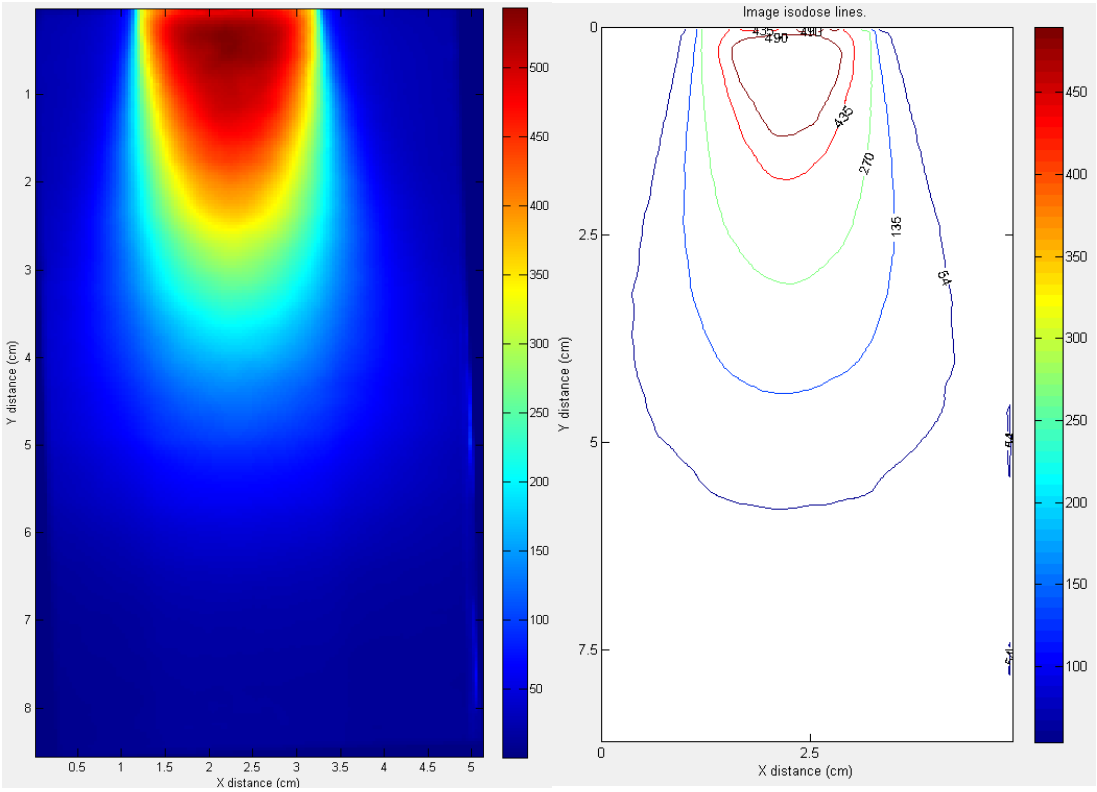

Figure 5.23. Image profile (left) and Isodose lines (right: *10%, 25%, 50%, 80%, 90%* isodose curves) for *1.905 mm* Al, *15 MeV* at *600 MUs*.

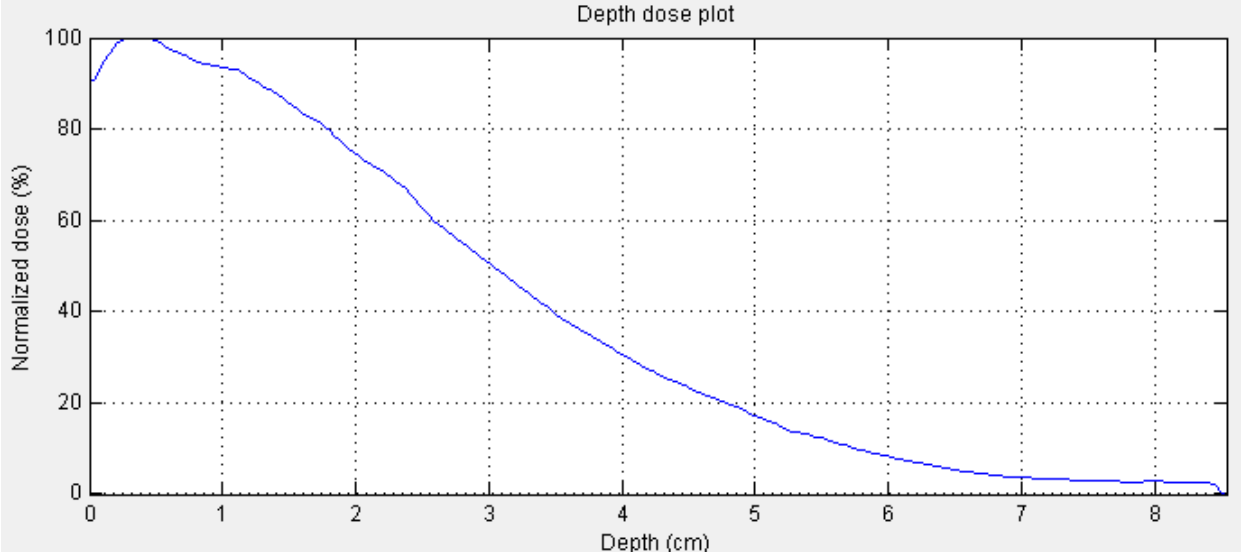

Figure 5.24. Normalized dose *PDD* at central axis for *1.905 mm* Al, *15 MeV* at *600 MUs.*

Table 24: Results for *1.905 mm* Al scatter foil for *15 MeV* electron beam.

Parameter	Results
Beam Energy	*15 MeV*
Foil Material	*Al*
Foil Thickness	*1.905 mm*
Most probable Energy E_{P0}	*10.70 MeV*
Maximum dose, and D_{max}	*543 cGy @ 0.32cm*
Practical Range R_p	*5.26 cm*
Diameter of *90% @* D_{max}	*1.34 cm*
Penumbra Size D_{max}, D_{90}, D_{50}, D_{25}	*0.31, 0.60, 1.11, and 1.30 cm*

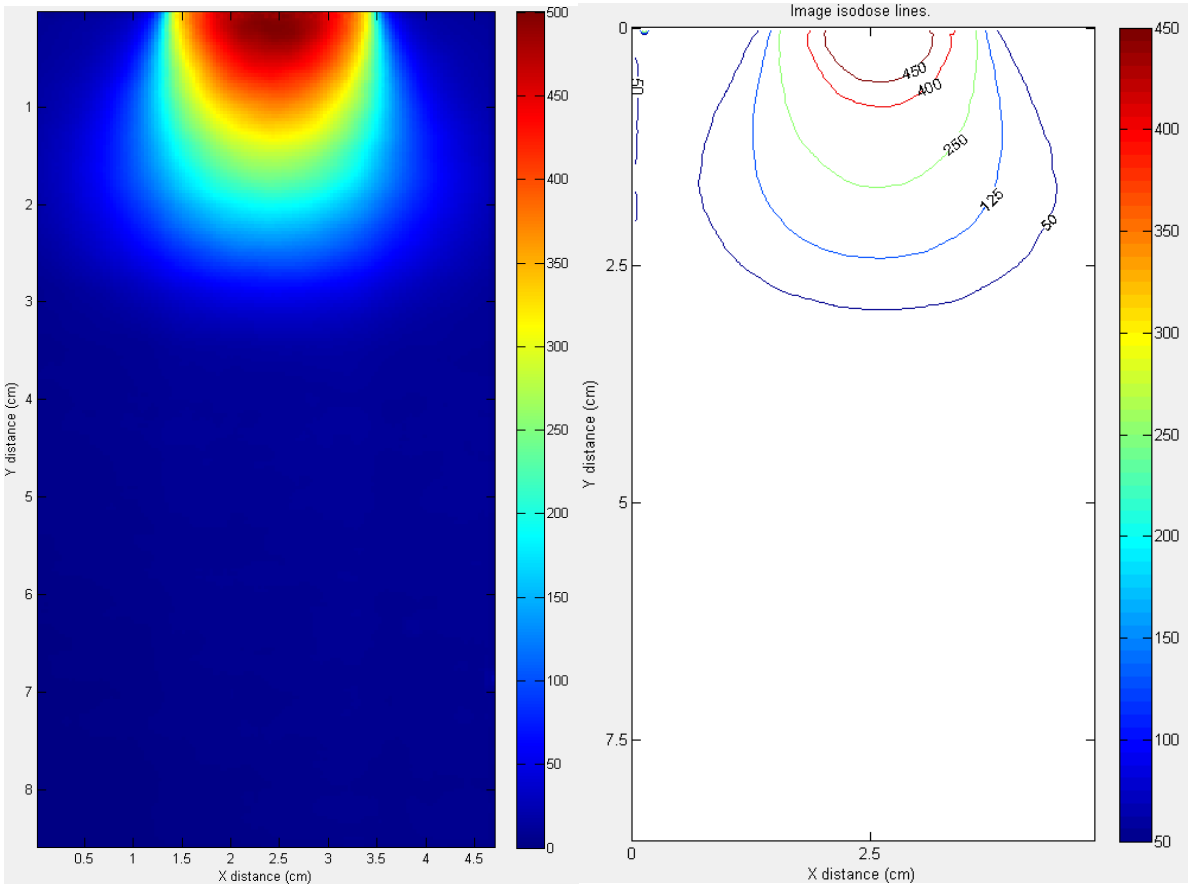

Figure 5.25. Image profile (left) and Isodose lines (right: *10%*, *25%*, *50%*, *80%*, *90%* isodose curves) for *2.54 mm* Al, *8 MeV* at *600 MUs*.

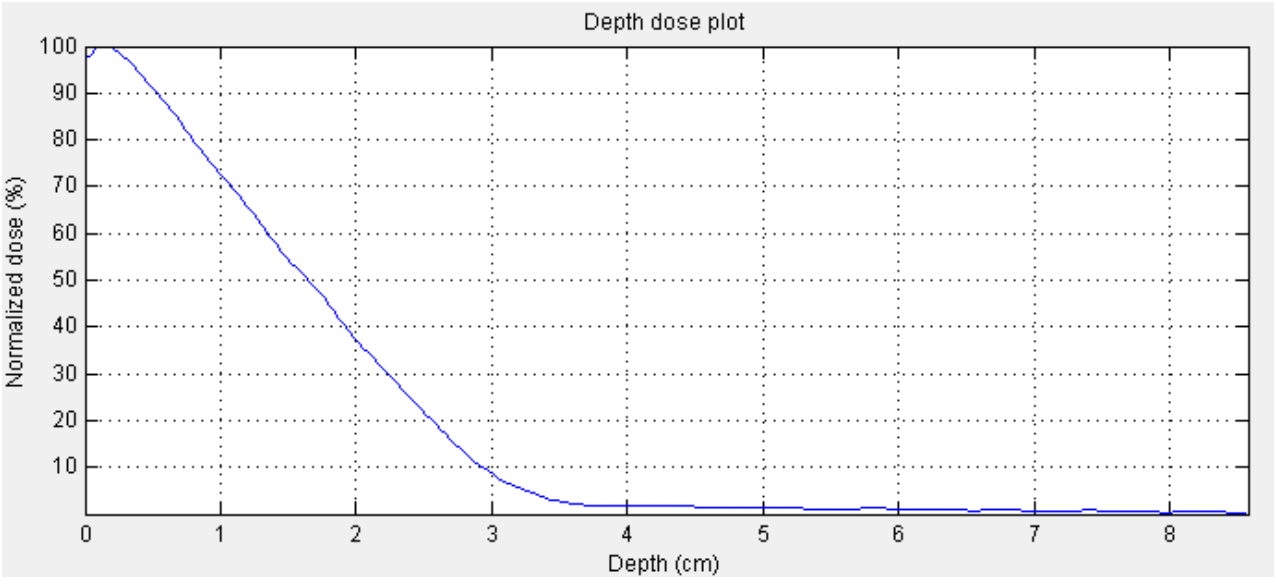

Figure 5.26. Normalized dose *PDD* at central axis for *2.54 mm* Al, *8 MeV* at *600 MUs*.

Table 25: Results for *2.54 mm* Al scatter foil for *8 MeV* electron beam.

Parameter	Results
Beam Energy	*8 MeV*
Foil Material	*Al*
Foil Thickness	*2.54 mm*
Most probable Energy E_{P0}	*6.45 MeV*
Maximum dose, and D_{max}	*500 cGy @ 0.14 cm*
Practical Range R_p	*3.13 cm*
Diameter of *90% @* D_{max}	*1.13 cm*
Penumbra Size D_{max}, D_{90}, D_{50}, D_{25}	*0.46, 0.64, 1.15, and 1.27 cm*

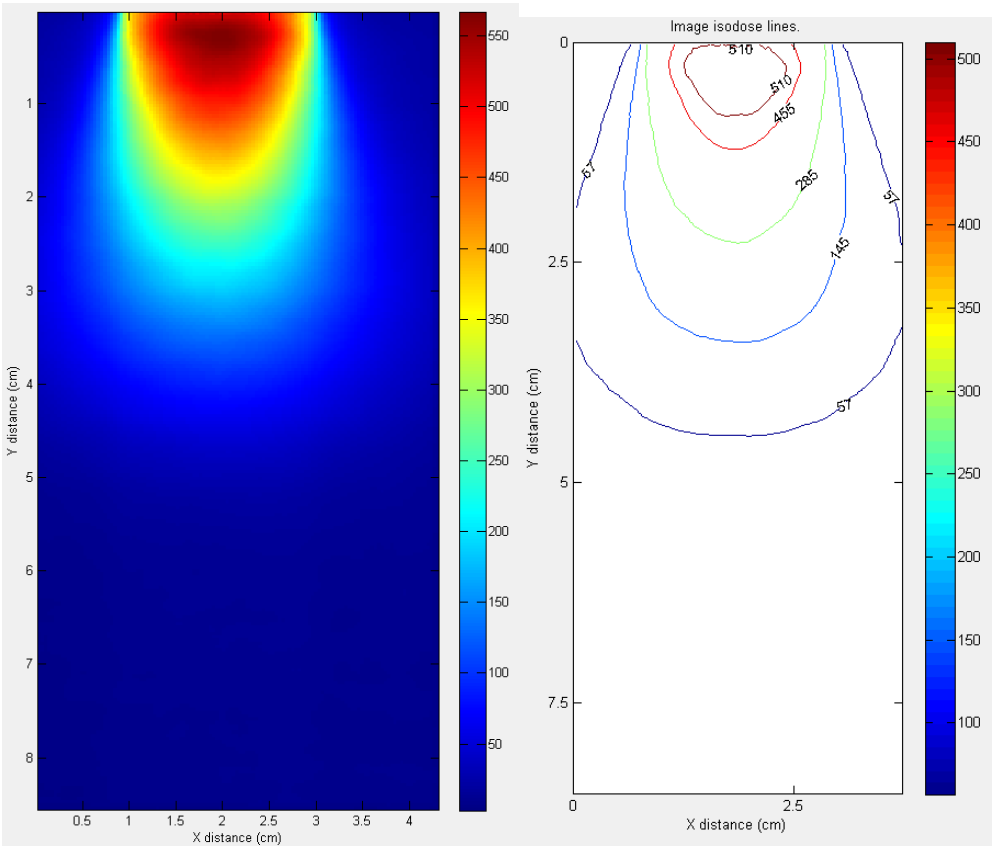

Figure 5.27. Image profile (left) and Isodose lines (right: *10%, 25%, 50%, 80%, 90%* isodose curves) for *2.54 mm* Al, *12 MeV* at *600 MUs*.

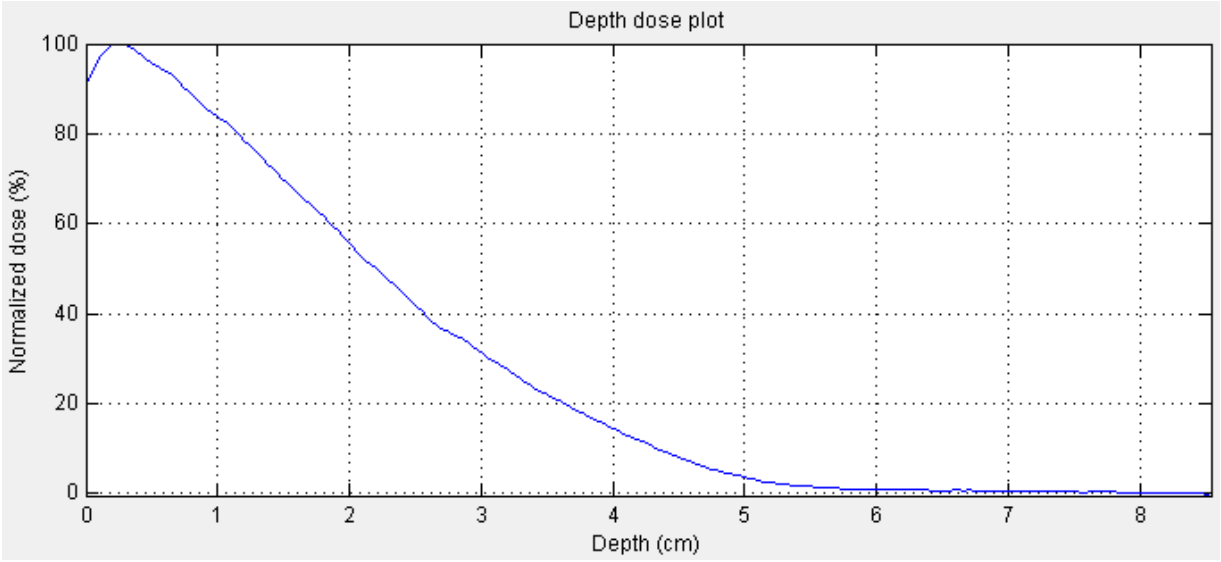

Figure 5.28. Normalized dose *PDD* at central axis for *2.54 mm* Al, *12 MeV* at *600 MUs*.

Table 26: Results for *2.54 mm* Al scatter foil for *12 MeV* electron beam.

Parameter	Results
Beam Energy	*12 MeV*
Foil Material	*Al*
Foil Thickness	*2.54 mm*
Most probable Energy E_{P0}	*8.20 MeV*
Maximum dose, and D_{max}	*565 cGy @ 0.25 cm*
Practical Range R_p	*4.01 cm*
Diameter of *90% @* D_{max}	*1.16 cm*
Penumbra Size D_{max}, D_{90}, D_{50}, D_{25}	*0.41, 0.58, 1.15, and 1.50 cm*

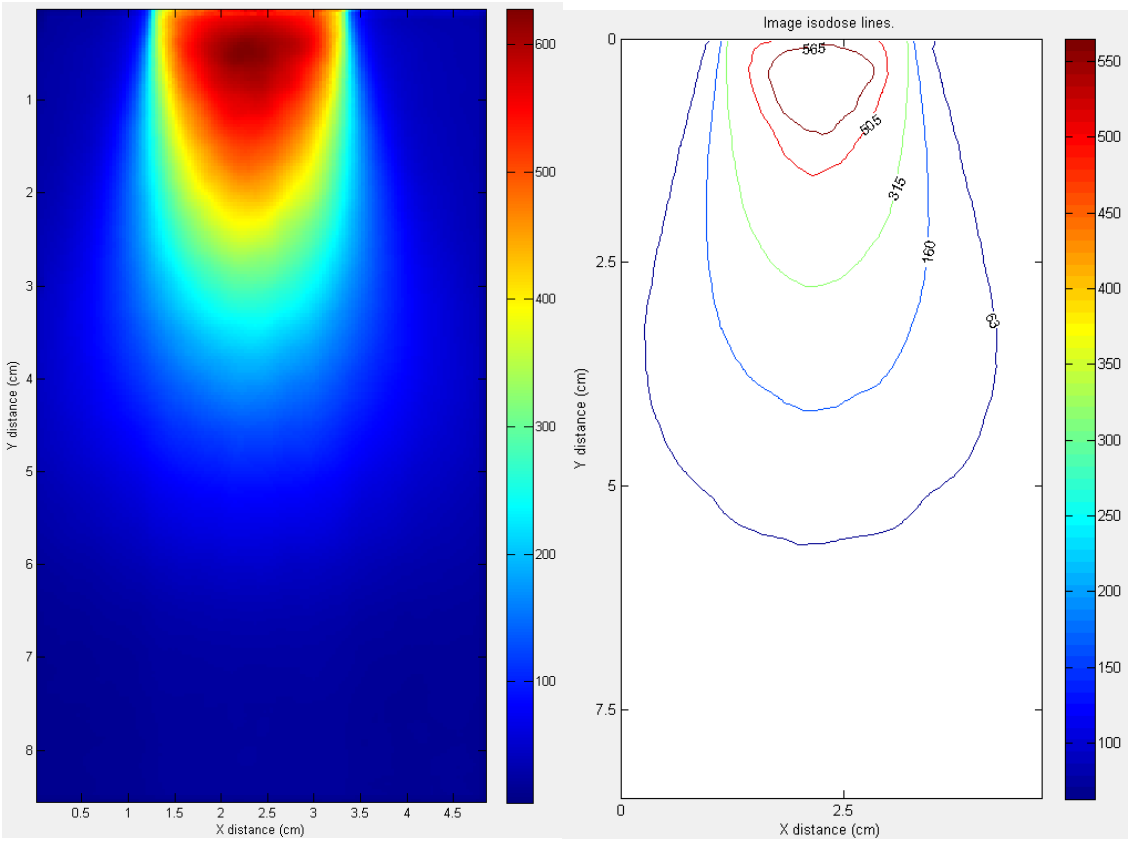

Figure 5.29. Image profile (left) and Isodose lines (right: *10%, 25%, 50%, 80%, 90%* isodose curves) for *2.54 mm* Al, *15 MeV* at *600 MUs*.

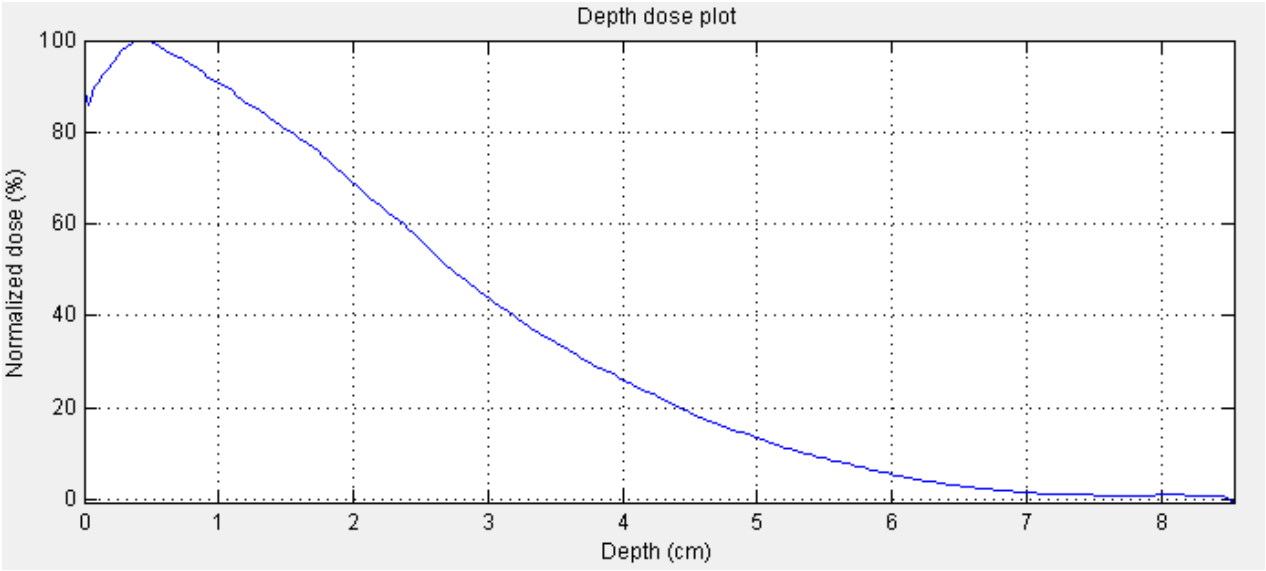

Figure 5.30. Normalized dose *PDD* at central axis for *2.54 mm* Al, *15 MeV* at *600 MUs*.

Table 27: Results for *2.54 mm* Al scatter foil for *15 MeV* electron beam.

Parameter	Results
Beam Energy	*15 MeV*
Foil Material	*Al*
Foil Thickness	*2.54 mm*
Most probable Energy E_{P0}	*9.78 MeV*
Maximum dose, and D_{max}	*628 cGy @ 0.43 cm*
Practical Range R_p	*4.80 cm*
Diameter of *90%* @ D_{max}	*1.15 cm*
Penumbra Size D_{max}, D_{90}, D_{50}, D_{25}	*0.36, 0.62, 1.15, and 1.63 cm*

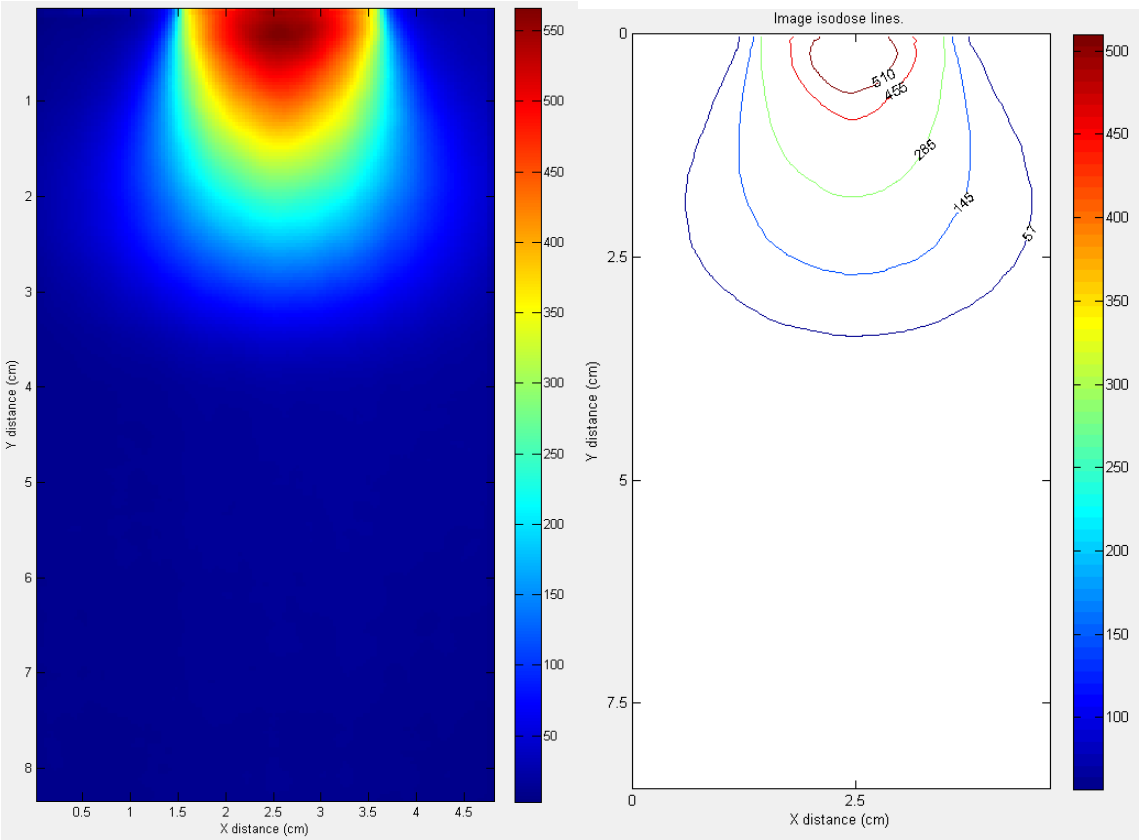

Figure 5.31. Image profile (left) and Isodose lines (right: *10%, 25%, 50%, 80%, 90%* isodose curves) for *0.1524 mm* Pb, *8 MeV* at *600 MUs*.

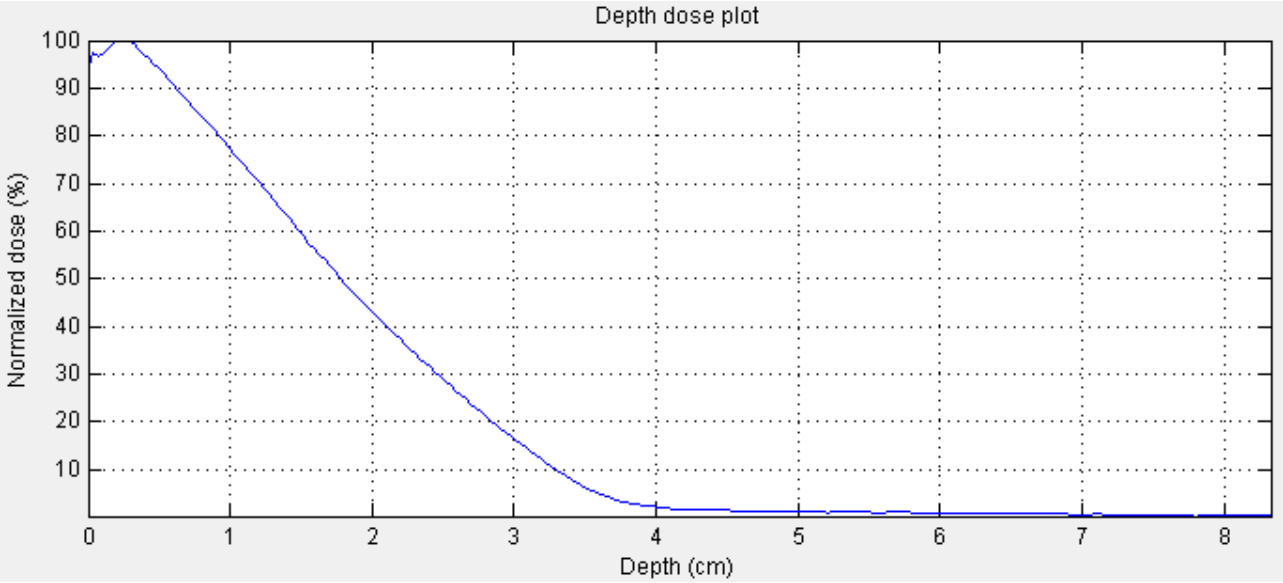

Figure 5.32. Normalized dose *PDD* at central axis for *0.1524 mm* Pb, *8 MeV* at *600 MUs*.

Table 28: Results for *0.1524 mm* Pb scatter foil for *8 MeV* electron beam.

Parameter	Results
Beam Energy	*8 MeV*
Foil Material	*Pb*
Foil Thickness	*0.1524 mm*
Most probable Energy E_{P0}	*6.80 MeV*
Maximum dose, and D_{max}	*567 cGy @ 0.25 cm*
Practical Range R_p	*3.31 cm*
Diameter of *90%* @ D_{max}	*0.97 cm*
Penumbra Size D_{max}, D_{90}, D_{50}, D_{25}	*0.50, 0.67, 1.14, and 1.48 cm*

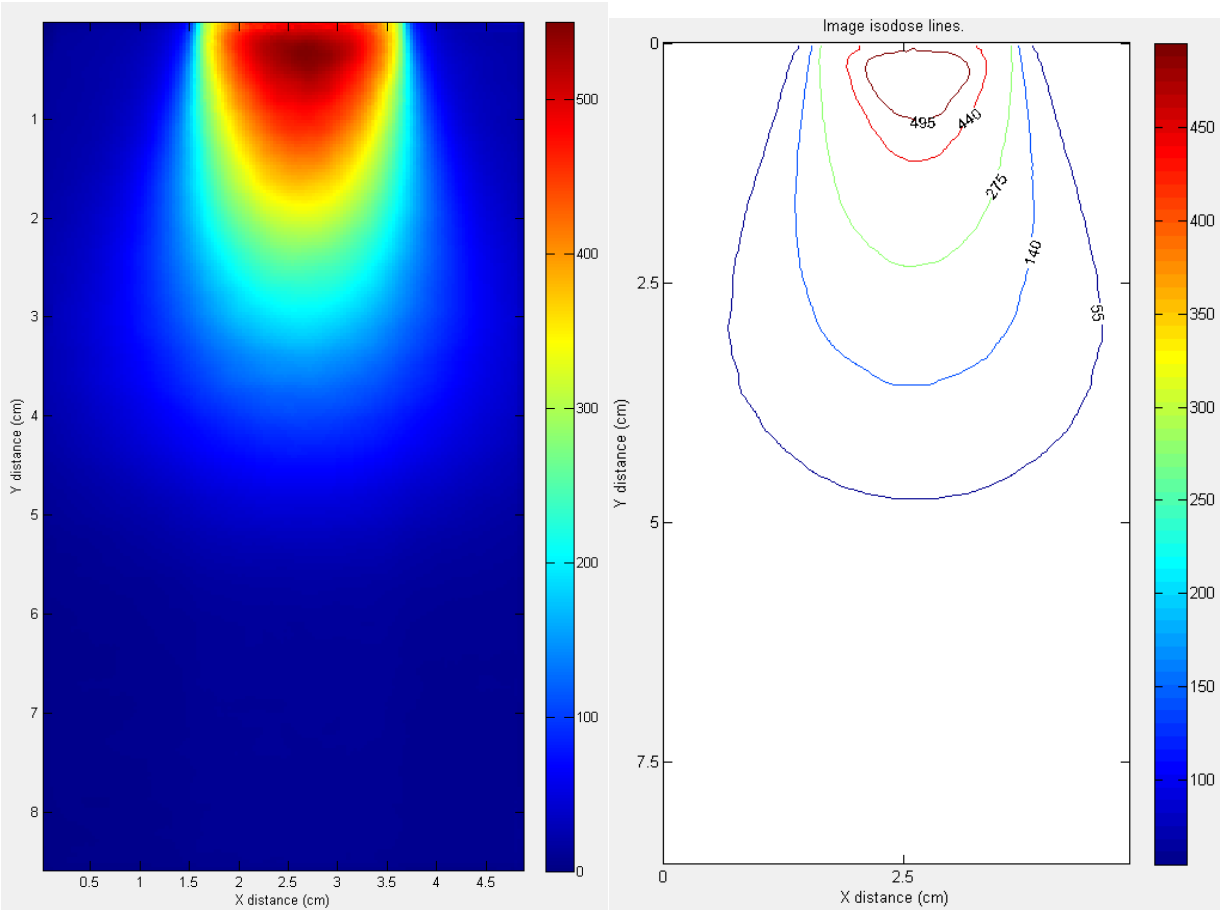

Figure 5.33. Image profile (left) and Isodose lines (right: *10%*, *25%*, *50%*, *80%*, *90%* isodose curves) for *0.1524 mm* Pb, *12 MeV* at *600 MUs*.

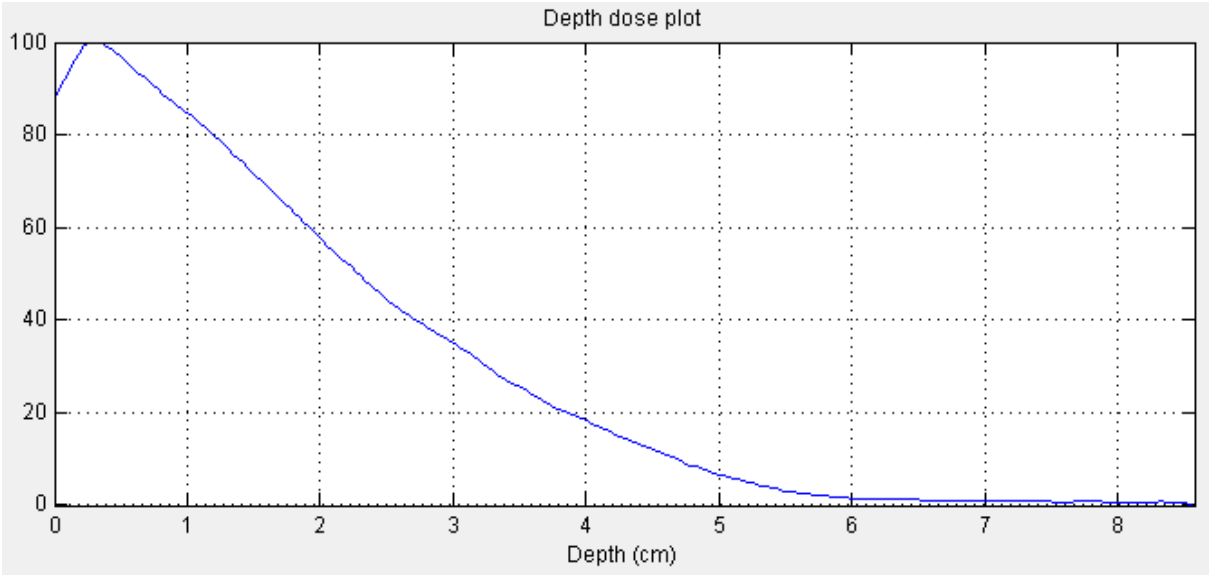

Figure 5.34. Normalized dose *PDD* at central axis for *0.1524 mm* Pb, *12 MeV* at *600 MUs*.

Table 29: Results for *0.1524 mm* Pb scatter foil for *12 MeV* electron beam.

Parameter	Results
Beam Energy	*12 MeV*
Foil Material	*Pb*
Foil Thickness	*0.1524 mm*
Most probable Energy E_{P0}	*8.72 MeV*
Maximum dose, and D_{max}	*551 cGy @ 0.32 cm*
Practical Range R_p	*4.27 cm*
Diameter of *90%* @ D_{max}	*1.08 cm*
Penumbra Size D_{max}, D_{90}, D_{50}, D_{25}	*0.48, 0.64, 1.16, and 1.62 cm*

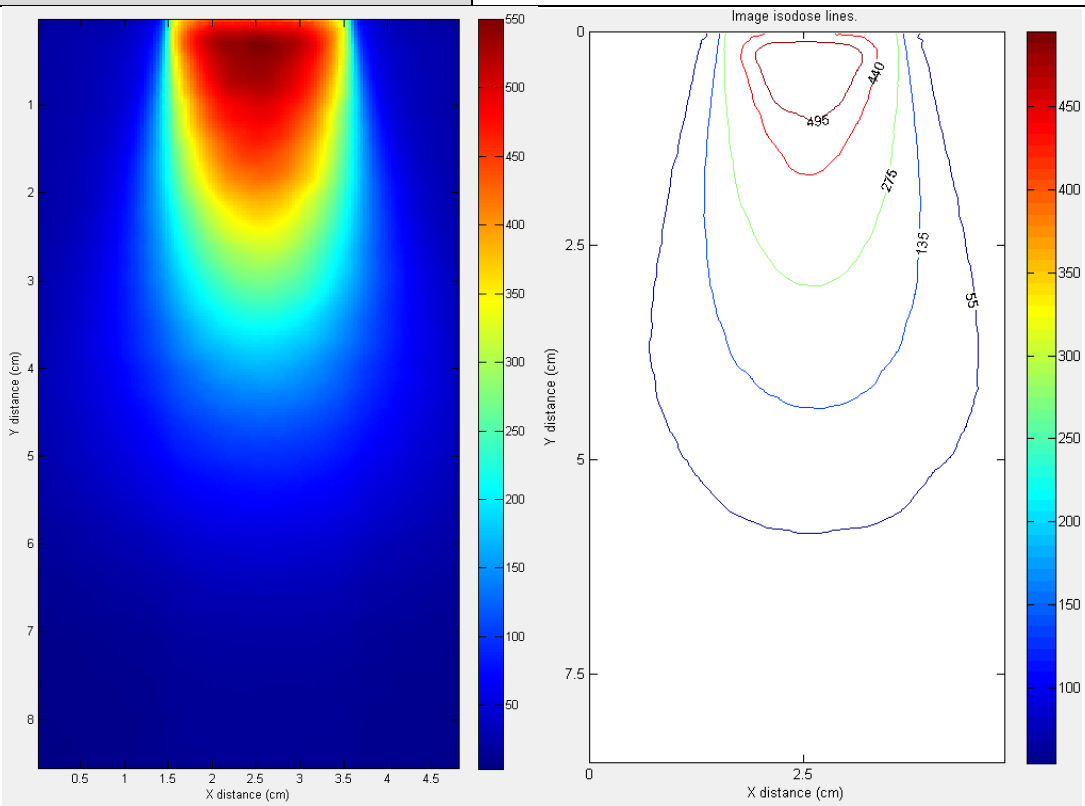

Figure 5.35. Image profile (left) and Isodose lines (right: *10%, 25%, 50%, 80%, 90%* isodose curves) for *0.1524 mm* Pb, *15 MeV* at *600 MUs*.

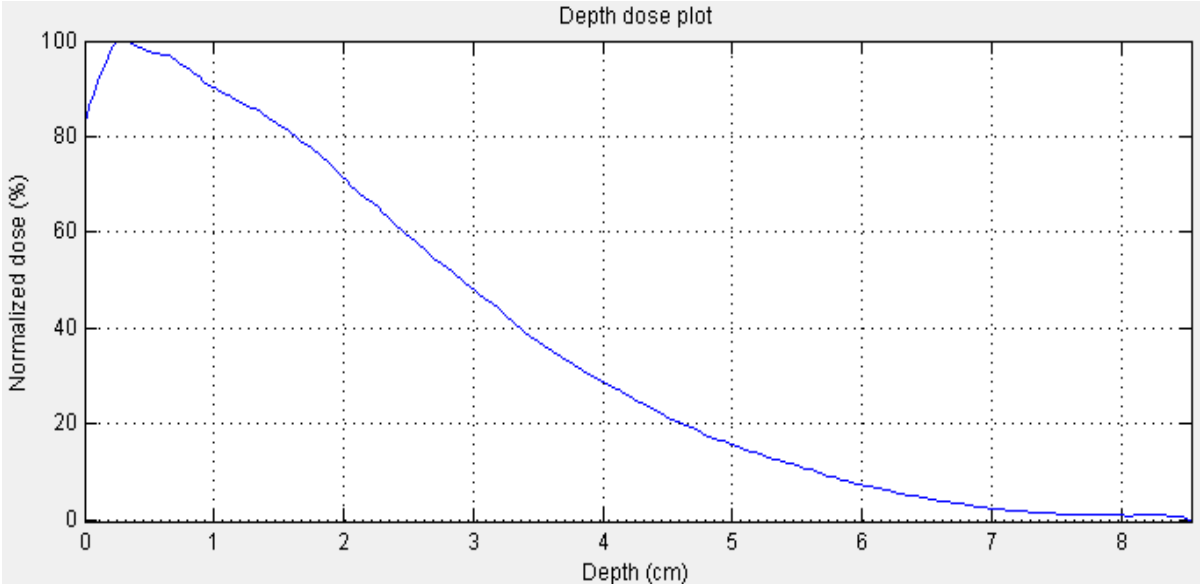

Figure 5.36. Normalized dose *PDD* at central axis for *0.1524 mm* Pb, *15 MeV* at *600 MUs*.

Table 30: Results for *0.1524 mm* Pb scatter foil for *15 MeV* electron beam.

Parameter	Results
Beam Energy	*15 MeV*
Foil Material	*Pb*
Foil Thickness	*0.1524 mm*
Most probable Energy E_{P0}	*10.56 MeV*
Maximum dose, and D_{max}	*550 cGy @ 0.28 cm*
Practical Range R_p	*5.19 cm*
Diameter of *90% @* D_{max}	*1.26 cm*
Penumbra Size D_{max}, D_{90}, D_{50}, D_{25}	*0.31, 0.57, 1.14, and 1.67 cm*

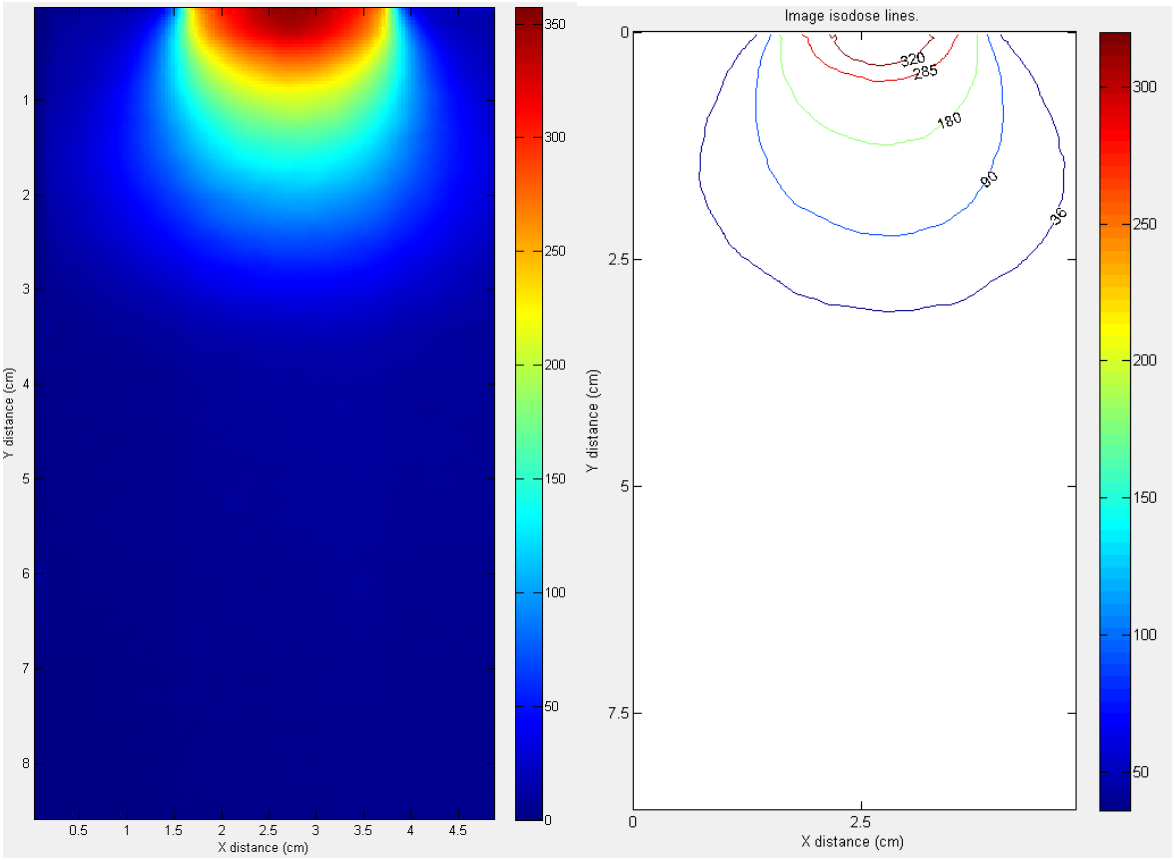

Figure 5.37. Image profile (left) and Isodose lines (right: *10%, 25%, 50%, 80%, 90%* isodose curves) for *0.4572 mm* Pb, *8 MeV* at *600 MUs*.

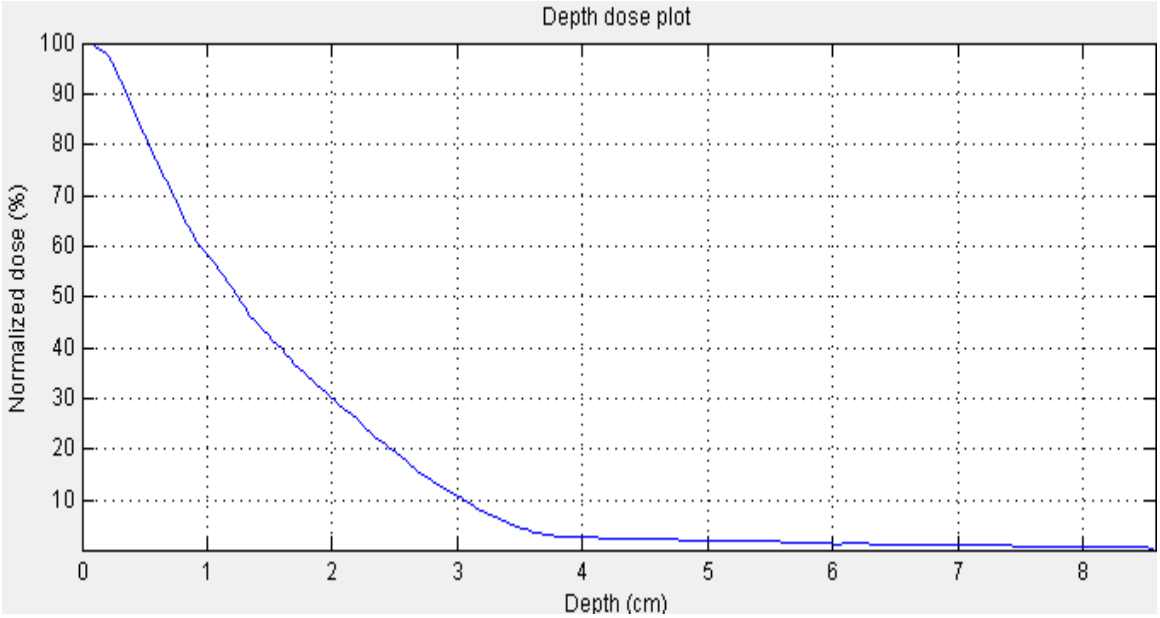

Figure 5.38. Normalized dose *PDD* at central axis for *0.4572 mm* Pb, *8 MeV* at *600 MUs*.

Table 31: Results for *0.4572 mm* Pb scatter foil for *8 MeV* electron beam.

Parameter	Results
Beam Energy	*8 MeV*
Foil Material	*Pb*
Foil Thickness	*0.4572 mm*
Most probable Energy E_{P0}	*5.78 MeV*
Maximum dose, and D_{max}	*358 cGy @ 0 cm*
Practical Range R_p	*2.80 cm*
Diameter of *90%* @ D_{max}	*1.07 cm*
Penumbra Size D_{max}, D_{90}, D_{50}, D_{25}	*0.42, 0.62, 1.24, and 1.47 cm*

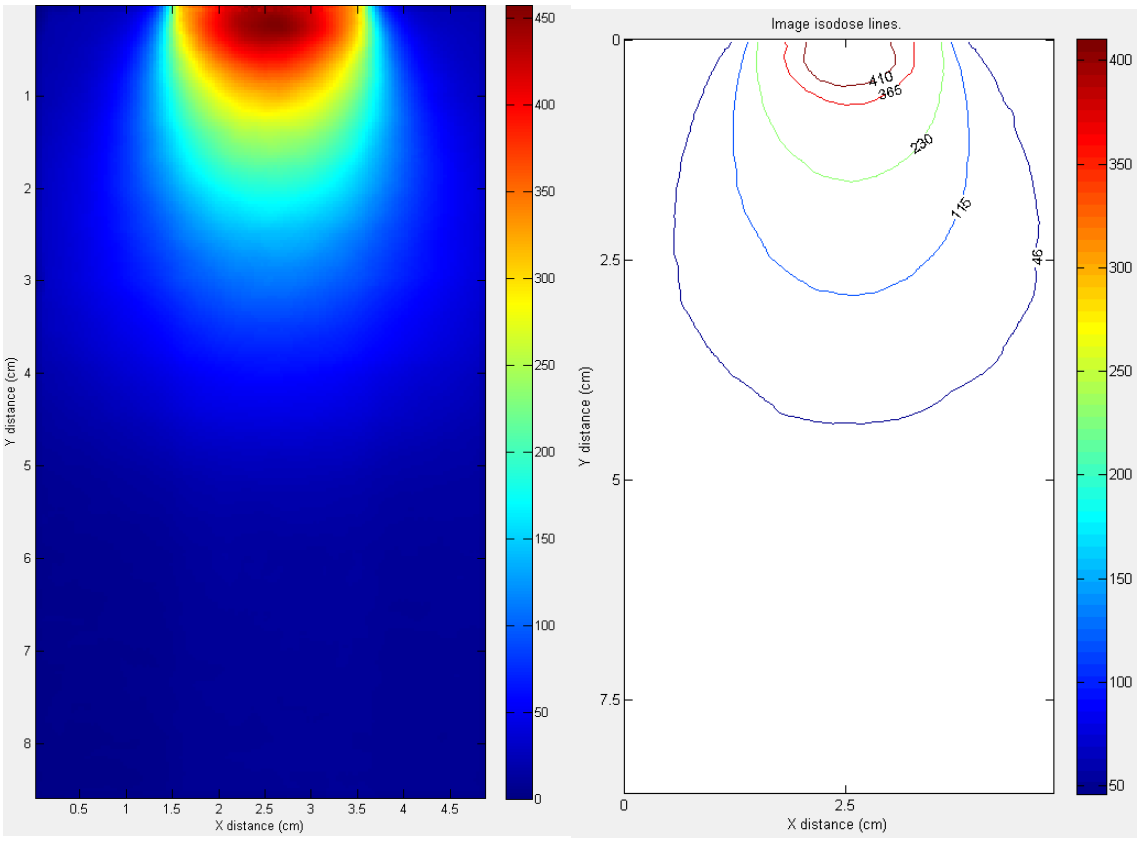

Figure 5.39. Image profile (left) and Isodose lines (right: *10%, 25%, 50%, 80%, 90%* isodose curves) for *0.4572 mm* Pb, *12 MeV* at *600 MUs*.

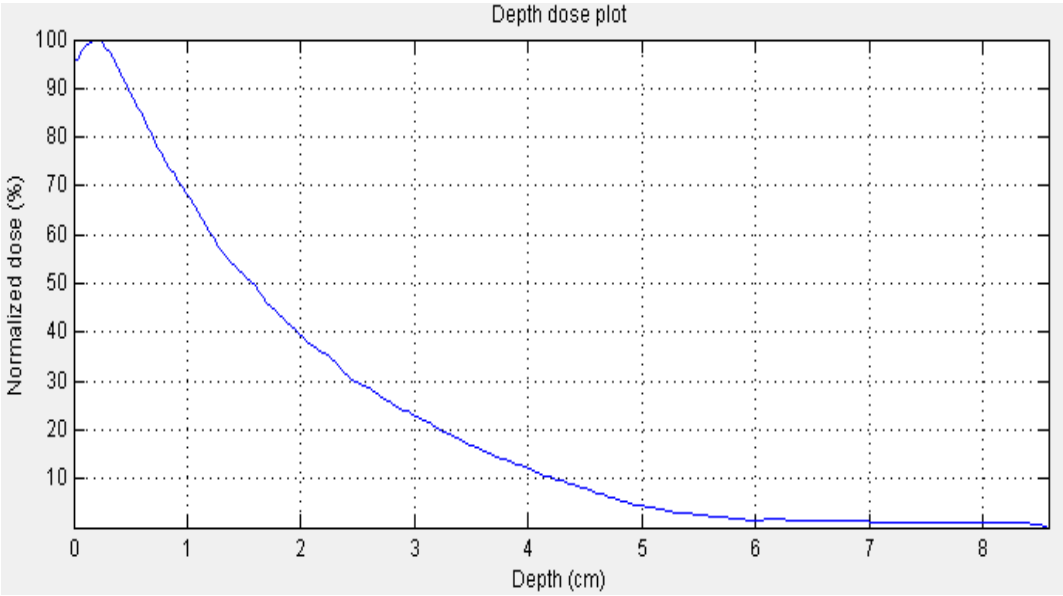

Figure 5.40. Normalized dose *PDD* at central axis for *0.4572 mm* Pb, *12 MeV* at *600 MUs*.

Table 32: Results for *0.4572 mm* Pb scatter foil for *12 MeV* electron beam.

Parameter	Results
Beam Energy	*12 MeV*
Foil Material	*Pb*
Foil Thickness	*0.4572 mm*
Most probable Energy E_{P0}	*7.19 MeV*
Maximum dose, and D_{max}	*458 cGy @ 0.21 cm*
Practical Range R_p	*3.50 cm*
Diameter of *90% @* D_{max}	*1.02 cm*
Penumbra Size D_{max}, D_{90}, D_{50}, D_{25}	*0.53, 0.64, 1.13, and 1.52 cm*

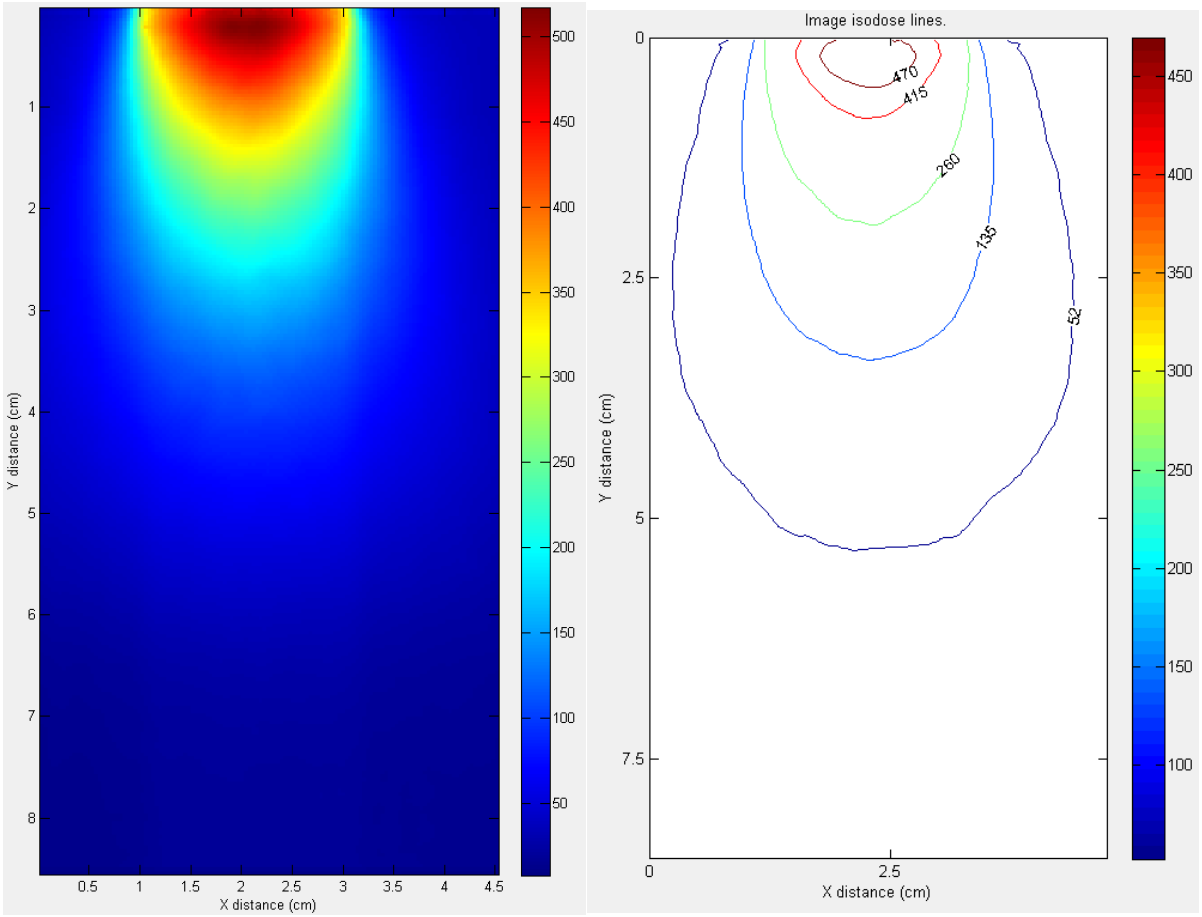

Figure 5.41. Image profile (left) and Isodose lines (right: *10%, 25%, 50%, 80%, 90%* isodose curves) for *0.4572 mm* Pb, *15 MeV* at *600 MUs*.

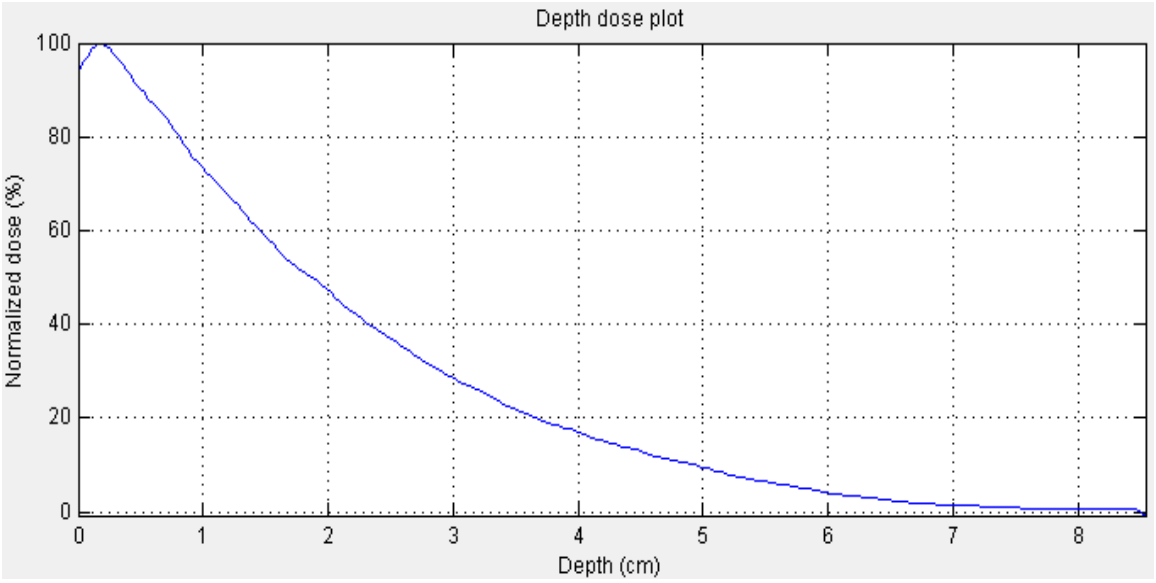

Figure 5.42. Normalized dose *PDD* at central axis for *0.4572 mm* Pb, *15 MeV* at *600 MUs*.

Table 33: Results for *0.4572 mm* Pb scatter foil for *15 MeV* electron beam.

Parameter	Results
Beam Energy	*15 MeV*
Foil Material	*Pb*
Foil Thickness	*0.4572 mm*
Most probable Energy E_{P0}	*8.39 MeV*
Maximum dose, and D_{max}	*518 cGy @ 0.18 cm*
Practical Range R_p	*4.11 cm*
Diameter of *90%* @ D_{max}	*1.04 cm*
Penumbra Size D_{max}, D_{90}, D_{50}, D_{25}	*0.54, 0.69, 1.24, and 1.41 cm*

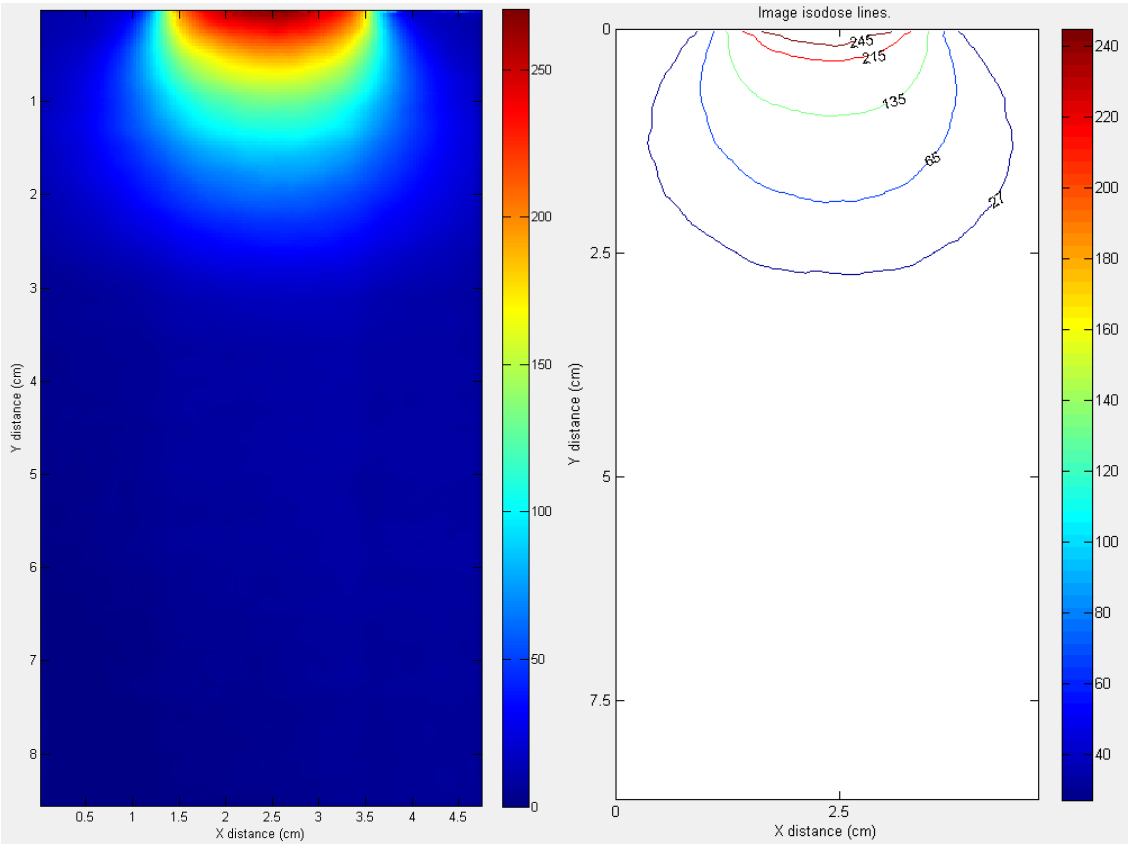

Figure 5.43. Image profile (left) and Isodose lines (right: *10%, 25%, 50%, 80%, 90%* isodose curves) for *0.762 mm* Pb, *8 MeV* at *600 MUs*.

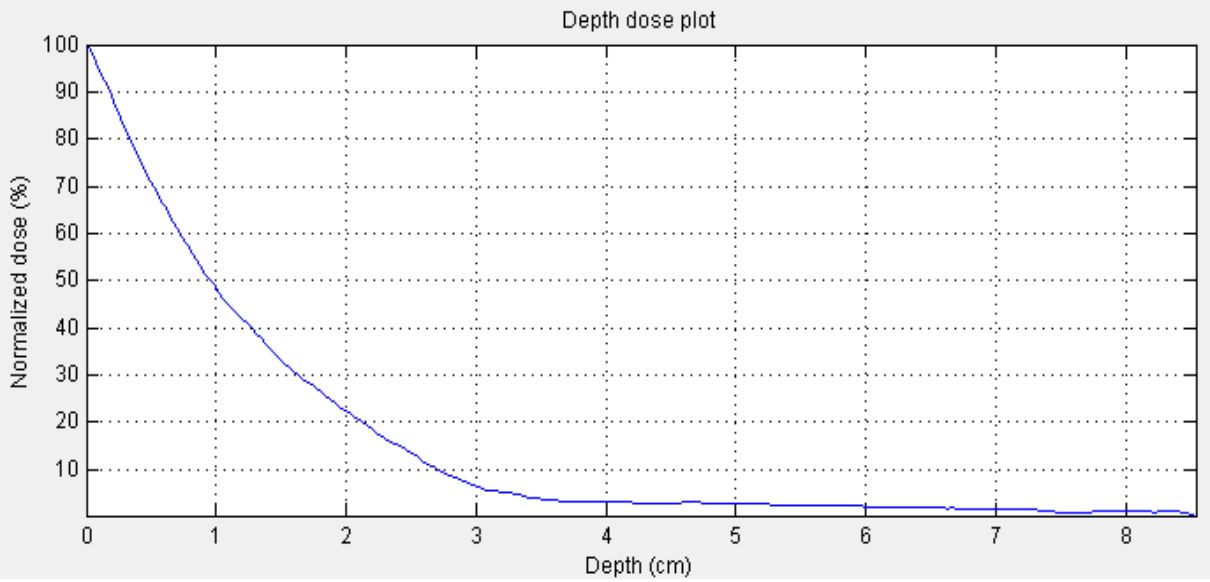

Figure 5.44. Normalized dose *PDD* at central axis for *0.762 mm* Pb, *8 MeV* at *600 MUs*.

Table 34: Results for *0.762 mm* Pb scatter foil for *8 MeV* electron beam.

Parameter	Results
Beam Energy	*8 MeV*
Foil Material	*Pb*
Foil Thickness	*0.762 mm*
Most probable Energy E_{P0}	*4.82 MeV*
Maximum dose, and D_{max}	*266 cGy @ 0 cm*
Practical Range R_p	*2.32 cm*
Diameter of *90% @* D_{max}	*1.58 cm*
Penumbra Size D_{max}, D_{90}, D_{50}, D_{25}	*0.09, 0.6, 1.11, and 1.50 cm*

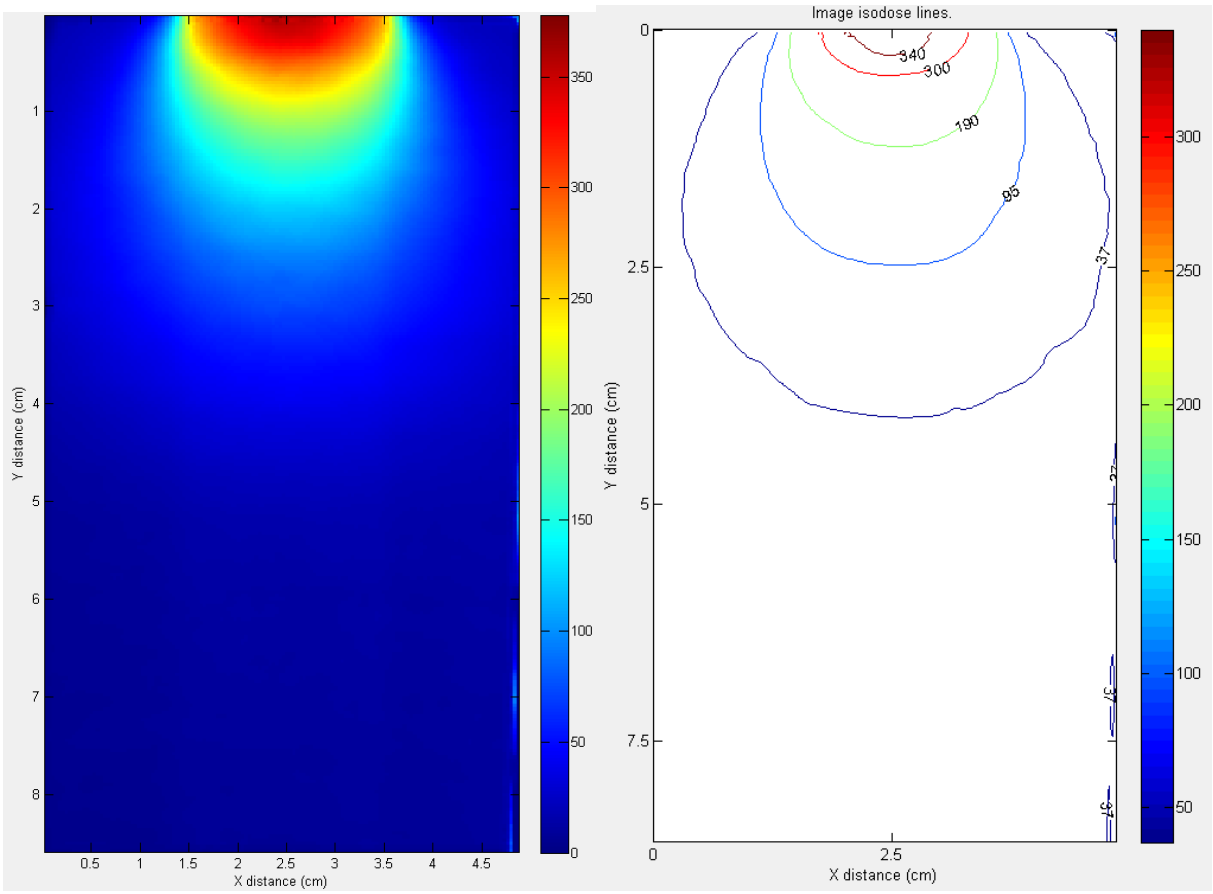

Figure 5.45. Image profile (left) and Isodose lines (right: *10%, 25%, 50%, 80%, 90%* isodose curves) for *0.762 mm* Pb, *12 MeV* at *600 MUs*.

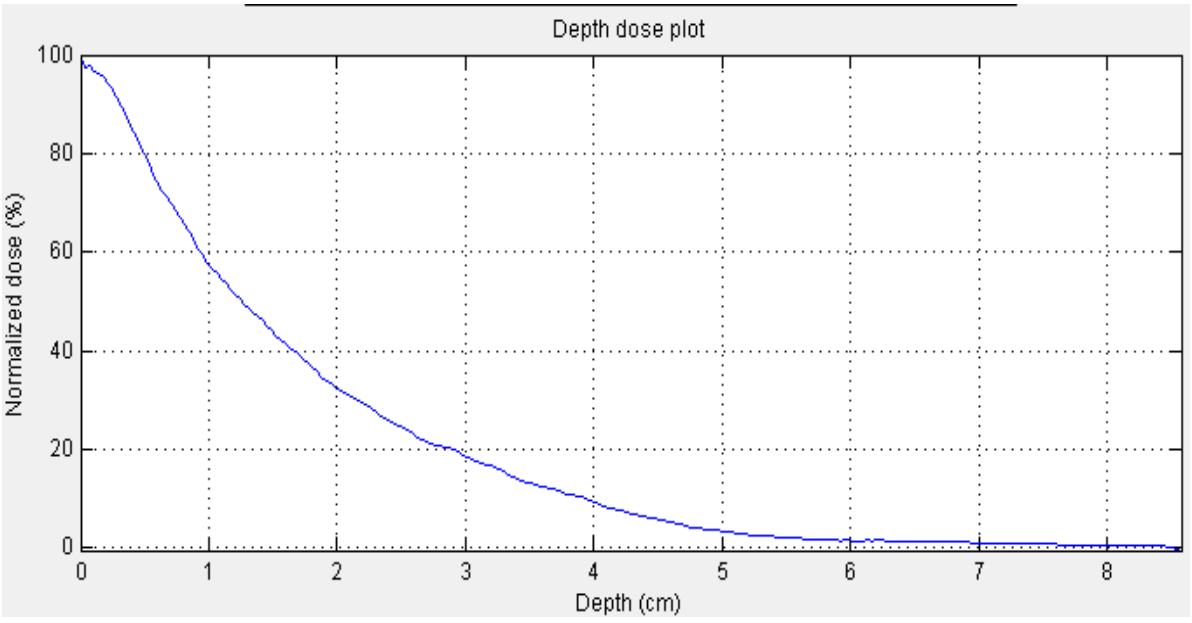

Figure 5.46. Normalized dose *PDD* at central axis for *0.762 mm* Pb, *12 MeV* at *600 MUs*.

Table 35: Results for *0.762 mm* Pb scatter foil for *12 MeV* electron beam.

Parameter	Results
Beam Energy	*12 MeV*
Foil Material	*Pb*
Foil Thickness	*0.762 mm*
Most probable Energy E_{P0}	*6.39 MeV*
Maximum dose, and D_{max}	*365 cGy @ 0 cm*
Practical Range R_p	*3.10 cm*
Diameter of *90%* @ D_{max}	*1.19 cm*
Penumbra Size D_{max}, D_{90}, D_{50}, D_{25}	*0.45, 0.67, 1.20, and 1.49 cm*

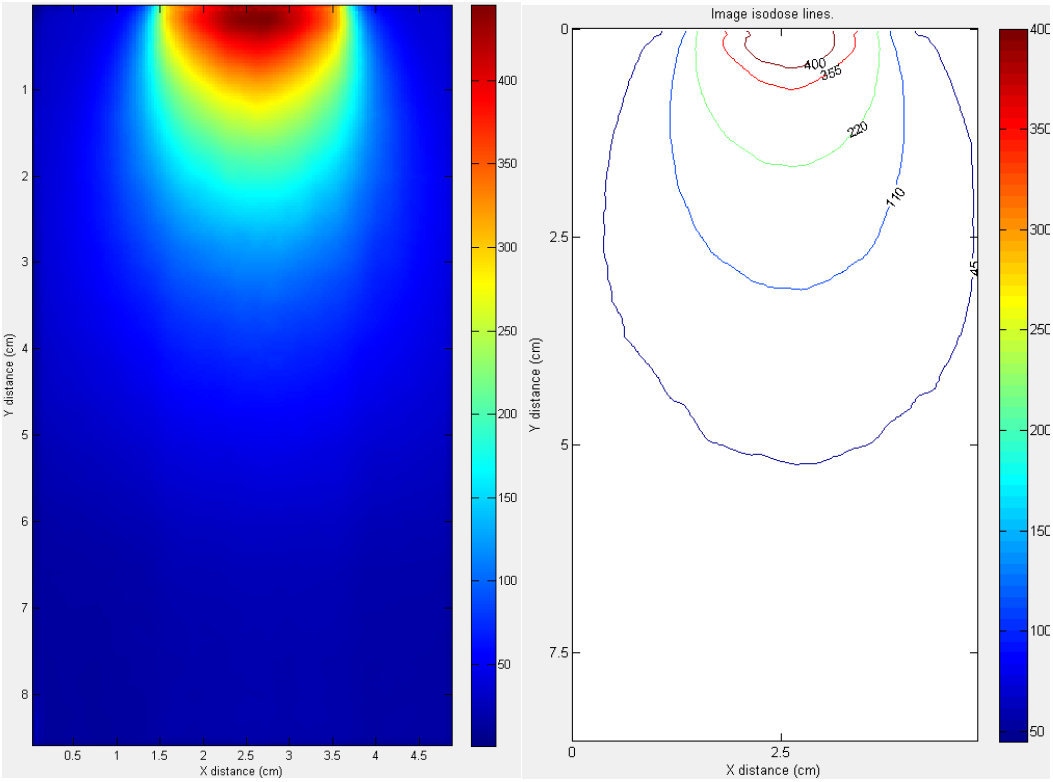

Figure 5.47. Image profile (left) and Isodose lines (right: *10%, 25%, 50%, 80%, 90%* isodose curves) for *0.762 mm* Pb, *15 MeV* at *600 MUs*.

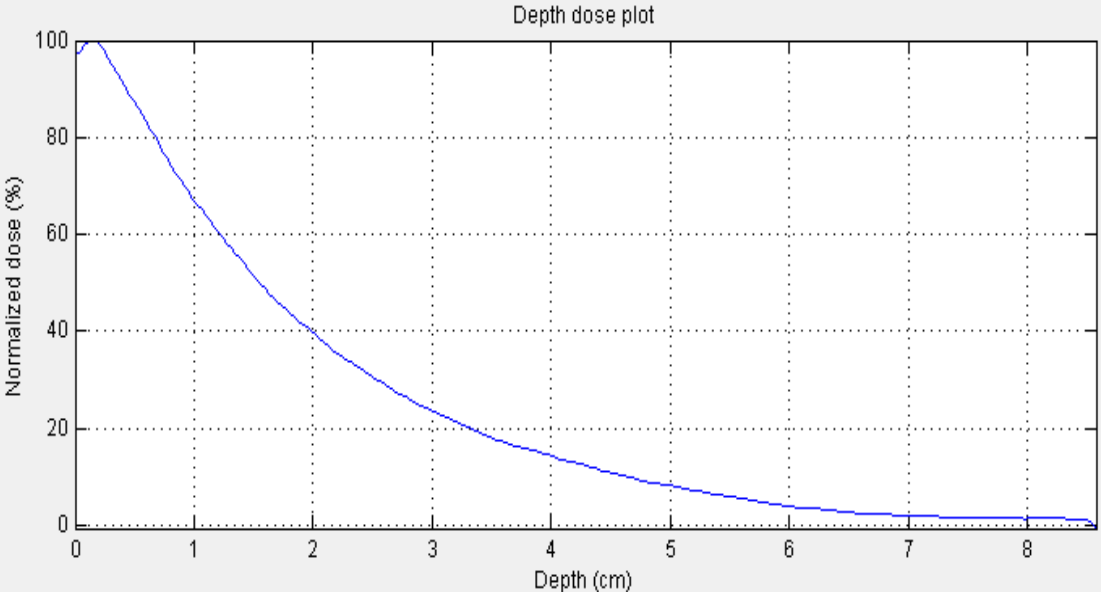

Figure 5.48. Normalized dose *PDD* at central axis for *0.762 mm* Pb, *15 MeV* at *600 MUs*.

Table 36: Results for *0.762 mm* Pb scatter foil for *15 MeV* electron beam.

Parameter	Results
Beam Energy	*15 MeV*
Foil Material	*Pb*
Foil Thickness	*0.762 mm*
Most probable Energy E_{P0}	*7.11 MeV*
Maximum dose, and D_{max}	*446 cGy @ 0.14 cm*
Practical Range R_p	*3.46 cm*
Diameter of *90%* @ D_{max}	*1.06 cm*
Penumbra Size D_{max}, D_{90}, D_{50}, D_{25}	*0.57, 0.72, 1.33, and 1.49 cm*

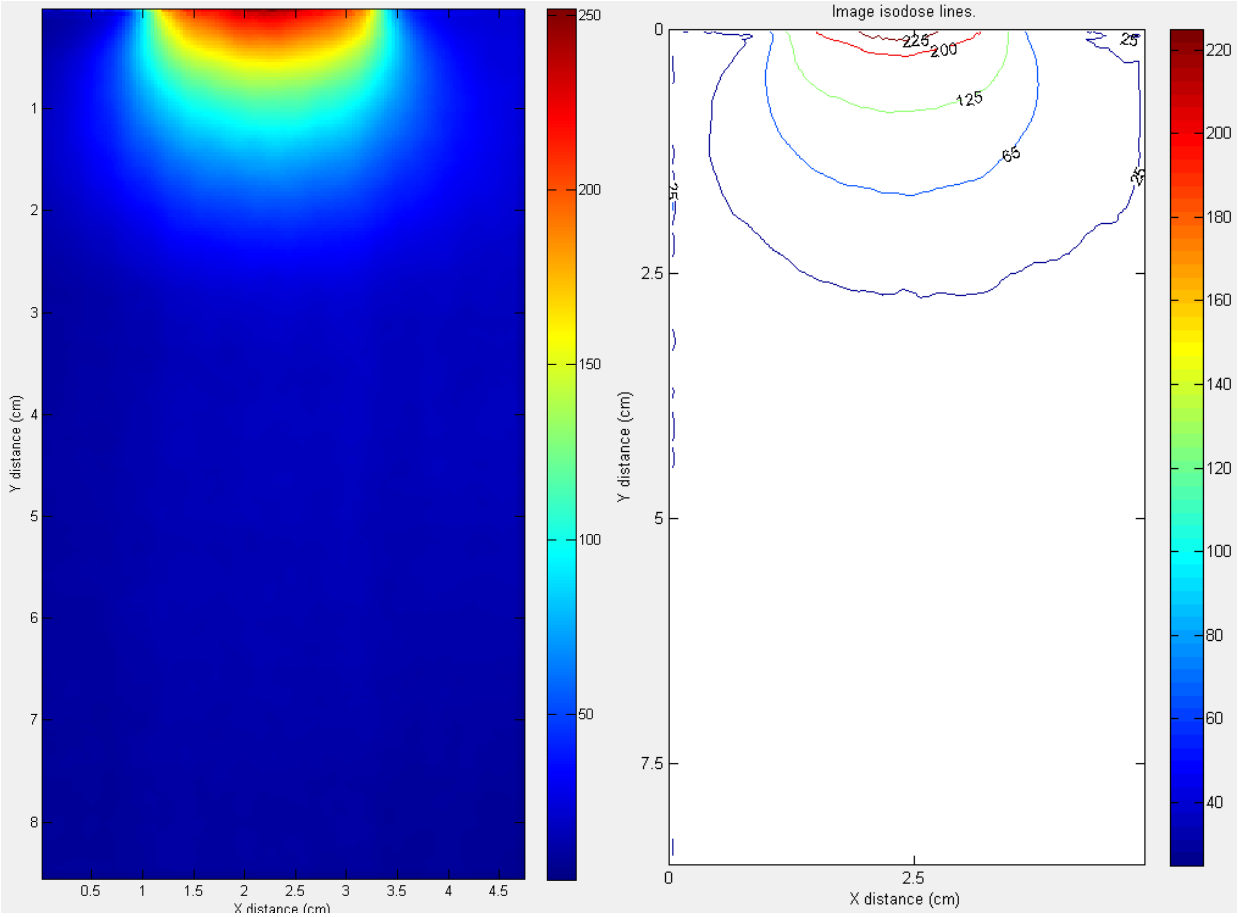

Figure 5.49. Image profile (left) and Isodose lines (right: *10%, 25%, 50%, 80%, 90%* isodose curves) for *1.0668 mm* Pb, *8 MeV* at *600 MUs*.

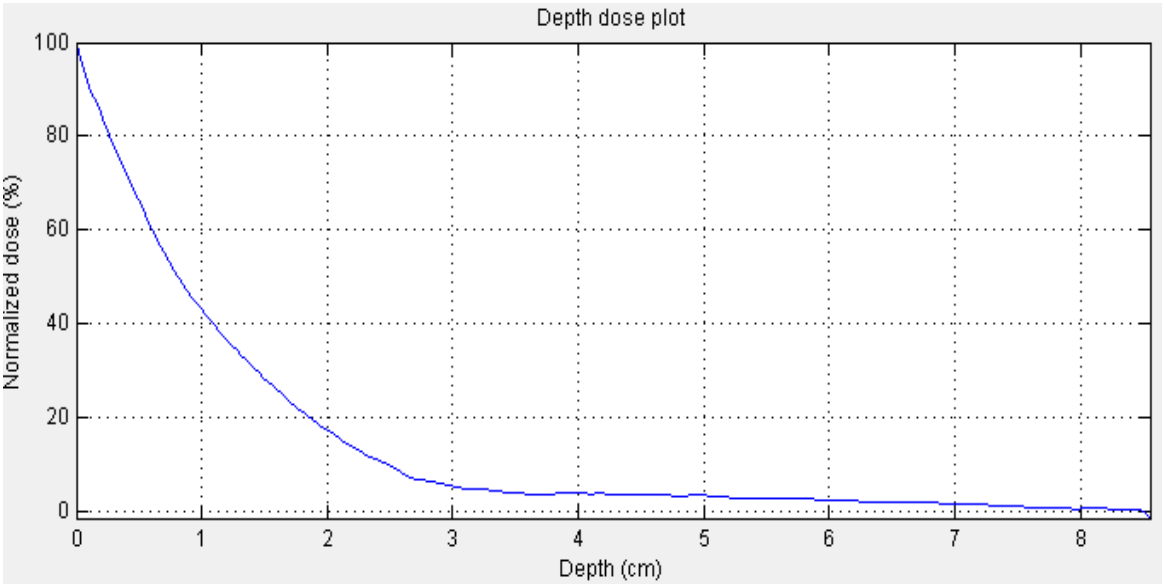

Figure 5.50. Normalized dose *PDD* at central axis for *1.0668 mm* Pb, *8 MeV* at *600 MUs*.

Table 37: Results for *1.0668 mm* Pb scatter foil for *8 MeV* electron beam.

Parameter	Results
Beam Energy	*8 MeV*
Foil Material	*Pb*
Foil Thickness	*1.0668 mm*
Most probable Energy E_{P0}	*4.29 MeV*
Maximum dose, and D_{max}	*253 cGy @ 0 cm*
Practical Range R_p	*2.05 cm*
Diameter of *90%* @ D_{max}	*0.73 cm*
Penumbra Size D_{max}, D_{90}, D_{50}, D_{25}	*0.54,0.50,1.00 and 1.57 cm*

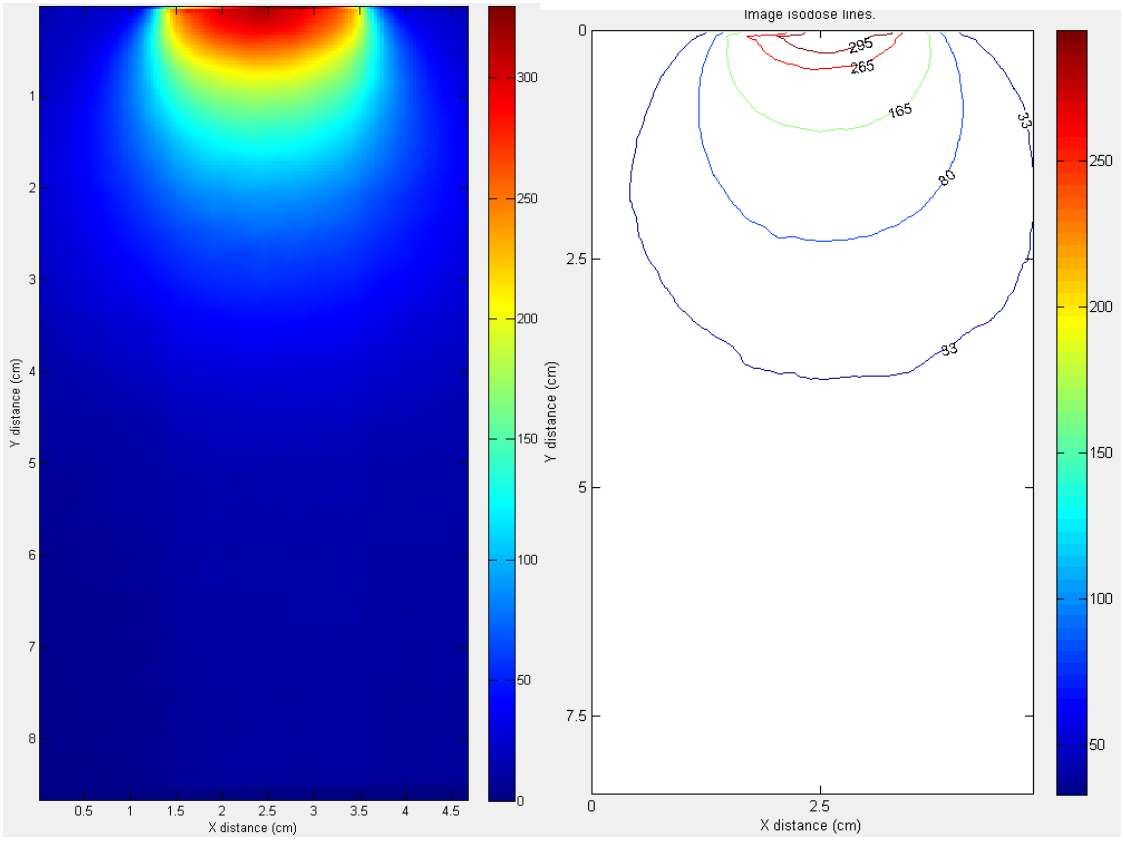

Figure 5.51. Image profile (left) and Isodose lines (right: *10%, 25%, 50%, 80%, 90%* isodose curves) for *1.0668 mm* Pb, *12 MeV* at *600 MUs*.

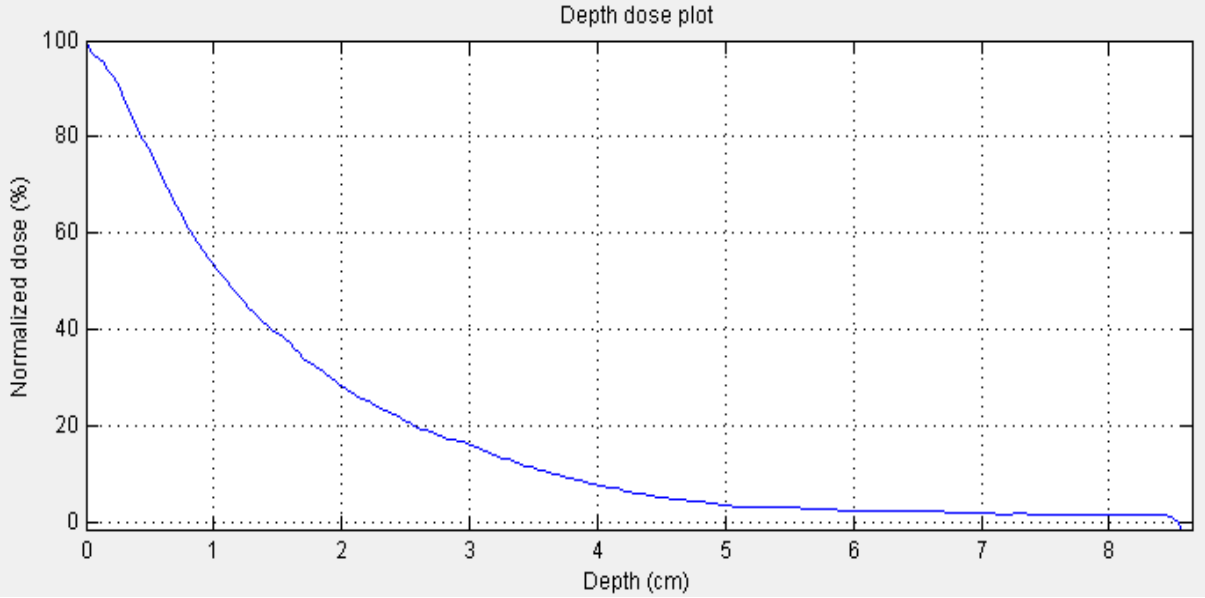

Figure 5.52. Normalized dose *PDD* at central axis for *1.0668 mm* Pb, *12 MeV* at *600 MUs*.

Table 38: Results for *1.0668 mm* Pb scatter foil for *12 MeV* electron beam.

Parameter	Results
Beam Energy	*12 MeV*
Foil Material	*Pb*
Foil Thickness	*1.0668 mm*
Most probable Energy E_{P0}	*5.52 MeV*
Maximum dose, and D_{max}	*325 cGy @ 0 cm*
Practical Range R_p	*2.67 cm*
Diameter of *90% @* D_{max}	*1.00 cm*
Penumbra Size D_{max}, D_{90}, D_{50}, D_{25}	*0.55, 0.54, 1.17, and 1.62 cm*

5.2. Scatter Foils Comparison Figures

Figures *5.53-5.61* are comparison figures that summarize the results from *section 5.1*. These figures show how a specific parameter behaves with respect to a combination of a scatter foil material (Pb and Al), a scatter foil thickness (*0-2.54 mm*) and an electron beam energy (*8, 12 & 15 MeV*). The nine parameters used for comparison are the practical range, the most probable energy, the maximum dose and its location, the size of the clinically relevant *90%* isodose line, and penumbra sizes at D_{max}, D_{90}, D_{50}, & D_{25}.

Reminder, all measurements were taken in solid water using EBT3 film under these conditions: *600 MU*, *100 SSD*, *6x6 cm*^{2} applicator, *2 cm* diameter circular skin collimator field.

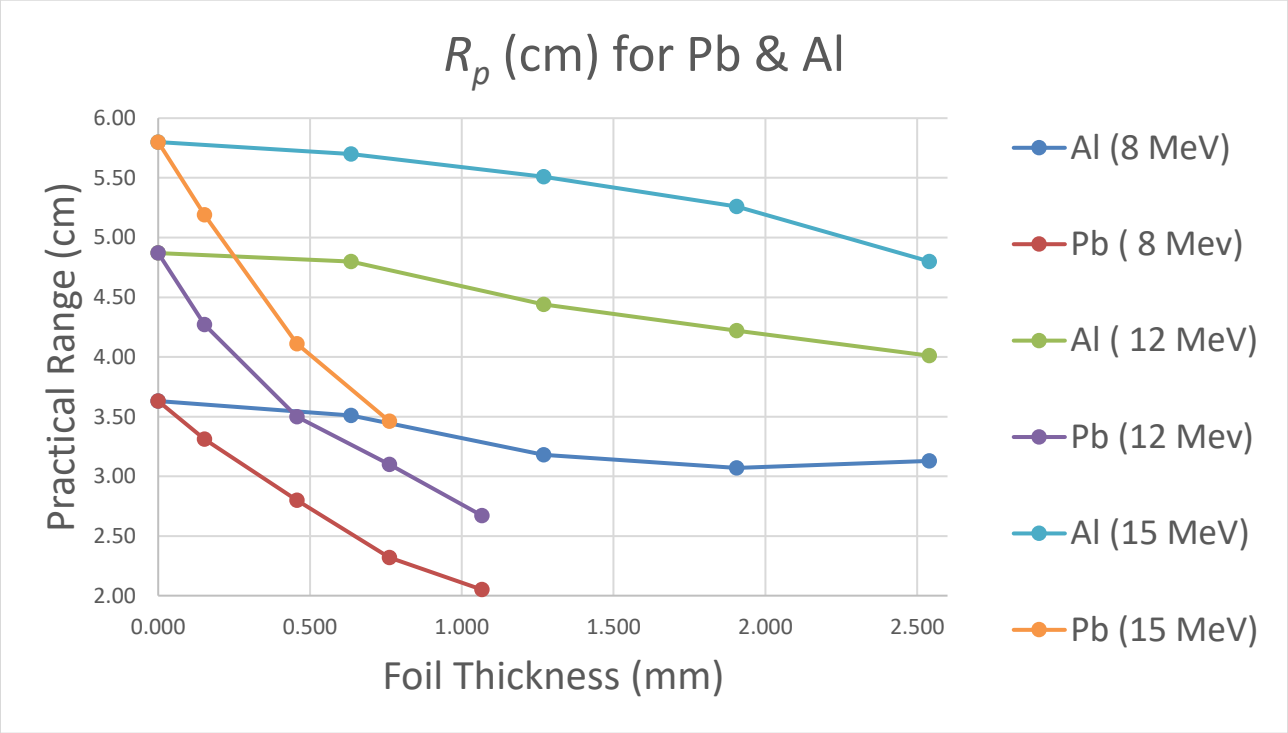

Figure 5.53. Practical range (*cm*) of Pb & Al scatter foils for *8, 12 & 15 MeV* electron beams at *600 MUs*.

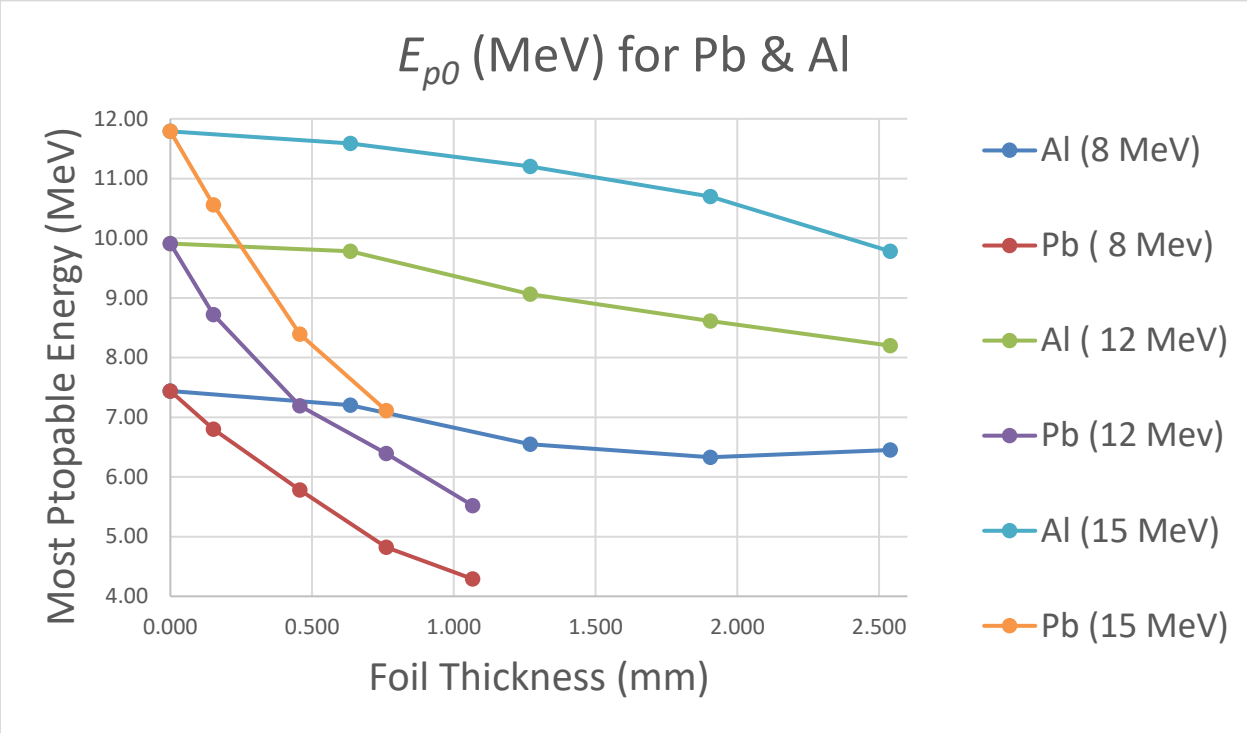

Figure 5.54. Most probable energy (*MeV*) of Pb & Al scatter foils for *8, 12 & 15 MeV* electron beams at *600 MUs*.

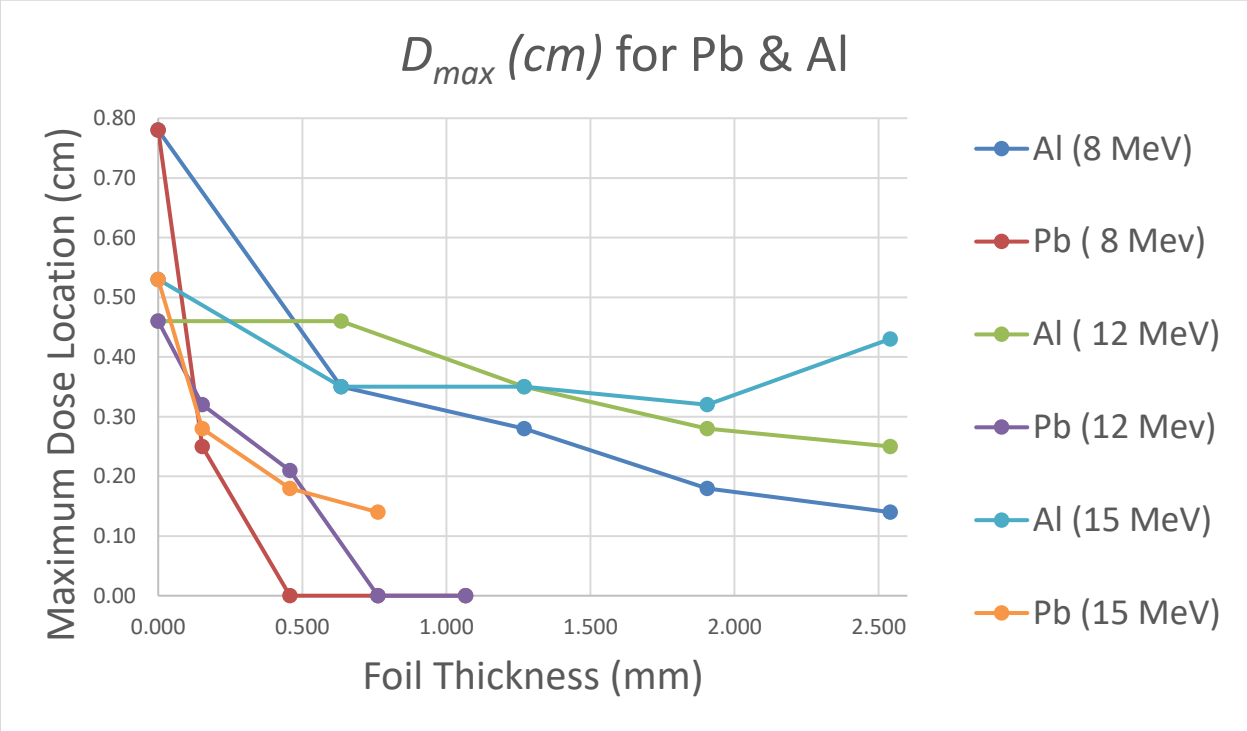

Figure 5.55. Maximum dose location (*cm*) of Pb & Al scatter foils for *8, 12 & 15 MeV* electron beams at *600 MUs*.

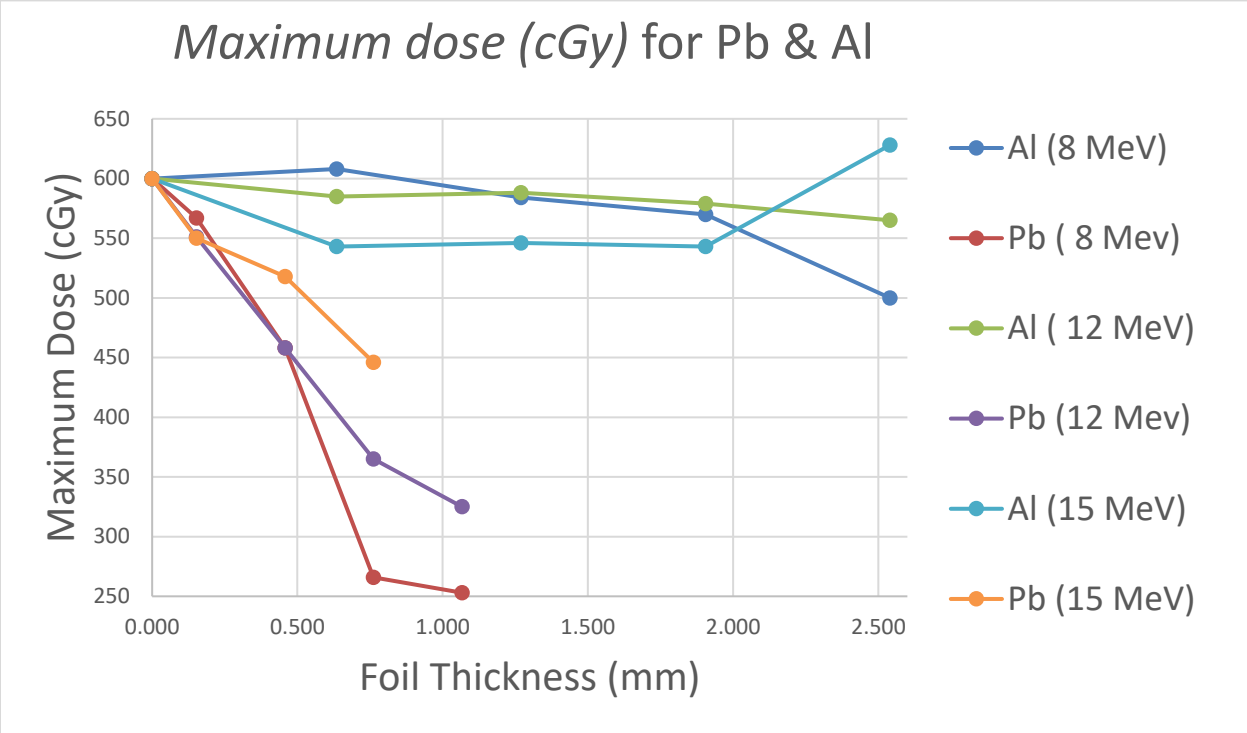

Figure 5.56. Maximum dose (*cGy*) of Pb & Al scatter foils for *8, 12 & 15 MeV* electron beams at *600 MUs*.

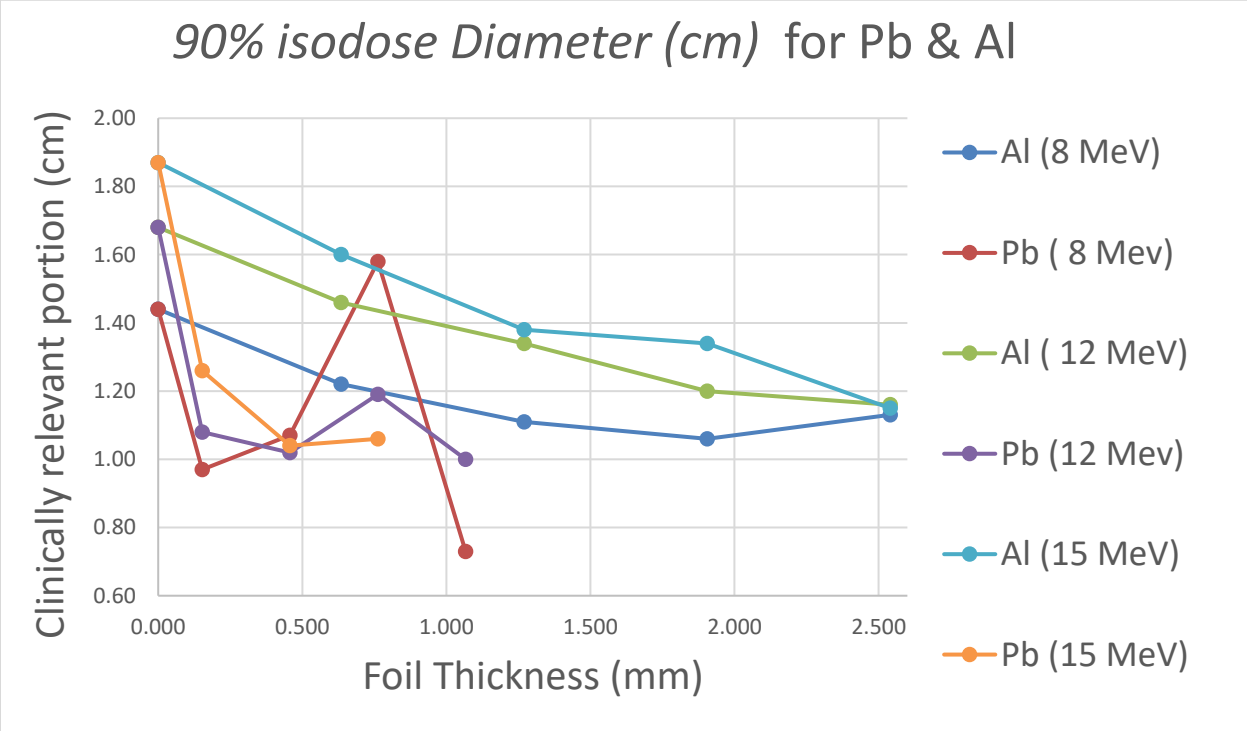

Figure 5.57. The clinically relevant portion of the field (*cm*) of Pb & Al scatter foils for *8, 12 & 15 MeV* electron beams at *600 MUs*.

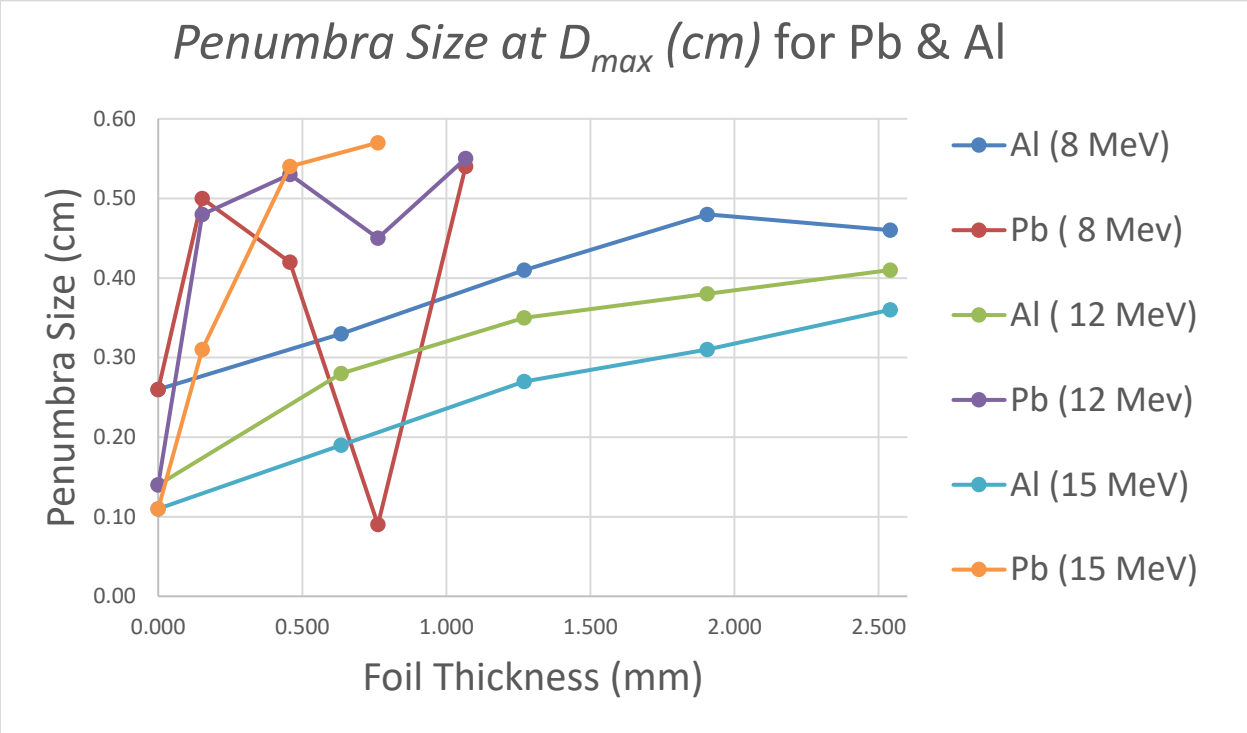

Figure 5.58. Penumbra size at D_{max} (*cm*) of Pb & Al scatter foils for *8, 12 & 15 MeV* electron beams at *600 MUs*.

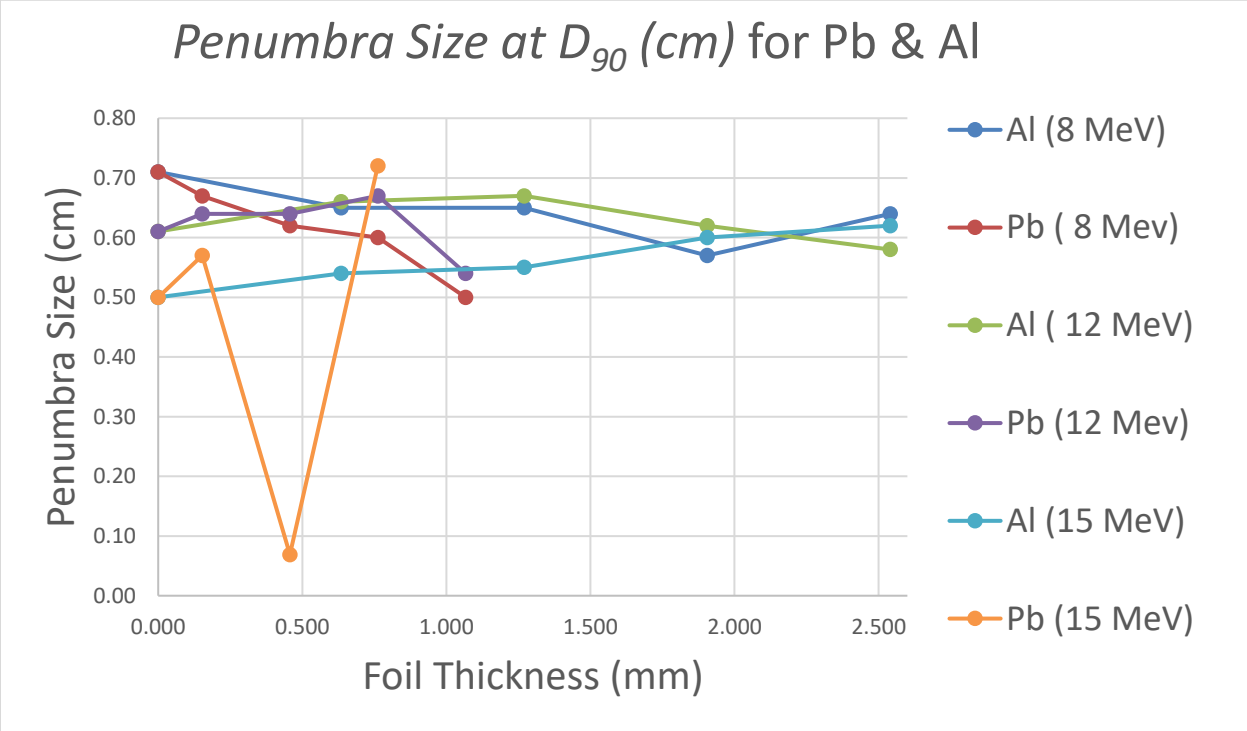

Figure 5.59. Penumbra size at D_{90} (*cm*) of Pb & Al scatter foils for *8, 12 & 15 MeV* electron beams at *600 MUs*.

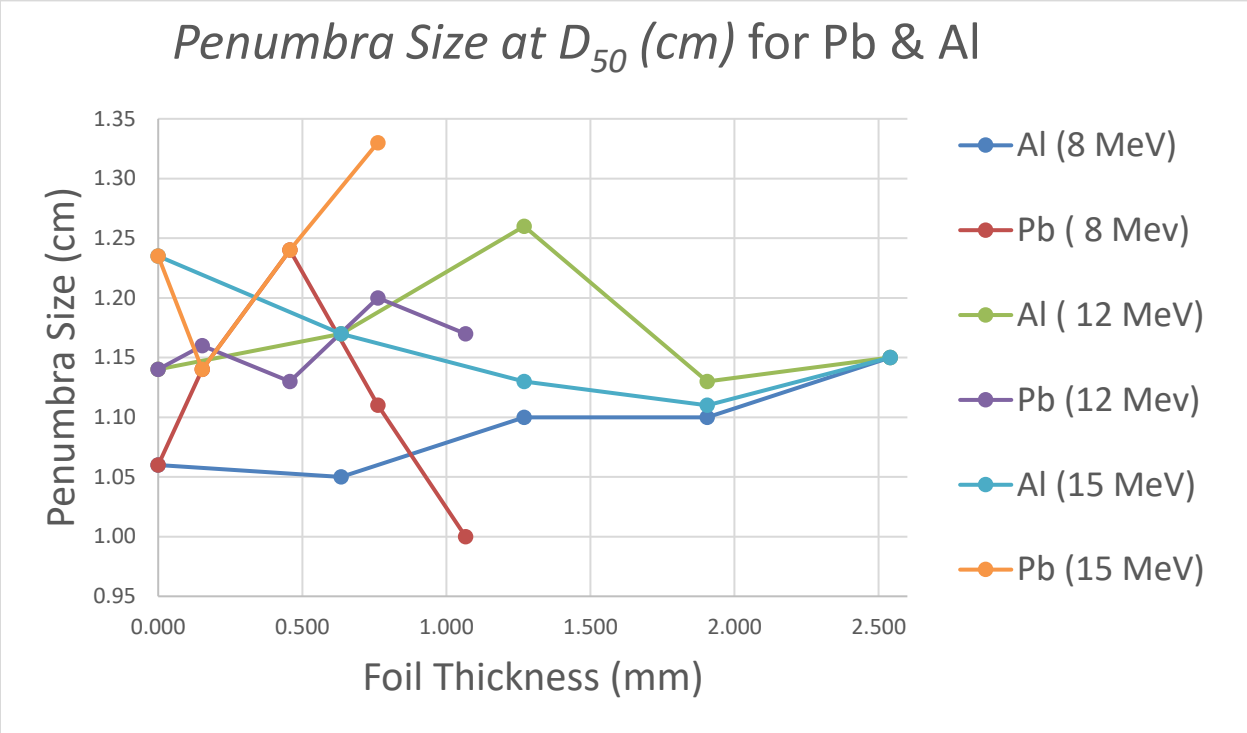

Figure 5.60. Penumbra size at D_{50} (*cm*) of Pb & Al scatter foils for *8, 12 & 15 MeV* electron beams at *600 MUs*.

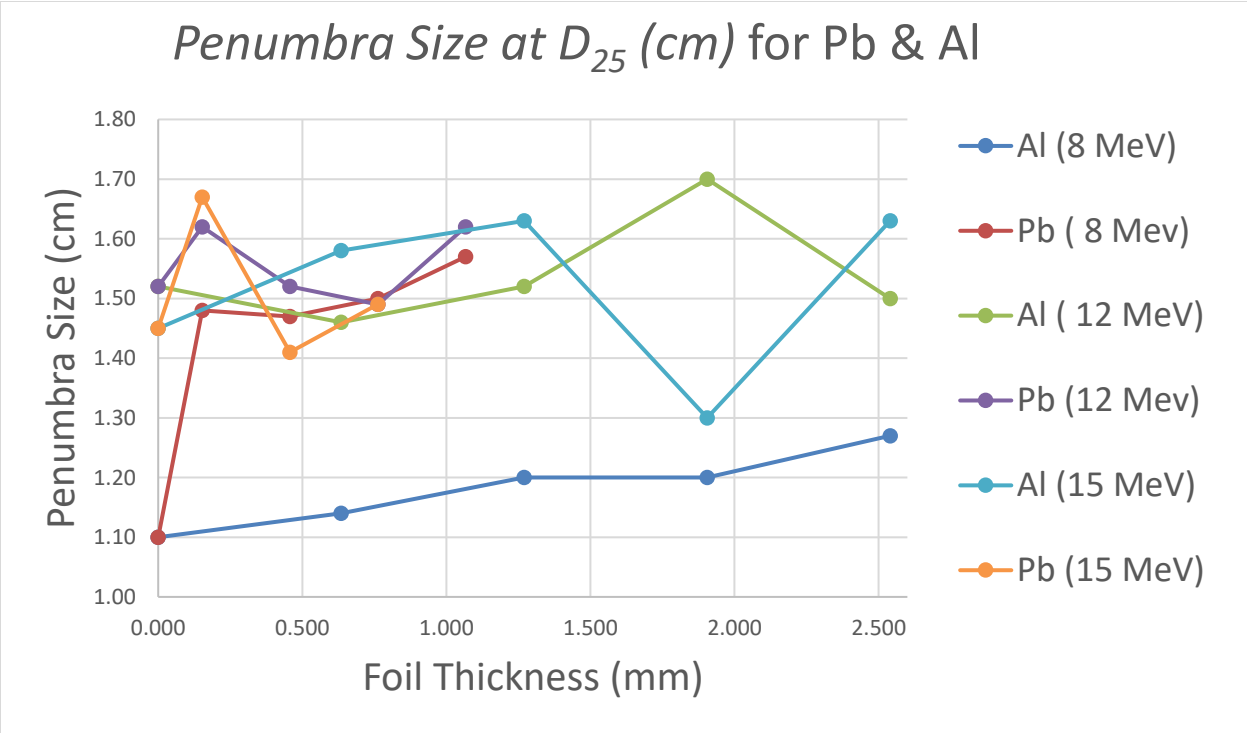

Figure 5.61. Penumbra size at D_{25} (*cm*) of Pb & Al scatter foils for *8, 12 & 15 MeV* electron beams at *600 MUs*.

6. DISCUSSION

This chapter contains a discussion of the findings of this experiment; the trend of the data collected, the reasoning behind the way this data behaved and its implications.

6.1. Scatter Foil Impact on R_p

The practical range is the maximum depth at which electrons come to a stop as they expend all their energy.[18] On a *PDD*, it is the intersection point of a trend line calculated from the descending linear portion of the depth dose profile and bremsstrahlung tail. The linear portion trend line is calculated using data between the R_{60} and R_{40}.[15] Clinically it represents the end of the dose deposited by electrons.[25] Beyond it, the only dose deposited in the medium is from bremsstrahlung tail.[18] High energy electrons loss *~2 MeV* of their energy per *cm* depth of water.[18] The practical range in cm can be estimated as $0.5E_0(MeV)$.[18] This formula did not hold true for this experiment as the measurements that were taken were no foils yielded slightly shorter practical ranges than what this formula would have predicted (*Figure 5.53*).

Figure *5.53* shows the practical range (*cm*) of Pb vs Al scatter foils for *8, 12 & 15 MeV* electron beams at *600 MUs*. The general trend of the data shows two things, the first one is an increase in the practical range as the energy increases which is expected because electrons have more energy to spend as they penetrate the solid water. The second one is a decrease in the practical range as the thickness of the scatter foil increases, which is also expected because the thicker the foil the more material electrons will encounter, the more energy electrons will loss, and thus the shorter their practical range will be. The decreases are roughly linear for both materials with a considerably larger slope for Pb.

It is also important to note that electrons have a much shorter practical range in Pb than in Al for the same beam energy. The huge decrease in practical range in Pb is attributed to its high

density (*11.34 g/cm³)* and high atomic number (*82*) compared to Al (*2.7 g/cm^3 & 13*, respectively).[18,25] This means that Pb has a higher number of electrons and the beam would loss more energy in it than in Al as its electrons absorb and scatter the energy.[39] With regards to bremsstrahlung radiation (*figures 5.2-5.52*), it had the same trend as practical range. Bremsstrahlung radiation increases as the energy of the electron beam increases and as the filtration decreases.

6.2. Scatter Foil Impact on E_{p0}

The most probable energy (E_{p0}) is the kinetic energy possessed by most of the incident electrons at phantom surface.[18,25] This is slightly larger than the mean energy ($\bar{E}_0$) which is the mean energy of the incident electrons at the surface of the phantom.[18,25] Their formulas are: $E_{p0} = 0.22 + 1.98R_p + 0.0025R_p^2$, & $\bar{E}_0 = 2.33 \times R_{50}$.[25] Since the most probable energy in dependent on the practical range, it is expected to behave similarly, as can be seen in figure *5.54*, which shows the most probable energy (*MeV*) of Pb vs Al scatter foils for *8, 12 & 15 MeV* electron beams at *600 MUs*. The first thing to notice is an increase in the most probable energy as the energy increases which is expected because the higher the energy of the beam, the more kinetic energy electrons will have. The second one is a decrease in the most probable energy as the thickness of the scatter foil increases, which is also expected because the thicker the foil more electrons will lose their kinetic energy, thus decreasing the most probable energy of most electrons as they reach the phantom surface.

Again, similar to practical range, the ability of Al to decrease the most probable energy is minimal compared to Pb, because of the reasons described in the previous section. For both materials the decrease is roughly linear. For Al, E_{p0} decreased by roughly $0.4\ \frac{MeV}{mm}$ for the *8 MeV,*

0.63 $\frac{MeV}{mm}$for the *12 MeV,* and *0.8* $\frac{MeV}{mm}$ for the *15 MeV.* For Pb, on the other hand, E_{p0} decreased by roughly *3.9 MeV/mm* for the *8 MeV, 5.9 MeV/mm* for the *12 MeV,* and *7.9 MeV/mm* for the *15 MeV.* It is worth pointing out that using Pb scatter foil of *0.4572 mm* with *12 MeV* yields similar practical range and most probable energy to using *0.762 mm* Pb foil with *15 MeV* and to similar results to that of *8 MeV* with no scatter foils.

6.3. Scatter Foil Impact on D_{max}

Depth of maximum dose is the location at which the maximum dose occurs. The first thing to notice is that as the foil gets thicker the location of the maximum dose gets closer to the surface for all energies. This is because electrons already spent some of their energy in the foil, thus, they cover less track in the phantom to deposit the rest of their energy after encountering the thick foil. This is especially evident for lower energy beams in Pb, where the maximum dose is at the surface. This decrement in depth of maximum dose is very apparent in all of the data except for the *2.54 mm* Al with the *15 MeV* electron beam which was not expected. This might have to do with the way the scatter foils were stacked on top of each other, which air gaps might have been present and added a complication to the measurement. It is advised to retake that measurement.

It can also be noted that the higher the energy the more penetrating the electrons are, thus they have more energy to deposit in the medium as they move in it, thus they have deeper maximum doses compared to lower energies.

6.4. Scatter Foil Impact on Maximum Dose

As anticipated, Pb was able to lower the maximum dose considerably, particularly for lower energy beams. In this case, the thin Pb foil acted as a shield filtering the electron beam and lowering the expected dose. For Al, doses were decreased overall but by a much smaller percentage compared to that of Pb, this explains why Al is not used as a shield against high energy electrons.

Note, even though the foils decreased the desired dose, an increase in the MUs delivered by some factor could bring the dose up to the desired dose for any of the measurements where foils were used.

Again, there were noticeable deviations from the rest of the data. One was for the same *2.54 mm* Al with the *15 MeV* electron beam. The other unexpected data was of the *0.635 mm* Al and *8 MeV* electron beam. These two discrepancies are most likely due to misalignment of the cutout or film with respect to the radiation field or error in the way the foils were piled.

6.5. *Scatter Foil Impact on 90% Isodose*

The *90%* isodose is of clinical relevance because it usually covers the region were doses are prescribed, that is because doses beyond the *90%* isodose curve characteristically decrease sharply.[18] Figure *5.57* shows the diameter of the *90%* isodose region for the different foil thicknesses and energies used. The diameter of the *90%* isodose region increases with increasing beam energy because electrons have more energy to spend. Foil usage did not improve the *90%* isodose region for any of the measurements. The decrease in the *90%* region diameter was more prominent for Pb than Al where it does level-off at *1.15 cm* for *2.5 mm* of Al regardless of the beam energy. This might be attributed to the fact that higher Z materials have more electron interactions and absorb more electrons than lower Z materials. There was an unusual increase in the *90%* region diameter for *0.762 mm* Pb at *8 MeV*. Retaking this measurement is recommended.

6.6. Scatter Foil Impact on Penumbra sizes

Penumbra is the region at the edge of a beam where dose rate rapidly decreases as a function of distance from the beam axis.[18] The penumbra width is typically defined as the distance between *20%* and *80%* isodose curves at a reference depth.[25] It consists of the geometrical (due to none-point source), the transmission (through jaws and collimators) and the scattering penumbras

(due to scattered electrons and photons).[25,39] Penumbra increases with SSD and decreases with beam energy.[18,25] Figures *5.58-5.61* show the width of the penumbra region at four depths D_{max}, D_{90}, D_{50}, & D_{25}, respectively, with respect to foil thickness and beam energy.

At D_{max}, lower energy beam has larger penumbras this is because electrons with higher energy are more penetrating with less lateral scatter and do not recoil at relatively larger angles like lower energy electrons.[45] Furthermore, Pb foils showed larger increase in penumbra width as foil thickness increases compared to that of Al. All the measurements (except for one) showed larger penumbras than when no foil was used. This means that there was a gradual (as opposed to sharp) decrease in dose rate at the edge of the beam due to greater electron range and the increase in scatter when foil thickness increases especially for lower energy electrons close to the surface. Generally speaking, the penumbras for both Pb and Al show similar behavior except for measurements at *0.762 mm* Pb where the case is reversed.

At D_{90}, the *8 MeV*, resulted in decreasing penumbra sizes regardless of the foil material used. While the *12 MeV* beam resulted in roughly the same penumbra size for both foil materials. On the other hand, the *15 MeV* resulted in an increase in penumbra size as foil thickness increases. Overall, the increase/decrease does not exceed 2 mm. Again, lower energy electrons resulted in slightly larger penumbras compared to higher energy electrons because at these depths lower energy electrons scatters more than higher energy electrons that penetrates more.

At D_{50}, all foils resulted in almost the same penumbra width for the three energies used. The one thing to notice is the higher the energy of the beam results in relatively larger penumbras at these depth because of electrons longer range. At these depths, the effect of the scatter foils is unobserved and the penumbra shape is more dependent of beam energy. At D_{25}, the general trend was that higher energy beams had larger penumbra width, and the thicker the foil the slightly larger

the penumbra size. The Al foils resulted in slightly larger penumbras widths with increasing foil thickness, but the Pb foils exhibited an initial increase in penumbra width then a level-off, with increasing foil thickness. At Pb thickness of *0.152 mm* electrons received the right amount of scatter to have enough range to widen the penumbra at this depth unlike that of the Al foils where thicker foils resulted in wider penumbras with no noticeable "peak" at the used foil thicknesses.

6.7. Study Limitations

Even though caution was taken during every step of this experiment, error could have befallen unintentionally. Potential of error in this experiment could be summarized as set-up related error and analysis related error. Examples of the set-up related errors are: film cutting and handling, alignment of film with respect to the phantom, alignment of the phantom with respect to the radiation field, alignment of the skin collimator with respect to the radiation field and with respect to the phantom, alignment of the scatter foils with respect to the collimator, with respect to the radiation field and with respect to each other. Analysis related error are attribute to handling and scanning irradiated films, scanner settings, manual calculation of penumbra widths and other parameters. These sources of uncertainty could explain why some of the data were unexpected.

Because everything is manually set in place, replicating the same exact positioning of every component in this experiment is very unlikely. Taking more measurements and isolating every factor should decrease the uncertainties but is very time consuming. A more realistic option would be to use a simulation software in which positioning uncertainties will be eliminated.

Very limited access to the facility for graduate students due to COVID-19 and time constrains caused by the lockout completely halted the progress of this project. This prevented retaking some of the measurements or even simulating the experiment. Thus, it is highly advised for the work to be reproduced to clarify inconstancies in data.

7. CONCLUSIONS

This work is a preliminary experiment to explore the effects of novel design of contact lead sheet collimation and filtration of high energy electron fields on electron depth dose distributions with application to uniform treatment of small skin lesions. When compared to the use of a bare skin collimator, the addition of scatter foils to the skin collimator has been demonstrated to reduce the practical range, the effective energy of electron beams, the *90%* isodose region diameter, the maximum dose and its depth, and to increase the penumbra width at several depths. These effects are especially evident for thicker scatter foils of high Z materials. In conclusion, the addition of scatter foils did not yield the hypothesized uniform, clinically-desirable, dose distributions. With the help of a Monte Carlo simulation program future studies might want to focus on investigating the effects of tweaking the shape of the scatter foil (e.g., thicker in the middle, mesh design…etc.), the use of other material or a combination of materials, and changing the location of the foil with respect to the skin collimator.

BIBLIOGRAPHY

[1]Adrich, Przemysław. “Technical Note: Monte Carlo Study on the Reduction of X-Ray Contamination of Therapeutic Electron Beams for Intraoperative Radiation Therapy by Means of Improvements in the Design of Scattering Foils.” *Medical Physics*, 2019, doi:10.1002/mp.13647.

[2]Allen, Christopher, et al. “Heavy Charged Particle Radiobiology: Using Enhanced Biological Effectiveness and Improved Beam Focusing to Advance Cancer Therapy.” *Mutation Research/Fundamental and Molecular Mechanisms of Mutagenesis*, vol. 711, no. 1-2, 2011, pp. 150–157., doi:10.1016/j.mrfmmm.2011.02.012.

[3]Amin, Md Nurul, et al. “Small Field Electron Beam Dosimetry Using MOSFET Detector.” *Journal of Applied Clinical Medical Physics*, vol. 12, no. 1, 2010, pp. 50–57., doi:10.1120/jacmp.v12i1.3267.

[4]Anjali V.R. (2020) Electrons. In: Mallick S., Rath G., Benson R. (eds) Practical Radiation Oncology. Springer, Singapore

[5]Attix, Frank Herbert. *Introduction to Radiological Physics and Radiation Dosimetry*. VCH, 2007.

[6]Beddar, A. Sam, et al. “Intraoperative Radiation Therapy Using Mobile Electron Linear Accelerators: Report of AAPM Radiation Therapy Committee Task Group No. 72.” *Medical Physics*, vol. 33, no. 5, 2006, pp. 1476–1489., doi:10.1118/1.2194447.

[7]Bieda, Michael R., et al. “The Effect of Scattering Foil Parameters on Electron-Beam Monte Carlo Calculations.” *Medical Physics*, vol. 28, no. 12, 2001, pp. 2527–2534., doi:10.1118/1.1420387.

[8]Brant, Timothy A. “Treating Skin Cancer with Radiation Traditional and New Approaches.” AOCD CURRENT CONCEPTS IN DERMATOLOGY MEETING. AOCD CURRENT CONCEPTS IN DERMATOLOGY MEETING, 2016, Santa Monica, California.

[9]Carlone, Marco, et al. “Technical Note: Enhancing the Surface Dose Using a Weak Longitudinal Magnetic Field.” *Medical Physics*, vol. 43, no. 6Part1, 2016, pp. 2927–2932., doi:10.1118/1.4949001.

[10]Carver, Robert L., et al. “Real-Time Simulator for Designing Electron Dual Scattering Foil Systems.” *Journal of Applied Clinical Medical Physics*, vol. 15, no. 6, 2014, pp. 323–342., doi:10.1120/jacmp.v15i6.4849.

[11]Chi, Pai-Chun M., et al. “Modeling Skin Collimation Using the Electron Pencil Beam Redefinition Algorithm.” *Medical Physics*, vol. 32, no. 11, 2005, pp. 3409–3418., doi:10.1118/1.2064808.

[12]Connell, T, and J Seuntjens. “Design and Validation of Novel Scattering Foils for Modulated Electron Radiation Therapy.” *Physics in Medicine and Biology*, vol. 59, no. 10, 2014, pp. 2381–2391., doi:10.1088/0031-9155/59/10/2381.

[13]Cooper, Geoffrey M. *The Cell: a Molecular Approach*. Sinauer Associates, 2019.

[14]Dodge, Daquan. “Radiation Protection in Radiotherapy - Ppt Download.” *SlidePlayer*, 2015, slideplayer.com/slide/2718772/.

[15]DoseLab Version 6.80, Rev 1.0, MOBIUS MEDICAL SYSTEMS, LP, Houston, TX, USA, 2016.

[16]Epson Expression 10000XL: Color Graphics Scanner User’s Guide, Epson America, Long Beach, CA, USA, 2007. Accessed on: July 22, 2020. [Online]. Available: https://files.support.epson.com/pdf/ex10kg/ex10kgu1.pdf

[17]Gajewski, Romuald. “An Enhanced Sector Integration Model for Output and Dose Distribution Calculation of Irregular Concave Shaped Electron Beams.” *Medical Physics*, vol. 36, no. 7, 2009, pp. 2966–2975., doi:10.1118/1.3148583.

[18]Gibbons, John P., and Faiz M. Khan. *Khan's the Physics of Radiation Therapy*. Wolters Kluwer, 2020.

[19]Gillespie, Sean, and Peter Woulfe. “Commissioning an Elekta Versa HD Linear Accelerator.” *Physica Medica*, vol. 32, no. 7, 2016, p. 954., doi:10.1016/j.ejmp.2016.05.031.

[20]Hall, Eric J., and Amato J. Giaccia. *Radiobiology for the Radiologist*. Wolters Kluwer, 2019.

[21]Hanahan, Douglas, and Robert A. Weinberg. “Hallmarks of Cancer: The Next Generation.” *Cell*, vol. 144, no. 5, 2011, pp. 646–674., doi:10.1016/j.cell.2011.02.013.

[22]Henzen, D., et al. “Forward Treatment Planning for Modulated Electron Radiotherapy (MERT) Employing Monte Carlo Methods.” *Medical Physics*, vol. 41, no. 3, 2014, p. 031712., doi:10.1118/1.4866227.

[23]Hogstrom, Kenneth R., et al. “Modulated Electron Therapy .” Intensity Modulated Radiation Therapy. AAPM Summer School, 2003, Colorado Springs, CO.

[24]Hogstrom, Kenneth. “Bolus Electron Conformal Therapy (ECT): Personalized Electron Beam Therapy Using Custom Treatment Devices .” AAPM Annual Meeting. AAPM Annual Meeting, 2017, Denver, CO.

[25]INTERNATIONAL ATOMIC ENERGY AGENCY, Radiation Oncology Physics, , IAEA, Vienna (2005).

[26]Johnson, G. (2010, December 28). Unearthing Prehistoric Tumors, and Debate. *The New York Times*, D1. Retrieved from: http://www.nytimes.com/2010/12/28/health/28cancer.html

[27]Kaiser, Adeel, et al. "Proton Therapy Delivery and Its Clinical Application in Select Solid Tumor Malignancies." *Journal of Visualized Experiments*, no. 144, 2019, doi:10.3791/58372.

[28]Khan, Faiz M., et al. "Effect of Air Space on Depth Dose in Electron Beam Therapy." *Radiology*, vol. 126, no. 1, 1978, pp. 249–251., doi:10.1148/126.1.249.

[29]Klein , Eric E., and Rojano Kashani. "Electron-Beam Therapy Dosimetry, Treatment Planning, and Techniques." *Oncohema Key*, 2 July 2016, oncohemakey.com/electron-beam-therapy-dosimetry-treatment-planning-and-techniques/.

[30]Kokurewicz, K., et al. "Focused Very High-Energy Electron Beams as a Novel Radiotherapy Modality for Producing High-Dose Volumetric Elements." *Scientific Reports*, vol. 9, no. 1, 2019, doi:10.1038/s41598-019-46630-w.

[31]Korevaar, Erik W, et al. "Mixing Intensity Modulated Electron and Photon Beams: Combining a Steep Dose Fall-off at Depth with Sharp and Depth-Independent Penumbras and Flat Beam Profiles." *Physics in Medicine and Biology*, vol. 44, no. 9, 1999, pp. 2171–2181., doi:10.1088/0031-9155/44/9/305.

[32]LeBlanc, Justin Deloy. "Design of Electron Dual Foil Scattering Systems for Elekta Infinity Radiotherapy Accelerators." *Louisiana State University* , Agricultural and Mechanical College, 2012.

[33]Ludewig, Harrison D. "Preliminary Investigation into Electron Beam Lensing Utilizing Beveled Cerrobend Geometries: a Thesis." *Oregon Health & Science University, June*, 2019.

[34]Ma, Lijun. "Dosimetric Properties of Magnetically Collimated Electron Beams for Radiation Therapy." *Medical Physics*, vol. 31, no. 11, 2004, pp. 2973–2977., doi:10.1118/1.1809780.

[35]McDermott, Patrick, and Colin G. Orton. *The Physics & Technology of Radiation Therapy*. Medical Physics Publishing, 2018.

[36]Mobile, Katherine. "The Use of Bolus Electron Conformal The Use of Bolus Electron Conformal Therapy in the Clinical Setting." The American Association of Medical Dosimetrists, Region 1. The American Association of Medical Dosimetrists, Region 1, Aug. 2013.

[37]National Research Council. (2006). Health Risks from Exposure to Low Levels of Ionizing Radiation: BEIR VII Phase 2. Washington, DC: The National Academies Press. doi: 10.17226/11340.

[38]Niroomand-Rad, Azam, et al. "Radiochromic Film Dosimetry: Recommendations of AAPM Radiation Therapy Committee Task Group 55." *Medical Physics*, vol. 25, no. 11, 1998, pp. 2093–2115., doi:10.1118/1.598407.

[39]Pawlicki, Todd, et al. *Hendee's Radiation Therapy Physics*. John Wiley and Sons, 2017.

[40]Phaisangittisakul, N., et al. "Magnetic Collimation and Metal Foil Filtering for Electron Range and Fluence Modulation." *Medical Physics*, vol. 31, no. 1, 2003, pp. 17–23., doi:10.1118/1.1630491.

[41]Pitcher, Garrett M., et al. "Improved Electron Collimation System Design for Elekta Linear Accelerators." *Journal of Applied Clinical Medical Physics*, vol. 18, no. 5, 2017, pp. 259–270., doi:10.1002/acm2.12155.

[42]Pohl, Ryan. *Skin Sparring with Electron Treatments*. ryanpohl.weebly.com/skin-sparring-with-electron-treatments.html.

[43]Purdy, James A., et al. "Lipowitz Metal Shielding Thickness for Dose Reduction of 6-20 MeV Electrons." *Medical Physics*, vol. 7, no. 3, 1980, pp. 251–253., doi:10.1118/1.594680.

[44]Rich, J. N. (2016). Cancer stem cells: understanding tumor hierarchy and heterogeneity. Medicine, 95(1 Suppl 1), S2-7. doi: 10.1097/MD.0000000000004764.

[45]Rivers, Charlotte I., et al. "The Dose Penumbra of a Custom-Made Shield Used in Hemibody Skin Electron Irradiation." *Journal of Applied Clinical Medical Physics*, vol. 17, no. 6, 2016, pp. 276–282., doi:10.1120/jacmp.v17i6.6367.

[46]Ross, C. K., et al. "Measurement of Multiple Scattering of 13 and 20MeV Electrons by Thin Foils." *Medical Physics*, vol. 35, no. 9, 2008, pp. 4121–4131., doi:10.1118/1.2968095.

[47]Siegel, R. L., Miller, K. D., & Jemal, A. (2016). Cancer statistics, 2016. CA: A Cancer Journal for Clinicians, 66(1),7-30. doi: 10.3322/caac.21332

[48]Sipilä, Petri, et al. "Gafchromic EBT3 Film Dosimetry in Electron Beams - Energy Dependence and Improved Film Read-Out." *Journal of Applied Clinical Medical Physics*, vol. 17, no. 1, 2016, pp. 360–373., doi:10.1120/jacmp.v17i1.5970.

[49]"Skin Cancer." *American Academy of Dermatology*, www.aad.org/media/stats-skin-cancer.

[50]"Skin Cancer: Melanoma and Nonmelanoma Skin Cancer." *Maryland Oncology Hematology*, marylandoncology.com/disease-drug-info/types-of-cancer/skin-cancer/.

[51]Toulany, Mahmoud. “Targeting DNA Double-Strand Break Repair Pathways to Improve Radiotherapy Response.” *Genes*, vol. 10, no. 1, 2019, p. 25., doi:10.3390/genes10010025.

[52]“Treating Basal & Squamous Cell Skin Cancer: Squamous Cell Treatment.” *American Cancer Society*, www.cancer.org/cancer/basal-and-squamous-cell-skin-cancer/treating.html.

[53]Ulin, Kenneth, and Edward S. Sternick. “An Isodose Shift Technique for Obliquely Incident Electron Beams.” *Medical Physics*, vol. 16, no. 6, 1989, pp. 905–910., doi:10.1118/1.596316.

[54]Venanzio, Cristina Di, et al. “Comparison between Small Radiation Therapy Electron Beams Collimated by Cerrobend and Tubular Applicators.” *Journal of Applied Clinical Medical Physics*, vol. 16, no. 1, 2015, pp. 329–335., doi:10.1120/jacmp.v16i1.5186.

[55]*VERSA HD System – ELEKTA*, DOSEO, www.plateformedoseo.com/en/wp-content/uploads/2016/06/accelerator-Elekta.pdf.

[56]Vilches, M., et al. “Multiple Scattering of 13 and 20 MeV Electrons by Thin Foils: A Monte Carlo Study with GEANT, Geant4, and PENELOPE.” *Medical Physics*, vol. 36, no. 9Part1, 2009, pp. 3964–3970., doi:10.1118/1.3183501.

[57]Vries, Rowen J. De, and Steven Marsh. “Evaluation of Backscatter Dose from Internal Lead Shielding in Clinical Electron Beams Using EGSnrc Monte Carlo Simulations.” *Journal of Applied Clinical Medical Physics*, vol. 16, no. 6, 2015, pp. 139–150., doi:10.1120/jacmp.v16i6.5563.

[58]Wild CP, Weiderpass E, Stewart BW, editors (2020). World Cancer Report: Cancer Research for Cancer Prevention. Lyon, France: International Agency for Research on Cancer. Available from: http://publications.iarc.fr/586.

[59]Wittke, James H. “Electron Interaction with Matter.” *GLG 510: Course Overview*, 19 Mar. 2006, www.cefns.nau.edu/geology/malabs/Microprobe/Course%20Overview.html.

[60]“Worldwide Cancer Statistics.” *Cancer Research UK*, 22 Aug. 2019, www.cancerresearchuk.org/health-professional/cancer-statistics/worldwide-cancer.

[61]Ye, Sung-Joon, et al. “Monte Carlo Techniques for Scattering Foil Design and Dosimetry in Total Skin Electron Irradiations.” *Medical Physics*, vol. 32, no. 6Part1, 2005, pp. 1460–1468., doi:10.1118/1.1924368.

[62] Pijls-Johannesma, Madelon et al. “Do we have enough evidence to implement particle therapy as standard treatment in lung cancer? A systematic literature review.” The oncologist vol. 15,1 (2010): 93-103. doi:10.1634/theoncologist.2009-0116